LBL--25057

DE88 010879

I. Photochemistry of Psoralen-DNA Adducts
II. Biological Effects of Psoralen-DNA Adducts
III. Applications of Psoralen-DNA Photochemistry

Yun-bo Shi
(Ph.D. Thesis)

Lawrence Berkeley Laboratory
1 Cyclotron Road
Berkeley, CA 94720
and
University of California, Berkeley
Berkeley, CA 94720

March 1988

Supported by the U.S. Department of Energy under Contract Number DE-AC03-76SF00098.

I. Photochemistry of Psoralen-DNA Adducts

II. Biological Effects of Psoralen-DNA Adducts

III. Applications of Psoralen-DNA Photochemistry

Yun-bo Shi

ABSTRACT

This thesis consists of three main parts and totally eight chapters. In part I, I will present studies on the photochemistry of psoralen-DNA adducts, specifically, the wavelength dependencies for the photoreversals of thymidine-HMT (4'-hydroxymethyl-4, 5', 8-trimenthylpsoralen) moncadducts and diadduct and the same adducts incorporated in DNA helices and the wavelength dependecies for the photocrosslinking of thymidine-HMT moncadducts in double-stranded helices. In part II, I will report some biological effects of psoralen-DNA adducts, i.e., the effects on double-stranded DNA stability, DNA structure, and transcription by *E. coli* and T7 RNA polymerases. Finally, I will focus on the applications of psoralen-DNA photochemistry to investigation of protein-DNA interaction during transcription, which includes the interaction of *E. coli* and T7 RNA polymerases with DNA in elongation complexes arrested at specific psoralen-DNA adduct sites as revealed by DNase I footprinting experiments.

DEDICATION

This work is dedicated to Theresa Ng.

ACKNOWLEDGEMENTS

I am deeply indebted to all my colleagues and friends, who not only made my life in this foreign culture so enjoyable but also helped me through my graduate career. The following list is in no way meant to cover all the people to whom I owe my thanks.

First of all, I'd like to thank my advisor John E. Hearst for his support, encouragement, and scientific guidance. During all these years in Berkeley, he showed me the way a scientist should be. While keeping me on the right track toward successful scientific research, he let me developed my own research interests. I also thank him and his wife, Jean, for all those memorable Thanksgiving and New Year parties.

I owe deep appreciation to George Cimino and Howard Gamper, with whom I worked most closely. I learned a lot of techniques and ideas from them and enjoyed all those fruitful discussions with them.

I am grateful to John Hubbard for helping me so much in using the computer systems and Steve Isaacs, Sam Lipson, and John Tessman for teaching me a lot of the laboratory techniques. I also want to thank them and others in the laboratory: Jason Kahn, Peter Spielmann, Suzanne Cheng, Enrique Dalmasso, Joe Monforte, Dae Yoon Chi, Martin Ferguson, Mark Gartenberg, Bethe Scalettar, Don Burke, Marie Alberti, Greg Armstrong, David Cook, David O'Brien, and Yu Sheng Zhu, for many stimulating discussions and their patience in correcting my bad scientific writings and English pronunciations. I also owe them thanks for helping me enjoy the American Culture.

People outside of the Hearst laboratory also deserve my thanks,

especially Joe Kao, Barbara Dengler, Helen Lok, David Koh, and Fareed Aboul-ela in the Tinoco laboratory and Aziz Sancar, Gwendolyn Sancar, Jack Griffith, and Bennett Van Houten at the University of North Carolina at Chapel Hill. All of them helped me in different aspects of my graduate career.

Special thanks go to Marian Malone, Kathy Mielke, Kathy Macbride, and Lisa Kona for technical and secretarial support.

Finally, I want to thank my parents, Gongjing Shi and Nanxiang Xing, for their long term support and encouragement.

TABLE OF CONTENTS

PART I

PHOTOCHEMISTRY OF PSORALEN-DNA ADDUCTS

CHAPTER I. WAVELENGTH DEPENDENCE FOR THE PHOTOREVERSAL OF A PSORALEN-DNA CROSSLINK

1. Introduction

Psoralens are a class of planar, three ring heterocyclic compounds (furocoumarins). The chemical properties of several natural and synthetic psoralens have been studied for over two decades (for reviews see: Song and Tapley, 1979, Parsons, 1980). These molecules have the ability to intercalate between the base pairs of a double helical nucleic acid (Isaacs et al, 1977, Isaacs et al, 1982). Upon exposure to long UV wavelength radiation (320-400 nm), a limited but well characterized set of covalent adducts are formed between psoralens and pyrimidine bases (Straub et al, 1981, Kanne et al, 1982). Covalent cyclo-addition occurs between the 5,6 double bond of pyrimidine bases and either the 3,4 double bond of a psoralen, which forms a "pyrone-side monoadduct or M_{Py}", or the 4',5' double bond of a psoralen, which yields a "furan-side monoadduct or M_{Fu}". Psoralens react primarily with thymidine in DNA and uridine in RNA, although a minor reaction with cytosine also occurs (Cimino et al, 1985). When a psoralen molecule is intercalated between adjacent pyrimidine bases on opposite strands of a double helical segment of DNA or RNA, a diadduct can be photochemically induced which covalently crosslinks the two nucleic acid strands. The formation of the diadduct is a polar reaction. The furan-side monoadduct must be formed initially. Continued irradiation of this monoadduct (320-380 nm) results in cycloaddition at the pyrone end of the psoralen if it is positioned in a crosslinkable

site (Kanne et al, 1982). Crosslinks and monoadducts are both photoreversable by exposure to shorter wavelength UV light (typically 254 nm). The structures of the adducts formed between thymidine and several psoralen derivatives have been determined by techniques such as mass spectroscopy, proton NMR, and X-ray crystallography (Straub et al., 1982; Kanne et al., 1982a, b; Peckler et al, 1982). A theoretical molecular structure of the diadduct in a DNA helix has recently been proposed (Pearlman et al, 1985). The structures of the adducts between the psoralen derivative HMT (4'-hydroxymethyl-4, 5', 8-trimethylpsoralen) and thymidine are shown in figure 1.

This thorough understanding of the chemistry and photochemistry of psoralens has resulted in their widespread use in the medical and biological fields. These compounds are used in the treatment of psoriasis and vitiligo (Fitspatrick, et al, 1982). Psoralens plus UV light (320-400 nm) have both lethal and mutagenic effect in cells (Fujita, 1984, Cassier et al, 1984), and form nucleic acid lesions that are recognized by repair systems (Ben-Hur and Song, 1984, Saffran and Cantor, 1984). Psoralens are also used widely as probes to study nucleic acid structure and function (for a review see Cimino et al, 1985). Procedures have been developed utilizing psoralens to map secondary and tertiary structure in large RNA molecules (Thompson et al, 1983). These procedures employ both the crosslinking and photoreversal reactions of psoralen molecules. Relatively little is known about the wavelength dependency of these photoreactions. Gasparro et al, 1984, have reported the action spectrum for the crosslinking of pBR322 DNA. They observed

Figure 1. Structures of HMT (4'-hydroxymethyl-4, 5', 8-trimethylpsoralen) and HMT-T (thymidine) photoproducts. M_{Fu}: HMT-T furan-side monoadduct; M_{Py}: HMT-T pyrone-side monoadduct; T-HMT-T: diadduct.

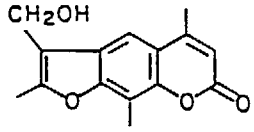

HMT

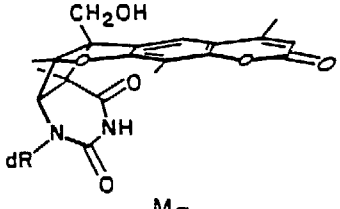

M_{Fu}

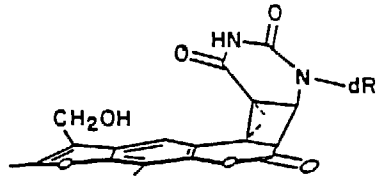

M_{Py}

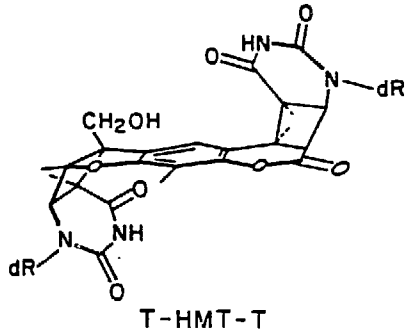

T-HMT-T

that the wavelength dependency for crosslink formation correlates with the absorption spectrum of the furan-side monoadduct.

In this chapter I report an action spectrum for the photoreversal of an isolated diadduct between HMT and thymidine (T-HMT-T) and an action spectrum for the photoreversal of the same T-HMT-T diadduct in the double-stranded Kpn I linker 5'-GGGTACCC-3' (a DNA-HMT crosslink). Some differences were observed which we interpret to be the result of the positioning of a diadduct in a nucleic acid helix. We also show that the formation of furan-side monoadduct and pyrone-side monoadduct from the photoreversal of a diadduct is dependent on the irradiation wavelength and the pH of the photoreversal solution. The incorporation of the diadduct into a DNA helix also has a dramatic effect on the formation of one monoadducted DNA vs. the other upon photoreversal. The results here have been published (Cimino et al., 1986).

2. Materials and Methods

A) Materials

HMT and [^{3}H]-HMT were gifts from HRI Associate Inc. (Berkeley, CA). The oligonucleotide, 5'-GGGTACCC-3' (Kpn I linker), was either purchased from New England Biolabs or synthesized on an automated DNA synthesizer (SAM ONE DNA Synthesizer, Biosearch). [γ-^{32}P]ATP was obtained from Amersham. T4 polynucleotide kinase was bought from Bethesda Research Laboratories. Poly(dAT), DNase II, bacterial alkaline phosphatase and phosphodiesterase II were from Sigma. Sephadex G-10 was purchased from Pharmacia Fine Chemicals. 1,10-Phenanthroline was bought from Aldrich Chemical Company, Inc. Potassium ferric oxalate was pur-

chased from ICN Pharmaceuticals, Inc. All the chemicals were used without further purification.

B) Irradiations

Broad-Band Irradiation. Samples were irradiated with the apparatus described in figure 2. Infrared radiation was removed by a water filter (9 cm) at position LF1. A aqueous solution of cobaltous nitrate (1.7% cobaltous nitrate, 2% sodium chloride, 9 cm pathlength) was placed at LF2, providing a band of light in the range of 320 nm to 380 nm (Hearst et al, 1984). A pyrex filter was required at position GF to prevent photodegradation of the cobaltous nitrate solution by short wavelength radiation. The intensity of the beam was measured with a Blackray Ultraviolet meter (Model No. J221, San Gabriel, CA). At the focal point, the beam had a diameter of 2.1 cm and a maximum intensity of 1 watt/cm^2.

Monochromatic Irradiation. Monochromatic light was selected as described in figure 2. The optical path contained only a water filter at position LF1. Position LF2 and GF were both unoccupied in order to pass short wavelength UV light. For irradiations above 313 nm, a pyrex filter was placed at the exit of the monochrometer. The band width for all monochromatic irradiations was maintained constant at 2.5 nm. Monochromatic radiation was continuously monitored with an in-line photodiode. This photodiode was calibrated by actinometry with $K_3Fe(C_2O_4)_3$ (de Mayo Shizuk, 1976). The amount of Fe^{2+} produced was determined by the absorption of the complex formed between Fe^{2+} and 1,10-phenanthroline at 510 nm. The maximum light intensity at 365 nm of

Figure 2. Schematic of the irradiation apparatus: The apparatus is designed to produce either high intensity monochromatic light or very high intensity broad-band light for preparative purposes. Light from an arc source (2.2kW Xe or 2.5kW Hg) is passed through a shutter (S) which is operated by an external clock. Broad-band radiation is selected by a combination of liquid filters (LF1 and LF2). Glass filters (GF) provide order sorting capacity when monochromatic light is desired, and are also used as cutoff filters. An iris diaphram (I) is used to adjust the intensity. Cuvettes, positioned at the intersection of axes B and C, can be exposed to either broad-band or monochromatic irradiation. When monochromatic radiation is desired, light enters the monochromator (Model CT-103, One-Meter Spectrometer, Interactive Technology, Los Gatos, CA) along axis A and emerges along axis A'. Mirror M1 deflects the monochromatic beam along axis B. A series of lenses focus the beam at the intersection of axes B and C. A photodiode (PD, Model HUV-4000B, EG and G Inc., Salem, Mass.), positioned behind a diffuser (Oriel UV diffuser 4812), continuously monitors the intensity of the beam. When broad-band radiation is desired, mirror M1 is removed and a second mirror (M2) is placed at the intersection of axis A and B. Mirror M2 deflects the beam from axis A to axis B. The beam is then focused onto the sample and monitored as described above. Mirror M2 can also deflect the beam perpendicular to the plane described by axis A and B. This capability permits irradiation of large volumes of solution, or cells attached to a flask or petri dish. The thermoregulated cuvette holder accepts a standard 1cm x 1cm cuvette or a 2.5 cm x 2.5 cm cuvette,

allowing volumes of up to 30 ml to be easily irradiated. The cuvette holder, which includes a magnetic stirrer, is mounted on a translatable rail. This holder is positioned at the intersection of axes B and C during irradiations. By translating the holder along axis C, a sample can be positioned in the optical beam of a Zeiss spectrometer. Any optical density changes that occur during irradiations are easily monitored without exposure to room light. This capability is desired when precise dosimetry is necessary. A viewing port along axis C in the side of the spectrometer box permits fluorescence measurements.

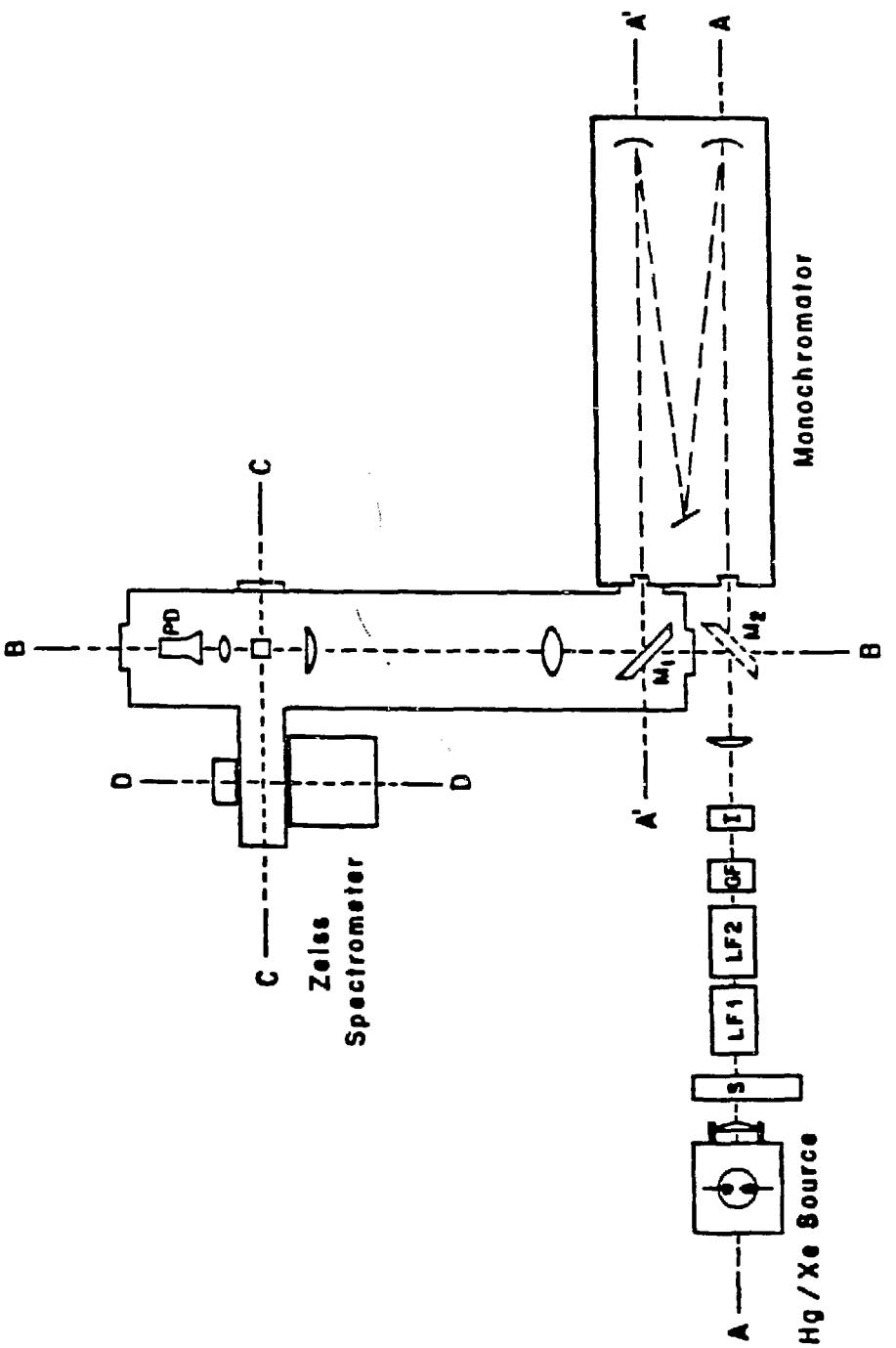
A'
A
Monochromator
C
B
PD
M1
M2
B
D
D
A'
T
OF
LF2
LF1
S
C
Zeiss
Spectrometer
A
Hg / Xe Source

this instrument with a 2.5 kilowatt Hg/Xe lamp is 10^{16} photons/second. The irradiation intensities used in the experiments varied between 10^{14} and 10^{16} photons/second.

C) Preparation of DNA-HMT Crosslink

25 µg Kpn I linker was 5'-end labelled with [γ-^{32}P]ATP and T4 polynucleotide kinase according to standard procedures (Maniatis et al, 1982). A solution (140 µl) containing the Kpn I linker, 0.9 mCi [γ-^{32}P]ATP (3000 Ci/mmole), 14 µl of 10X linker kinase buffer (700 mM TrisHCl, 100 mM $MgCl_2$, 50 mM dithiothreitol, pH 7.6), and 10 units of T4-Polynucleotide kinase was incubated at 37°C for 30 min. 10 additional units of the kinase were added to the solution which was then incubated for another 30 min. This reaction was subsequently chased with cold ATP by adding 21 µl of 10 mM ATP, 3 µl of 10X linker kinase buffer, 10 additional units of the kinase, and incubating again at 37°C for 30 min. Unreacted ATP was removed by chromatography on a Sephadex G-10 column, which was equilibrated with irradiation buffer (pH 7.6, 50 mM TrisHCl, 0.1 mM EDTA, 75 mM NaCl, 3 mM $MgCl_2$). 5 µl of 2.5 mM HMT in EtOH was then added to the labeled DNA solution (160 µl). This solution was irradiated for 3 min. at 4°C with broad-band light in a 1.5 ml Eppendorf tube. HMT addition and subsequent irradiation were repeated three times. Unreacted and photodamaged HMT were removed by extracting twice with chloroform-isoamyl alcohol (24:1 v/v) and twice with water-saturated ether. The DNA was then EtOH-precipitated, washed, and electrophoresed on a 20% polyacrylamide-7M urea gel (20 cm x 40 cm x 0.08 cm). The crosslink band was located by autoradiography, excised

and eluted from the gel into a solution of 50 mM NaCl, 1 mM EDTA solution. The crosslink was further purified by EtOH precipitation and dissolved in 200 µl TE buffer (PH 7.6, 10 mM TrisHCl, 1 mM EDTA), and stored at -20°C.

D) Preparation of HMT-Thymidine Diadduct

45 µl of [^{3}H]HMT solution (2.5 µg/µl in EtOH, 4.4 Ci/mmole) was added to 3 ml of 500 µg/ml poly(dAT) in 10 mM TrisHCl, 1 mM EDTA, pH 7.5, and the mixture was irradiated with broad-band light for 8 min. at 4°C. Another 45 µl of the concentrated HMT stock solution was added and the mixture was irradiated for an additional 8 min. The photoreacted poly(dAT) was purified by extracting twice with chloroform-isoamyl alcohol (24:1 v/v) twice with water-saturated ether, and then EtOH-precipitation. Finally, the precipitate was digested sequentially with DNAse II, phosphodiesterase II, and alkaline phosphatase as previously described (Kanne et al, 1982). The diadduct was isolated by adding the digest to a 10 mm x 25 cm reverse phase (C_{18}) HPLC column (Ultrasphere ODS, Altex-Beckman, Berkeley, CA.) and eluting with a linear 10 mM KH_2PO_4(pH 2.2)-CH_3OH gradient. The purified diadduct was vacuum dried, and dissolved back in a acetate buffer (150 mM NaOAc, 27 mM KH_2PO_4, PH5.0), and stored at -20°C.

E) Photoreversals

The DNA-HMT crosslink ($5x10^{-9}$ M) was photoreversed in a 1 cm pathlength quartz cuvette in 1/10 TE buffer (pH 7.5, 1 mM TrisHCl, 0.1 mM EDTA, ca 2 mM NaCl) at room temperature with monochromatic light. During photoreversal, the samples were continuously stirred under a N_2

atomsphere. After photoreversal, the samples were dried without heating in a speedvac concentrator (Savant Intrument Inc.), dissolved in 7 M urea, 0.05% bromophenol blue, and 0.05% xylene cyanol FF solution, and then electrophoresed on a 20% polyacrylamide-7M urea gel. Band positions of the crosslinked, monoadducted, and free oligonucleotides were located by autoradiography (Gamper et al, 1984), excised, and quantified by Cerenkov counting with a Beckman LS-230 liquid scintillation counter.

The HMT-thymidine diadduct ($1.3x10^{-7}$ M) was photoreversed with monochromatic light in a stirred cuvette in 20 mM NaOAc, 0.4 mM KH_2PO_4, pH 5.45 solution at room temperature. The photoreversed samples were run through the reverse phase HPLC column with a linear KH_2PO_4-CH_3OH gradient. The diadduct, monoadducts, and free HMT were identified by their retention time on the column as characterized by Kanne et al (1982a) and quantified by ^3H scintillation counting. The diadduct, furan-side monoadduct, pyrone-side monoadduct, and HMT eluted at fractions 29, 39, 50, and 55, respectively.

F) Analysis of the Photoreversal Kinetics

Under denaturing conditions complete photoreversal of the crosslink is a two step reaction (see figure 3). The initial photoreversal of a crosslink (XL) yields two distinct monoadducted oligonucleotides. An oligonucleotide with a furan-side monoadduct (M_{Fu}) is formed when photoreversal occurs at the pyrone end of the HMT, and an oligonucleotide with a pyrone-side monoadduct (M_{Py}) is formed when photoreversal occurs at the furan end of the HMT. The rate constants

Figure 3. A model for photoreversal of the diadduct or crosslink under conditions where free Kpn I linker is denatured.

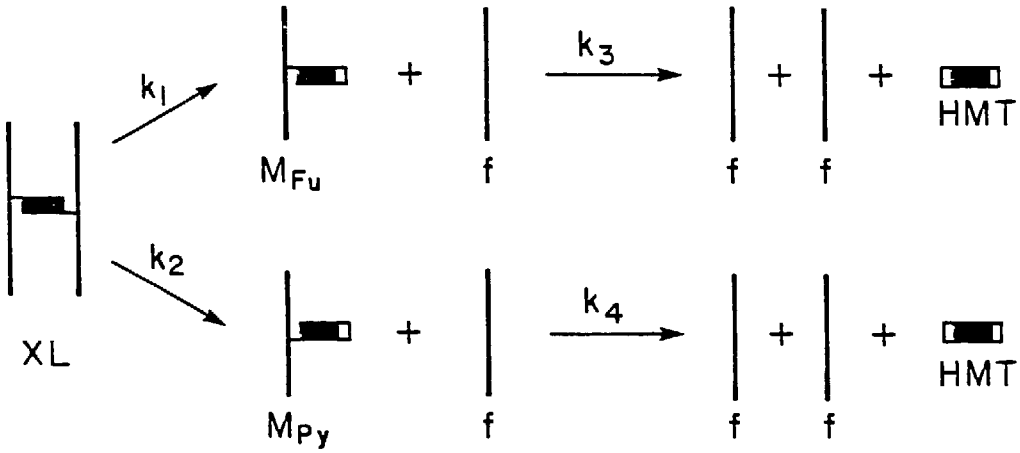
k1
k2
XL
MFu
MPy
f
k3
k4
HMT

for the two processes are k_1 and k_2, respectively. The second step is the photoreversal of the monoadducted oligonucleotides to produce free DNA (f) and free HMT. The rate equations for these reactions are:

$$dC/dt = -a[k_1 + k_2]C \quad (1)$$

$$dC_{Fu}/dt = ak_1C - ak_3C_{Fu} \quad (2)$$

$$dC_{Py}/dt = ak_2C - ak_4C_{Py} \quad (3)$$

$$dC_f/dt = a[k_1 + k_2]C + ak_3C_{Fu} + ak_4C_{Py} \quad (4)$$

where a is a constant that is defined as $a = I_0 l/VN_0$, in which V is the reaction volume (liters), N_0 is Avogadro's number, I_0 is the photon intensity (photons/sec.), and l is the path length (cm); C, C_{Fu}, C_{Py}, C_f are the concentrations in moles/liter of XL, M_{Fu}, M_{Py}, and f respectively; k_i (i = 1, 2, 3, 4) are the correspoding rate constants (liters/einstein cm).

The solutions to these equations at initial conditions: $C_f = C_{Fu} = C_{Py} = 0$, $C = C^0$, are,

$$C = C^0\exp[-a(k_1 + k_2)t] \quad (5)$$

$$C_{Fu} = \{k_1C^0/(k_1 + k_2 - k_3)\}\exp[-ak_3t] - \{k_1C^0/(k_1 + + k_2 - k_3)\}\exp[-a(k_1 + k_2)t] \quad (6)$$

$$C_{Py} = \{k_2C^0/(k_1 + k_2 - k_4)\}\exp[-ak_4t] - \{k_2C^0/(k_1 + + k_2 - k_4)\}\exp[-a(k_1 + k_2)t] \quad (7)$$

$$C_f = C^0\{1-\exp[-a(k_1 + k_2)]\} + \{k_2k_4C^0/[(k_1 + k_2)(k_1 + + k_2 - k_4)]\}\{\exp[-a(k_1 + k_2)t] - 1\} + + \{k_1C^0/(k_1 + k_2 - - k_3)\}\{1 - \exp[-ak_3t]\} + \{k_2C^0/(k_1 + k_2 - k_4)\}\{1 - - \exp[-ak_4t]\} + \{k_1k_3C^0/[(k_1 + k_2)(k_1 + k_2 - - k_3)]\}\{\exp[-a(k_1 + k_2)t] - 1\} \quad (8)$$

At low concentrations of the crosslink, the rate constants k_i (i = 1, 2, 3, 4) are related to the molecular properties of the reactant molecules in a simple manner:

$$k_i = 2.303\varepsilon_i\phi_i \qquad (9)$$

where ε_i and ϕ_i are the corresponding extinction coefficients (liters/mole·cm) and quantum yields (see Appendices at the end of the chapter).

When photoreversal is minimized such that the second step is negligible, the following equation holds true:

$$C_{Fu}/C_{Py} = k_1/k_2 \qquad (10)$$

The same analysis is also applicable to the diadduct photoreversal with replacements of free thymidine for free DNA as the meaning of f, monoadducts for monoadducted oligonucelotides as the meanings of M_{Fu} and M_{Py}, and diadduct for crosslink as the meaning of XL.

3. RESULTS

A) Identification of the Site of HMT Crosslinkage in DNA

There are two types of crosslinking sites in the double stranded Kpn I linker. These are T-HMT-T and T-HMT-C. In order to identify precisely the crosslinking site in the isolated crosslinked molecules, DNA-[^{3}H]HMT crosslink, generated as described in the method section, was digested to nucleosides by sequential treatment with DNAse II, phosphodiesterase II, and alkaline phosphatase. The digest was analyzed by HPLC eluting with the linear CH_3OH-KH_2PO_4 gradient. Almost all the ^{3}H counts eluted in the peak corresponding to T-HMT-T diadduct. The crosslinking site is, therefore, the thymidine base on each Kpn I link-

er of the crosslink. Monoadducts of HMT with cytidine were not observed in the digest. Monoadducts of HMT with thymidine were observed at a level of less than 3% of the total ^3H recovered, which were probably produced during the enzymatic digestions as a result of lengthy exposure to room and window lighting. These results are in agreement with those of Gamper et al (1984).

B) Photoreversal of the DNA-HMT Crosslink

The DNA-HMT crosslink was photoreversed under denaturing conditions by irradiating with monochromatic light. The photoreversal products were separated by polyacrylamide gel electrophoresis. An autoradiogram of a time course of the photoreversal is shown in figure 4. With increasing exposure, the concentration of the crosslink decreased as the concentrations of the free Kpn I linker and the monoadducted oligonucleotides increased. The band labelled as M' is tentatively identified as the pyrone-ring opened form of the pyrone-side monoadducted oligonucleotide. A detailed discussion of this band is given in a later section. In order to determine the concentrations of each product, the bands were excised and counted. Under the electrophoretic conditions used, the two types of monoadducted oligonucleotides M_{Fu} and M_{Py} were not resolved. Therefore, only the sum of $k_1 + k_2$ could be determined. These values were obtained by plotting $\ln(C^0/C)$ versus the irradiation dose. The plots of $\ln(C^0/C)$ vs. dose for the photoreversal at three wavelengths are shown in figure 5. The rate constant $k_1 + k_2$ was calculated from the slope of the straight lines. The experiments were repeated at different wavelengths from 240 nm to 365 nm. The final

Figure 4. Photoreversal of the crosslink at 296 nm. Sample C is a control which was exposed to 254 nm light from a low pressure 40 watt germicidal lamp (3 min. at a distance of about 6 cm). Sample 1 is a dark control. Samples 2, 3, 4, and 5, were photoreversed for 15, 75, 300, and 520 seconds, respectively. The light intensity was 3.80×10^{14} photons/second. V = 750 µl, l = 1 cm and pH = 7.5. XL is the crosslink band, M is the monoadducted DNA band, M′ is discussed in the text, 8-mer is the free Kpn I linker band.

C
2
1
xd
M
M'
8 mer

Figure 5. $\ln(C^0/C)$ vs irradiation dose for the photoreversal of the DNA-HMT crosslink at three different wavelengths: (——), photoreversal at 249 nm, I_0 = 1.85 x 10^{14} photons/second. (-------), photoreversal at 266 nm, I_0 = 2.68 x 10^{14} photons/second. (— —), photoreversal at 288 nm, I_0 = 3.80 x 10^{14} photons/second. V = 750 µl, l = 1 cm, and pH = 7.5.

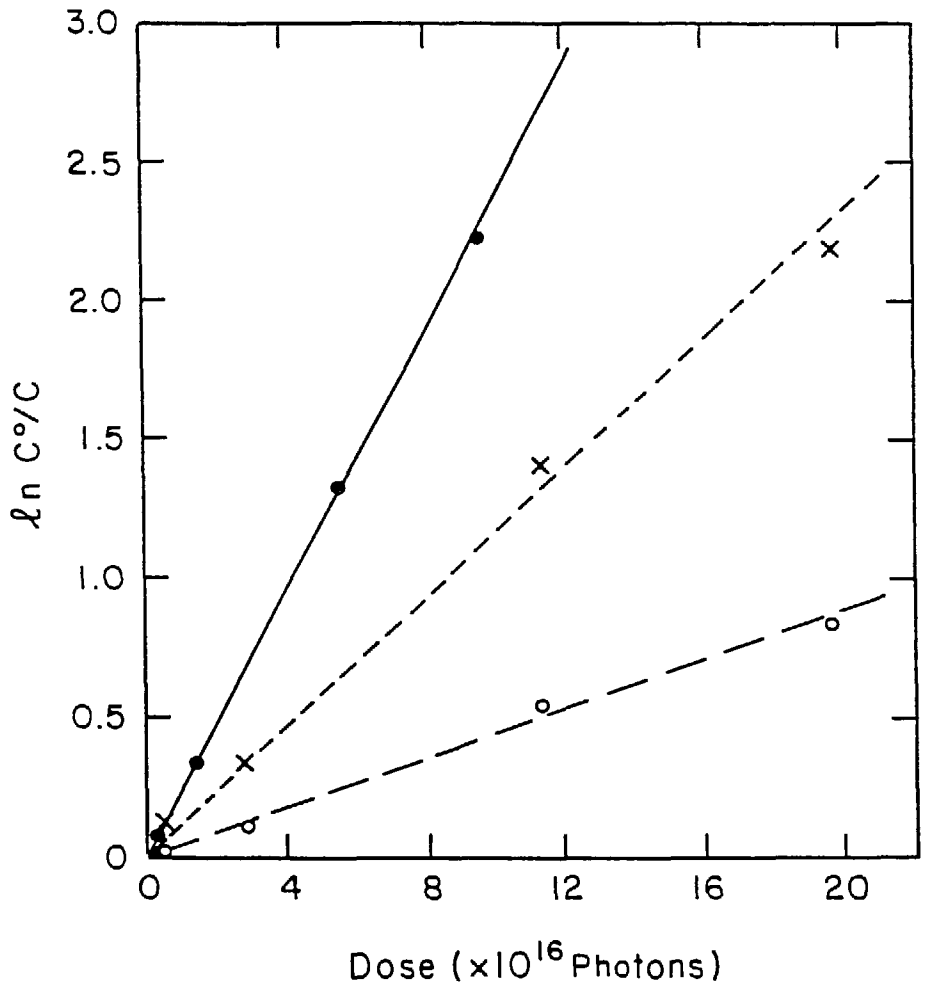
3.0
2.5
2.0
1.5
1.0
0.5
0
ℓn C°/C
0
4
8
12
16
20
Dose (×10^16 Photons)

results are shown in the action spectrum in figure 6. At $\lambda \geq 334$ nm, there is no detectable photoreversal.

The reciprocity of photoreversal was confirmed by exposing several identical samples to a constant dose (2.70×10^{16} photons) at 296 nm. The light intensity seen by each sample differed by up to a factor of four. The irradiation times were changed correspondingly to maintain the constant dose. All irradiated samples photoreversed to an identical extent. Thus under our experimental conditions, the photoreversal reaction is dependent only on the total irradiation dose and not on the light intensity. The initial photoreversal to give monoadducted oligonucleotides is a one photon process.

C) Photoreversal of T-HMT-T Diadduct

The T-HMT-T diadduct was photoreversed at pH 5.5. The products were analyzed by high performance liquid chromatography (HPLC). The amounts of diadduct, furan-side monoadduct, pyrone-side monoadduct, and free HMT were determined by ^3H scintillation counting. These data were analyzed similarly to the crosslink photoreversal data. The plots of $\ln(C^0/C)$ vs dose for the photoreversal at three wavelengths are shown in figure 7. The value of $k_1 + k_2$ is calculated from the slope of the line. The individual values of k_1 and k_2 can also be obtained from the sum of $k_1 + k_2$ and the use of equation (10). The experiments were repeated from 240 nm to 334 nm to obtain the action spectrum for the photoreversal of the diadduct. These results are also shown in figure 6. There is no detectable photoreversal at 334 nm.

The extinction spectrum of the diadduct was measured with a Cary

Figure 6. Action spectra for the photoreversal of the DNA-HMT crosslink and T-HMT-T diadduct. At 334 nm, $k_1 + k_2$ is equal to 0 for both the crosslink and diadduct.

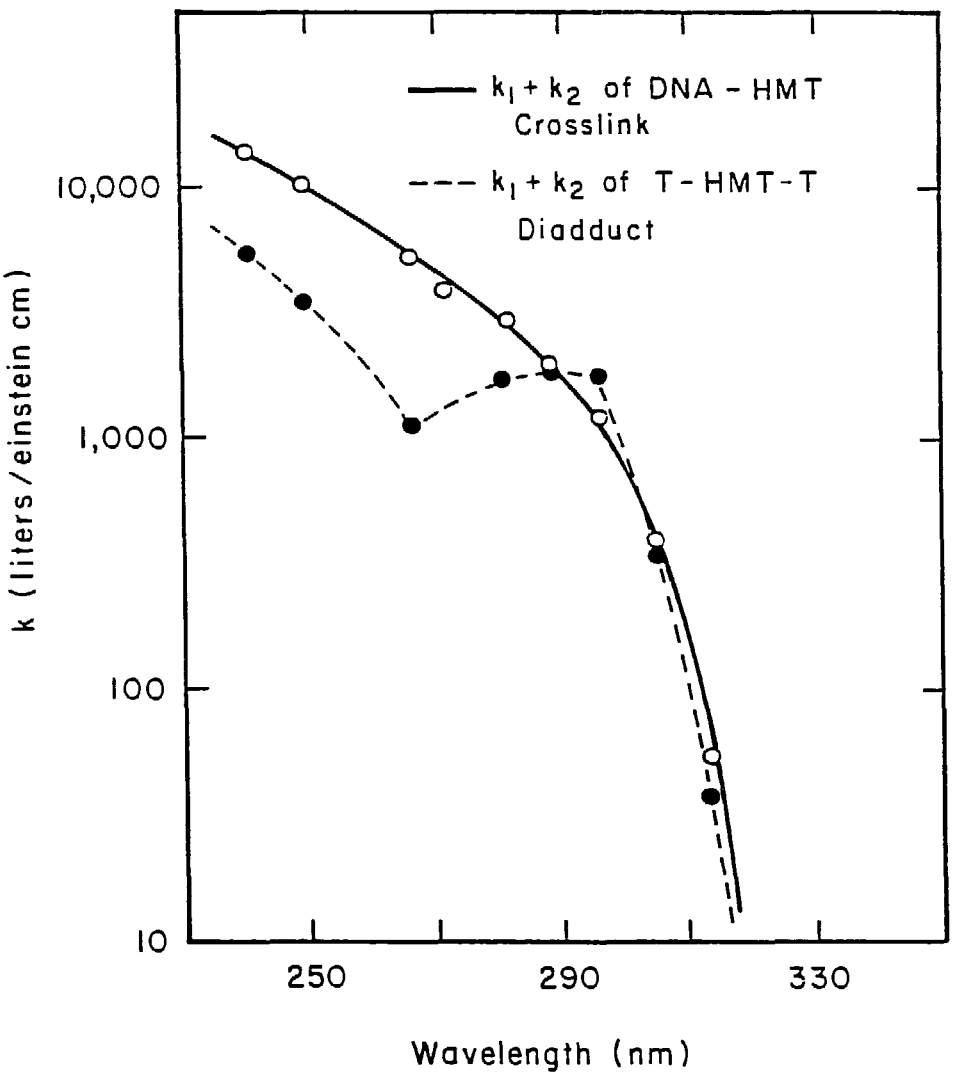
$k_1 + k_2$ of DNA - HMT Crosslink
$k_1 + k_2$ of T-HMT-T Diadduct
10,000
1,000
100
10
k (liters/einstein cm)
250
290
330
Wavelength (nm)

Figure 7. $\ln(C^0/C)$ vs irradiation dose for the photoreversal of the T-HMT-T diadduct at three different wavelengths. (——), photoreversal at 249 nm, I_0 = 2.70 x 10^{14} photons/second. (-------), photoreversal at 266 nm, I_0 = 1.08 x 10^{14} photons/second. (--- ---), photoreversal at 288 nm, I_0 = 2.42 x 10^{14} photons/second. V = 1500 µl, l = 1 cm, and pH = 5.5.

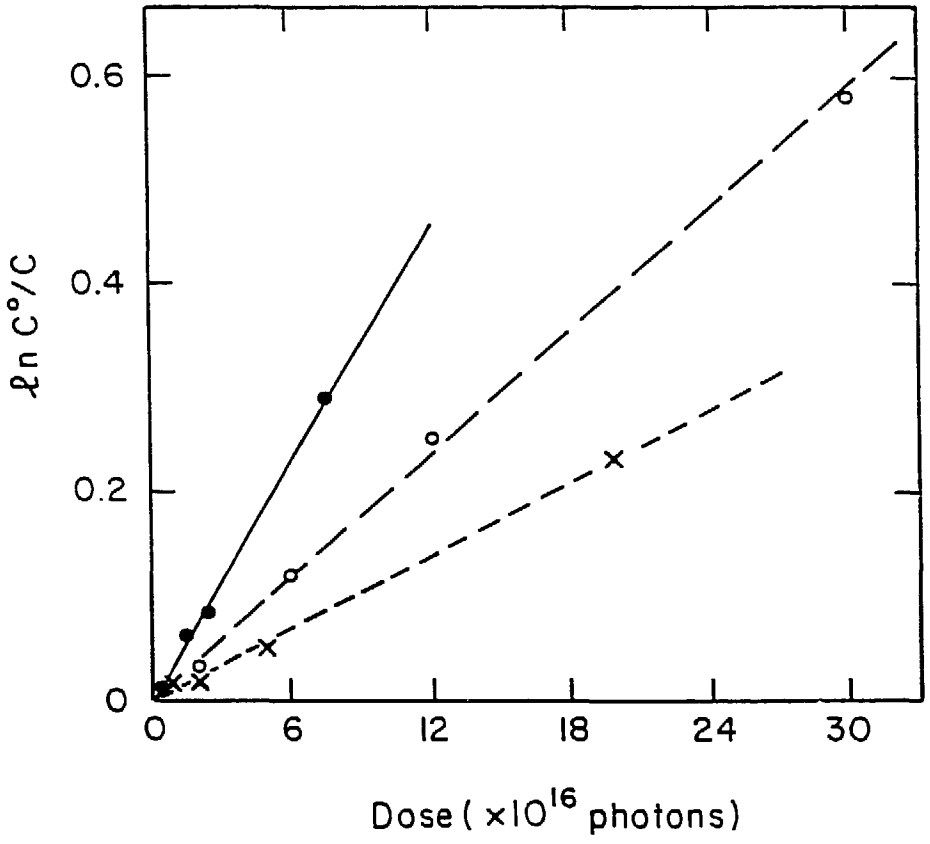
0.6
0.4
0.2
0
ℓn C°/C
0
6
12
18
24
30
Dose (×10^16 photons)

118 spectrophotometer in an acetate buffer (pH 5.5). It is plotted together with the action spectrum of the diadduct in figure 8. The extinction spectrum was determined by measuring the absorption spectrum of a sample of the HPLC purified diadduct on a Cary 118 spectrophotometer at room temperature. The concentration of this same sample of diadduct was then calculated by measuring the tritium decay from the [^{3}H]HMT in the diadduct. By use of the data in figure 8, the total quantum yield for the photoreversal of the diadduct can be estimated. The quantum yield is 0.16 ± 0.04 at wavelengths between 240 nm and 280 nm, and 0.30 ± 0.04 at wavelengths between 280 nm and 305 nm. These results indicate that two distinct absorption bands are contributing to photoreversal. For wavelengths below 280 nm, the major contribution is probably from excitation of the adducted pyrimidines. Above 280 nm, the benzene ring remaining in the adducted psoralen may be contributing to photoreversal.

D) Origin of M'

To investigate the origin of M', tritium labelled DNA-HMT crosslink was photoreversed by exposure to 254 nm light from a low pressure germicidal lamp and electrophoresed on a 20% polyacrylamide-7 M urea gel. In order to resolve the two types of monoadducted oligonucleotides, a thinner gel was used (0.4 mm compared to 0.8 mm previously used). An autoradiogram of the gel showed that in addition to the M' band, two distinct bands at the monoadducted oligonucleotide position could be resolved (for an example, see figure 9). These two bands were isolated, digested to nucleosides, and then analyzed by HPLC. The HPLC

Figure 8. The extinction spectrum and the action spectrum of the T-HMT-T diadduct. The absorption of the diadduct was measured with a Cary 118 spectrophotometer in a solution (pH 5.5) of 110 mM NaCAc, 25 mM Na_2HPO_4, and the concentration of the diadduct was determined by ^3H scintillation counting.

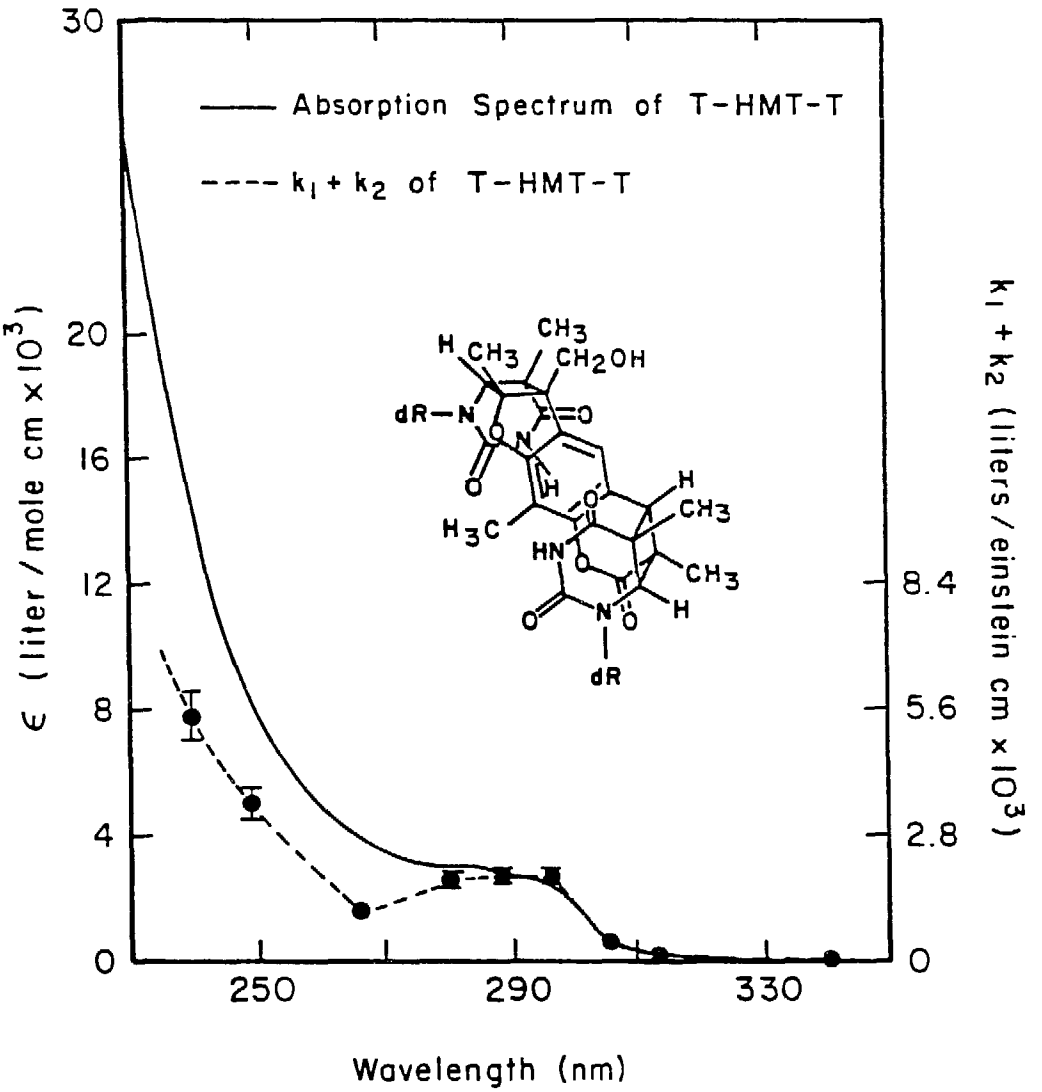
Absorption Spectrum of T-HMT-T
$k_1 + k_2$ of T-HMT-T
ϵ (liter / mole cm x 10^3)
$k_1 + k_2$ (liters / einstein cm x 10^3)
Wavelength (nm)
30
20
16
12
8
4
0
8.4
5.6
2.8
0
250
290
330
dR-N
dR
CH_3
CH_2OH
H_3C
HN
H

Figure 9. Acidic and basic incubation of the furan-side monoadducted DNA (M_{Fu}) and pyrone-side monoadducted DNA (M_{Py}). The starting material of the right lane of each pair is M_{Fu}, and that of the left lane is M_{Py}. C denotes starting materials before incubation. These samples were excised as single bands from a preparative gel, eluted at pH 7, 37°C, and kept at 4°C for several days before use. The sample set labelled pH = 10.0 was incubated at 60°C for two hours in 20 mM borate buffer, pH 10.0. The sample set labelled pH = 4.0 was incubated at 60°C for two hours in 20 mM succinate buffer, pH 4.0.

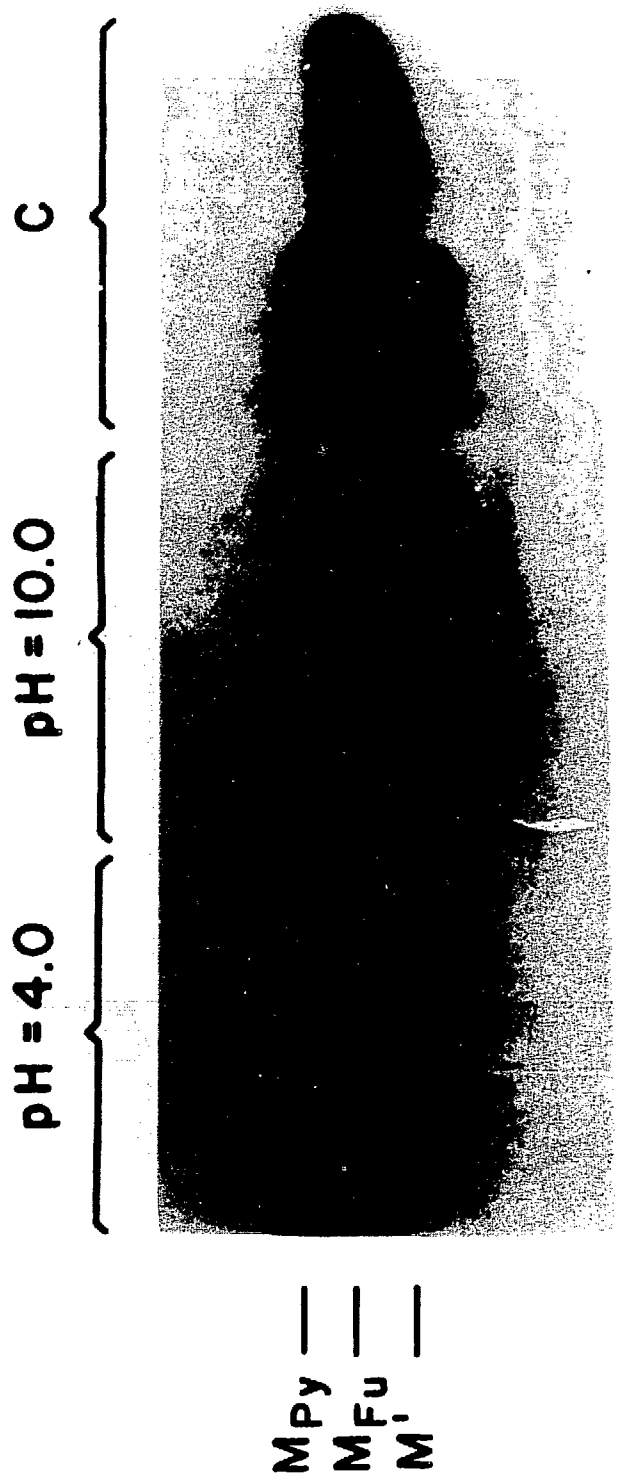
C
pH=10.0
pH=4.0
MPy
MFu
M'

results showed that the faster moving band, M_{Fu}, contained a furan-side monoadduct, and the slower moving band, M_{Py}, contained a pyrone-side monoadduct. The origin of M' was identified by incubating samples of M_{Fu} and M_{Py} in acidic and basic solutions at 60°C for two hours. These samples were then electrophoresed on a thin polyacrylamide gel. The autoradiogram of this gel shown in figure 9 indicates that M' and M_{Py} are interconvertable. There was no conversion between M' and M_{Fu}. It has been reported (Kanne et al, 1982) that the pyrone-ring of the diadduct can be opened in non-acidic solutions at positions 1 and 2 of the psoralen moiety to yield a carboxylic group. A pyrone-ring opened adduct in a DNA oligonucleotide would carry an additional negative charge on the carboxylic group at pH 8.5 during gel electrophoresis, and therefore, would migrate faster. Based on these results, it is concluded that M' is the pyrone-ring opened form of the pyrone-side monoadducted oligonucleotide. The nature of the resolution of the two types of monoadducted oligomucleotides, M_{Fu} and M_{Py}, under refined electrophoretic conditions is not understood at this time. Possible explanations include the differences in hydration and the differences in steric hindrance.

E) Factors Affecting Photoreversal at the Pyrone vs. Furan Ends of a Psoralen Diadduct or Crosslink

The initial photoreaction of a diadduct yields either a furan-side monoadduct or a pyrone-side monoadduct and free thymidine. Similarly the initial photoreversal of a crosslinked DNA produces either M_{Fu} or M_{Py} and a free strand of DNA. While collecting the data for the pho-

toreversal action spectrum of the diadduct, it was observed that photoreversal is not symmetric. Pyrone-side monoadduct is obtained in higher yield compared to furan-side monoadduct. Furthermore, it is also observed that the ratio of pyrone-side monoadduct to furan-side monoadduct varied with both the wavelength of incident light and the pH of the photoreversal solution. Consequently, the ratio of the rate of pyrone-side monoadduct production to the rate of furan-side monoadduct production (k_2/k_1) was examined further. Solutions of the diadduct at different pH (range from 2.2 to 8.0) were incubated at 37°C for one hour and then photoreversed. After photoreversal, the samples were brought back to pH 2.2 for 30 minutes to ensure ring closure of the pyrone-side adduct and the diadduct. These samples were then analyzed by HPLC. The ratio of k_2/k_1 was calculated according to equation(10) at several different wavelengths. In table 1, it is shown that k_2/k_1 varies with wavelength at pH 5.5 (20 mM NaOAc). The k_2/k_1 ratio at 249 nm is 2.5 compared to 4.5 for wavelengths above 280 nm. This result also supports the notion that there are two distinct photoreversal bands in the region of 240 nm to 313 nm. Both bands appear to preferentially effect photoreversal at the furan end of a diadduct. The longer wavelength band ($\lambda \geq 280$ nm) is about two times more effective in photoreversal at the furan end of the diadduct than the shorter wavelength band ($\lambda < 280$ nm). Similar k_2/k_1 ratios were obtained when photoreversal was done at pH 2.2 (10 mM KH_2PO_4, data not shown). The pyrone-ring of a pyrone-side monoadduct and diadduct are closed at pH 2.2. Since identical k_2/k_1 ratios were obtained at pH 2.2 and pH 5.5, it is believed

Table 1
k_2/k_1 Ratio for the Photoreversal of T-HMT-T Diadduct and DNA-HMT Crosslink

	pH	Wavelength (nm)		
		249	268	313
T-HMT-T Diadduct	5.5	2.5 ± 0.5	4.5 ± 0.9	4.5 ± 0.9
	7.5	2.5 ± 0.5	≥20	≥20
	8.0	2.8 ± 0.6	≥20	≥20
DNA-HMT Crosslink	7.5	0.42 ± 0.11	0.24 ± 0.07	0.28 ± 0.04
	10.0	0.68 ± 0.02	0.79 ± 0.05	1.2 ± 0.03
	12.0	6.3 ± 1.3	4.9 ± 1.0	4.7 ± 0.95

that only the closed form of the diadduct is present at pH 5.5. At pH 7.5 (1/10 TE) the k_2/k_1 ratio is greater than 20 at 288 nm and 313 nm. Further increase of pH to 8.0 (10 mM TrisHCl, 1 mM EDTA) did not change the ratio. Based on these observations, it is proposed that the pyrone-ring opened form of the diadduct is the predominant form at pH 7.5 or above and that the photoreversal of the pyrone-ring opened diadduct at the longer wavelengths (288 nm and 313 nm) yields only pyrone-side monoadduct because of the loss of the conjugation of the pyrone-ring to the benzene-ring. Prolonged irradiation at longer wavelengths did not produce free HMT at pH 7.5 or 8.0, suggesting the open form of a pyrone-side monoadduct is the terminal product of the photoreversal of a diadduct at these wavelengths. At 249 nm, however, the k_2/k_1 ratio does not change with pH. This suggests that the photoreversal at this wavelength is caused predominantly by the absorption of the remaining thymidine group in the diadduct, and consequently it is independent of the pyrone-ring opening.

Similar experiments were performed with the crosslink by electrophoresing with thin gel (0.4 mm) to resolve the two types of monoadducted oligonucleotides. The k_2/k_1 ratio was calculated according to equation (10) with the assumption that M' is the pyrone-ring opened form of the pyrone-side monoadducted DNA. At pH 7.5, the k_2/k_1 ratio is again wavelength dependent. In contrast to diadduct photoreversal, the crosslink photoreversal is preferentially at the pyrone end at all wavelengths. At this pH the k_2/k_1 ratios are slightly reduced at longer wavelengths. This is the reverse of that observed for the closed form

of the diadduct. Identical k_2/k_1 ratios were obtained for the crosslink at both pH 5.5 and 7.5 (data not shown). Consequently, it is assumed that the closed form of the crosslink is the only species at pH 7.5. These results imply that the DNA helix alters the chemistry of the photoreversal. A diadduct in a DNA helix would be expected to be more resistant to pyrone ring opening because of charge repulsion between the phosphates and the additional negative charge formed upon ring opening. Therefore, photoreversal at even higher pH was performed. Samples of crosslink solution at pH 10.0 (20 mM borate buffer) were incubated at 60°C for 2 hours and photoreversed. The samples were then acidified to ca pH 5, EtOH-precipitated with carrier t-RNA and analyzed by gel electrophoresis. Similar experiments were done at pH 12.0 (20 mM phosphate buffer) except that the crosslink solution was kept at room temperature for 4 hours instead of incubating at 60°C. Control samples showed that there is a negligible amount of damage to the crosslink at these high pH conditions. From the results in table 1, it is apparant that the k_2/k_1 ratio increases at all wavelengths as the pH of the photoreversal solution increases. Again it is consistent with the idea that photoreversal of the pyrone-ring opened form of the crosslink yields only the pyrone-side monoadducted DNA. In contrast to the diadduct photoreversal, the k_2/k_1 ratio for the crosslink photoreversal at 249 nm does increase when the pH increases. At these high pH different mechanisms may be contributing to the photoreversal of the crosslink compared to that of the diadduct.

4. DISCUSSION

A) Quantum Yield of the Diadduct Photoreversal

The extinction coefficient of the diadduct in figure 8 clearly shows that there are at least two absorption bands in the wavelength region between 240 nm to 350 nm. There is a pronounced absorption band that is centered at about 290 nm and a very large shoulder that continues to rise for wavelengths less than 270 nm. The action spectrum is also shown in figure 8 for comparison. The action spectrum is analogous in shape to the absorption spectrum of the diadduct. There is a peak in photoreversal at 290 nm and a shoulder that rises in parallel with the absorption spectrum at wavelengths less than 270 nm. Calculation of the quantum yield for photoreversal from the data of figure 8 also indicates that two distinct absorption bands contribute to photoreversal. Below 280 nm, the quantum yield is a constant value of 0.16 ± 0.04. Above 280 nm, the quantum yield is about twice as large (0.30 ± 0.04) and again appears to be constant within the wavelength region 289-313 nm. Thus, we conclude that photoreversal can be effected through two distinct absorption bands. In analogy with pyrimidine dimer photoreversal, it is likely that excitation of the adducted pyrimidines leads to photoreversal of the psoralen-pyrimidine diadducts, particularly at wavelengths below 280 nm. The quantum yield for photoreversal of a psoralen-pyrimidine diadduct in this wavelength region is much smaller than the quantum yield for photoreversal of a pyrimidine dimer, which is about unity (Deering and Setlow, 1963). Both electronic and steric factors may contribute to this difference in quantum yield.

B) Effects of Local Helical Structure and Adjacent Bases

The action spectra for photoreversal of the diadduct and crosslink are compared in figure 6. The wavelength dependence for the sum of the rate constants ($k_1 + k_2$) for both the diadduct and crosslink is almost identical at wavelengths above 290 nm. However, the crosslinked DNA photoreverses more efficiently at wavelengths between 240 nm and 290 nm than does the isolated diadduct. Several factors may contribute to this enhancement of the rates of photoreversal. The absorption spectrum of the diadduct may be different in a DNA helix compared to the free diadduct. It is not possible to measure the absorption spectrum of the diadduct in a helix because of hyperchromic effects of the adjacent DNA bases and the unknown deformation created by a diadduct in the helix. The photoreversal enhancement may also reflect a true quantum yield difference induced by increased strain of the cyclobutane bridges when the diadduct is incorporated into a helix. If this were contributing significantly, we would expect to see an equal enhancement at wavelengths above 290 nm. Since the photoreversal rate constants are about equal above 290 nm, we do not believe that we are observing an increase in quantum yield for a reversal reaction. A third source of photoreversal enhancement is energy migration from excited DNA bases to the diadduct. The shape of the difference of the two action spectra of figure 6 is similar to the absorption spectra of DNA. The wavelength dependence for the enhancement we have observed is consistent with absorption by DNA bases.

C) Selective Production of Monoadducts

Photoreversal of a diadduct or crosslink yields two types of monoadducts or monoadducted oligonucleotides. The data in table 1 show that the pyrone-side monoadduct is the major product of the diadduct photoreversal, whereas the furan-side monoadducted-oligonucleotide is the major product of the crosslink photoreversal. It is clear that the local structure of the DNA helix adjacent to a diadduct affects the photochemistry of the reversal reaction.

The selective production of monoadducts is highly dependent on the pH of the solution. From the results in table 1, we propose a mechanism for the photoreversal of both the diadduct and crosslink at high pH. This is shown in figure 10. At low pH, the pyrone-ring closed form of the diadduct or crosslink is predominant. The pyrone-ring of the adduct opens as the pH increases (figure 10), shifting the equilibrium to the open forms. Photoreversal of the pyrone-ring opened diadduct or crosslink at the pyrone-side is blocked because of the loss of the conjugation between the pyrone-ring and the benzene-ring. Consequently, only pyrone-side monoadduct or pyrone-side monoadducted DNA is produced upon photoreversal. The pyrone-side monoadduct or pyrone-side monoadducted DNA is resistant to further photoreversal for the same reason. There is, however, still a difference between the diadduct and the crosslink. At 249 nm, the ratio of k_2/k_1 for the diadduct is insensitive to the pH change, whereas this same ratio for the crosslink increases when the pH of the solution goes up. To explain this observation, we propose that the diadduct photoreversal at 249 nm is

Figure 10. Photoreversal of the pyrone-ring opened diadduct (or crosslink). T stands for free thymidine or DNA.

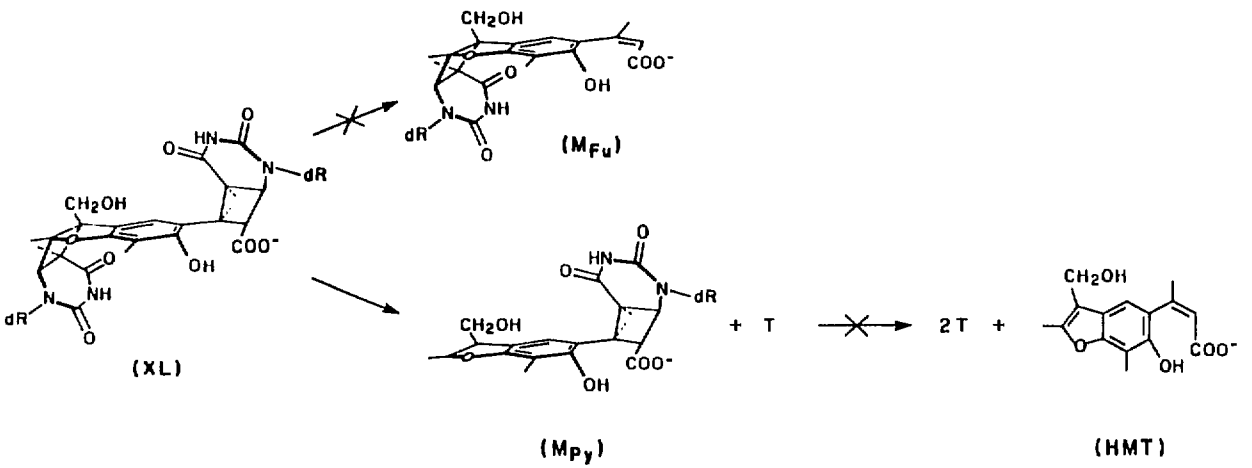
(XL)
(M$_{Fu}$)
(M$_{Py}$)
+ T
2T +
(HMT)

predominantly due to the absorption of the adducted thymidine group. Therefore, the ring opening has no effect on the k_2/k_1 ratio and on the further photoreversal of the monoadducts. On the other hand, it is possible that the photoreversal of the crosslink at 249 nm is caused in part by energy transfer from adjacent bases to the psoralen moiety of the crosslink. This is supported by the enhanced-photoreversal rate constant (k_1+k_2) at wavelengths below 290 nm for the crosslink compared to the isolated adduct. Consequently, photoreversal is still sensitive to the pyrone-ring opening, since photoreversal is effected through excitation of the benzene group of the parent psoralen.

The ability to selectively photoreverse one of the two cyclobutane rings of a crosslink in DNA might allow for the site-specific placement of a psoralen molecule within a large RNA or DNA. The site-specific placement procedure would be a three step process. First, a monoadducted oligonucleotide with a psoralen attached at a specific pyrimidine and in a specific orientation (either furan-side monoadduct or pyrone-side monoadduct) must be generated. An oligonucleotide with these characteristics can be easily obtained by following the procedures described in this paper. Second, the monoadducted oligonucleotide would be hybridized to its complement in a large DNA or RNA and subsequently crosslinked. The crosslinked complex would then be photoreversed under conditions which favor retention of the psoralen on the larger RNA or DNA molecule. The monoadducted RNA or DNA could then be used for secondary and tertiary structure analysis by re-irradiating to form intramolecular crosslinks site-specifically in the RNA or DNA.

If this latter goal is to be achieved, it would be best to start with a pyrone-side monoadducted oligonucleotide. The psoralen transferred to the larger RNA or DNA as a monoadduct would then be of the furan-side type, which is favored upon photoreversal and easily crosslinked by exposure to 320-400 nm light. The transfer procedure just described has two drawbacks. First, a pyrone-side monoadduct must be driven to crosslink. We have preliminary evidence which demonstrates that a pyrone-side monoadducted oligonucleotide is crosslinkable when it is irradiated (≥320 nm) in the presence of a suitable triplet sensitizer, such as triphenylene (G. Cimino and M. Gartenberg, unpublished observations). The second drawback is the exposure of the crosslinked oligonucleotide/DNA (or RNA) complex to photoreversal light. Since the action spectrum for photoreversal of a psoralen crosslink overlaps with nucleic acid absorption spectrum, there will certainly be some damage introduced into the larger DNA or RNA of the crosslinked complex. To estimate the potential damage created by a photoreversal step, we have calculated the crosssections for photoreversal (cm^2/base/quanta of photon, see equation 24 in the appendix). These are listed in table 2 along with the crosssections of several types of nucleic acid UV damage.

It is seen from table 2 that in both the bacteria and eucaryotic cells, the single strand breaks represent only a minor form of damage. (These cross sections cm^2/quanta base, were derived from the author's original data.) All the nucleic acid UV damage crosssections decrease faster than the photoreversal cross section of the crosslink as the

Table 2
Cross-Sections of DNA-HMT Crosslink Photoreversal and Nucleic Acid Photodamages (x 10^{-19} cm^2/quanta base)

Photochemical Event	Wavelength (nm) 240	254	266	280	290	302	313	Source
Photoreversal of DNA-HMT Crosslink	229	139	91.3	49.0	29.1	10.1	0.92	Data of Figure 5
Single-Strand Break Formation in Cells	1.2 x 10^{-4}	2.3 x 10^{-4}	3.2 x 10^{-4}	2.3 x 10^{-4}	1.0 x 10^{-4}	1.3 x 10^{-5}	3.1 x 10^{-6}	Rosenstein & Ducore, 1983
Single-Strand Break Formation in Bacteria		2.1 x 10^{-3}	9.2 x 10^{-4}	2.1 x 10^{-4}		2.0 x 10^{-5}	5.1 x 10^{-6}	Peak & Peak, 1982
T^T Dimer Formation in Poly dT	9.9	20	19	8.8				Deering & Setlow, 1963
U^U Dimer Formation in Poly rU	3.90	7.97	7.32	1.52	0.40			Pearson et al, 1966
U Hydrate Formation in Poly rU	1.49	3.65	4.12	1.44	0.20			Pearson et al, 1966
T^T Dimer Formation in cells		1.68	1.35	1.08	0.67	3.8 x 10^{-2}	6.8 x 10^{-4}	Rothman & Setlow, 1979

irradiation wavelength increases. Therefore, UV damage to nucleic acids can be minimized by photoreversing psoralen nucleic acid crosslinks at longer wavelengths, eg. 313 nm. Another kind of DNA damage that is not listed in the table is the formation of monomeric thymine ring saturation products. These products are as large as 73% of the thymidine dimer formed at 313 nm. Combining all the nucleic acid UV damage crosssections together (including monomeric thymine saturation products), it is estimated that photoreversing one crosslink at 313 nm will cause one photodamage per ca. 600 bases of nucleic acid. This level of damage can be tolerated when analyzing the secondary structure of an RNA molecule of the size of 23S rRNA or smaller.

5. Appendix: Kinetics of Photoreversal

The following analyses are concerned only with the DNA-HMT crosslink. The same treatments are also applicable to the diadduct.

a) Kinetic Equations of Crosslink

According to figure 2, the crosslink concentration change is

$$-dC/dt = \{\phi_1 I_0/VN_0\}\{1-\exp[-2.303\varepsilon Cl]\} + \{\phi_2 I_0/VN_0\}\{1 - \\ - \exp[-2.303\varepsilon Cl]\} \qquad (11)$$

where ϕ_1, ϕ_2 are the quantum yields of crosslink photoreversal to give furan-side monoadducted DNA and pyrone-side monoadducted DNA, respectively. The other terms are defined in the text.

Under conditions where $2.303\varepsilon Cl$ is much smaller than 1, equation (11) can be simplified to

$$-dC/dt = \{2.303\varepsilon\phi_1 + 2.303\varepsilon\phi_2\}CI_0 l/VN_0 \qquad (12)$$

Set $k_1 = 2.303\varepsilon\phi_1$, $k_2 = 2.303\varepsilon\phi_2$, $a = I_0 l/VN_0$. The above equation

is then identical to equation (1). Equations (2), (3), (4) are similarly obtained.

Set the initial concentrations of the crosslink, furan-side monoadducted DNA, pyrone-side monoadducted DNA, and free DNA, as C^0, C^0_{Fu}, C^0_{Py}, and C^0_f, respectively. The integration of equation (1) gives, then,

$$\ln[C^0/C] = a(k_1 + k_2)t \text{ or}$$

$$C = C^0\exp[-a(k_1 + k_2)t] \tag{13}$$

Substituting equation (13) into equations (2) and (3) gives

$$dC_{Fu}/dt = ak_1C^0\exp[-a(k_1 + k_2)] - ak_3C_{Fu} \tag{14}$$

$$dC_{Py}/dt = ak_2C^0\exp[-a(k_1 + k_2)] - ak_4C_{Py} \tag{15}$$

The solutions to these two equations are

$$C_{Fu} = \{k_1C^0/(k_1 + k_2 - k_3)\}\exp[-ak_3t] - \{k_1C^0/(k_1 + k_2 - k_3)\}\exp[-a(k_1 + k_2)t] + C^0_{Fu}\exp[-ak_3t] \tag{16}$$

$$C_{Py} = \{k_2C^0/(k_1 + k_2 - k_4)\}\exp[-ak_4t] - \{k_2C^0/(k_1 + k_2 - k_4)\}\exp[-a(k_1 + k_2)t] + C^0_{Py}\exp[-ak_4t] \tag{17}$$

Substituting equations (13), (16), and (17) into equation (4) gives

$$dC_f/dt = a(k_1 + k_2)C^0\exp[-a(k_1 + k_2)t] + ak_3C^0_{Fu}\exp[-ak_3t] + \{ak_3k_1C^0/(k_1 + k_2 - k_3)\}\exp[-ak_3t] - \{ak_3k_1C^0/(k_1 + k_2 - k_3)\}\exp[-a(k_1 + k_2)t] + ak_4C^0_{Py}\exp[-ak_4t] + \{ak_4k_2C^0/(k_1 + k_2 - k_4)\}\exp[-ak_4t] - \{ak_4k_2C^0/(k_1 + k_2 - k_4)\}\exp[-a(k_1 + k_2)t] \tag{18}$$

The solution to the above equation is

$$C_f = C^0_f + C^0\{1 - \exp[-a(k_1 + k_2)t]\} + C^0_{Fu}\{1 -$$

$$- \exp[-ak_3t]\} + \{k_1C^0/(k_1 + k_2 - k_3)\}\{1 - \exp[-ak_3t]\} + \{k_1k_3C^0/(k_1$$

$$+ k_2)(k_1 + k_2 - k_3)\}\{\exp[-a(k_1 + k_2)t] - 1\} + C^0_{Py}\{1 -$$

$$- \exp[-ak_4t]\} + \{k_2C^0/(k_1 + k_2 - k_4)\}\{1 - \exp[-ak_4t]\} + \{k_2k_2C^0/(k_1$$

$$+ k_2)(k_1 + k_2 - k_4)\}\{\exp[-a(k_1 + k_2)t] - 1\} \quad (19)$$

If the initial conditions are such that

$C^0_f = C^0_{Fu} = C^0_{Py} = 0$, then, equations (13), (16), (17), and (19) can be simplified to give equations (5), (6), (7), and (8), respectively.

b) Relationship between the Rate Constant $(k_1 + k_2)$ and the Reaction Cross Section $(\sigma_1 + \sigma_2)$ of the Crosslink

Substituting $a = I_0 l/VN_0$ back into equation (13) gives

$$C = C^0\exp[-(k_1 + k_2)I_0 lt/VN_0] \quad (20)$$

Set $D = I_0 tl/1000V$, which is the correspoding irradiation dose per unit area (photons/cm^2), then the above equation becomes

$$C = C^0\exp[-1000(k_1 + k_2)D/N_0] \quad (21)$$

By definition, the crosssections of the crosslink photoreversal to give furan-side monoadducted DNA and pyrone-side monoadducted DNA are, respectively,

$$\sigma_1 = 1000k_1/N_0 = 2303\phi_1\varepsilon/N_0 \quad (22)$$

$$\sigma_2 = 1000k_2/N_0 = 2303\phi_2\varepsilon/N_0 \quad (23)$$

and the total photoreversal cross section is

$$\sigma_1 + \sigma_2 = 1000(k_1 + k_2)/N_0 \quad (24)$$

CHAPTER II. WAVELENGTH DEPENDENCE FOR THE PHOTOREVERSAL OF PSORALEN-DNA MONOADDUCTS

1. Introduction

In the previous chapter, I reported the action spectra for the photoreversal of the T-HMT-T diadduct and the same diadduct in an HMT crosslinked double-stranded DNA oligonucleotide. We found that the photoreversal of the diadduct correlates with its absorption spectrum. The incorporation of the diadduct in a double-stranded DNA helix enhances the photoreversal below 290 nm where DNA bases absorb. In this chapter, I report the wavelength dependence for the photoreversal of T-HMT monoadducts (both M_{Fu} and M_{Py}) and the same monoadducts incorporated in a DNA oligonucleotide. We find that again the action spectra for the photoreversal of both M_{Fu} and M_{Py} are similar to the corresponding absorption spectra. The quantum yields for different absorption bands, however, are quite different. In the case of M_{Fu}, the incorporation of the monoadduct in DNA reduces the photoreversal rate constant at wavelengths above 285 nm. No effect was observed for the photoreversal of M_{Py} upon incorporating the monoadduct into the DNA oligonucleotide. In the following chapter, I will report the wavelength dependence for the photocrosslinking of the DNA-HMT monoadducts in the presence of a complementary oligonucleotide. The results in this chapter have been published (Shi and Hearst, 1986 and 1987a).

2. Materials and Methods

A) Materials

Oligonucleotides were synthesized on an automated DNA synthesizer

by the phosphotriester method (SAMONE DNA Synthesizer, Biosearch). After synthesis, the oligonucleotides were deprotected and purified by electrophoresis on a 20% polyacrylamide-7 M urea gel followed by EtOH precipitation. For the rest, see Chapter I.

B) Irradiations

The irradiation apparatus for both the broad-band (320-380 nm) and the monochromatic irradiations has been described in the previous chapter. The band width for all monochromatic irradiations was maintained constant at 2.5 nm. Monochromatic radiation was continuously monitored with an in-line photodiode, which was calibrated by actinometry with $K_3Fe(C_2O_4)_3$.

C) 5'-End Labelling of DNA oligonucleotides

Oligonucleotides with 5'-OH were labelled with [γ-^{32}P]ATP and T4 polynucleotide kinase and subsequently chased with cold ATP (Maniatis et al., 1982) The amount of enzyme in each aliquot used in the following experiments was approximately equal to the amount required to completely phosphorylate the 5'-end of the oligonucleotide, which was estimated based on the amount of DNA present, the incubation time (usually two to five hours), and the assumption that one unit of enzyme will kinase one nanomole of oligonucleotide in half an hour at 37°C. A 1X linker kinase buffer (70 mM Tris HCl, 10 mM $MgCl_2$, 5 mM dithiothreitol, pH 7.6) containing the oligonucleotide to be labelled, [γ-^{32}P]ATP, and an aliquot of kinase was incubated at 37°C for a few hours. The reaction was then chased by adding cold ATP to a final concentration of 1 mM, another aliquot of enzyme, 10X linker kinase buffer to maintain a

1X buffer concentration, and incubating at 37°C. To ensure complete kinasing, a third aliquot of kinase was added and the solution was incubated again at 37°C. The mixture was either used directly or EtOH precipitated (10 mM $MgCl_2$, 0.2 M NaCl, 2.5 v/v EtOH). After EtOH precipitation, the DNA was then dissolved in water or the appropriate buffer and stored at -20°C.

To label oligonucleotides with 5'-phosphate, the kinase exchange reaction was used (Maniatis et al., 1982). The kinase exchange solution (50 µl) containing ca. 3 µg oligonucleotide, 0.15-0.3 mCi [γ-^{32}P]ATP (3000 Ci/mmole), 5 µl 10X exchange reaction buffer (0.5 M imidazole chloride, 0.1 M $MgCl_2$, 50 mM dithiothreitol, 1 mM spermidine, 1 mM EDTA, pH 6.6), 3 µl 5 mM ADP, and 11 units of T4-polynucleotide kinase was incubated at 37°C for ca. 3 hours. The reaction was stopped with an EtOH precipitation at -20°C (10 mM $MgCl_2$, 0.2 M NaCl, 2.5 v/v EtOH). After the EtOH precipitation, the DNA was purified by 20% polyacrylamide-7 M urea gel electrophoresis. All the gels in this chapter had a 30:1 acrylamide to N, N'-methylene-bis-acrylamide ratio and were run in 1X TBE buffer (50 mM Tris base, 50 mM boric acid, 1 mM EDTA, pH 8.3).

D) Preparation of the Adducts

T-HMT monoadducts. T-[^{3}H]HMT-T diadduct was prepared from poly(dAT) and [^{3}H]HMT as described in the previous chapter. The diadduct (70 nanomole in 2.6 ml 9 mM KH_2PO_4, 40 mM NaOAc buffer, pH 5) was photoreversed at 249 nm for 40 min. (light intensity was 2.7 x 10^{14} photons/sec.). After photoreversal, the solution was concentrated in a speedvac concentrator (Savant Instrument Inc.) to 1.5 ml and adjusted

to pH 2. The photoreversal products were then isolated by loading the solution onto a 10 mm x 25 cm reverse phase (C_{18}) HPLC column (Ultrasphere ODS, Altex-Beckman, Berkeley, CA.) and eluting with a linear 10 mM KH_2PO_4 (pH 2.2)-CH_3OH gradient (Kanne, et al., 1982a; Cimino et al., 1986). The diadduct, furan-side monoadduct, pyrone-side monoadduct, and HMT eluted at 29, 39, 50, and 55 minutes, respectively. The purified adducts were then vacuum dried and redissolved back in an acetate buffer. About 3.5 nanomoles M_{Fu} (in 50 mM NaOAc, 19 mM KH_2PO_4, pH 5.0) and 9.5 nanomoles M_{Py} (in 40 mM NaOAc, 14 mM KH_2PO_4, pH 5.0) were thus obtained.

DNA-HMT Monoadducts. The HMT modified oligonucleotides used are 5'-GAAGCTACGAGC-3' (oligonucleotide A) with an HMT molecule attached to the thymidine residue as either a furan-side monoadduct or a pyrone-side monoadduct, i.e., 5'-GAAGC[T(HMT)$_{Fu}$]ACGAGC-3' (M_{Fu}-A) or 5'-GAAGC[T(HMT)$_{Py}$]ACGAGC-3' (M_{Py}-A), respectively. In order to make the desired monoadducted oligonucleotides, the HMT crosslinks between 5'-GAAGCTACGAGC-3' and 5'-TCGTAGCT-3' through the middle thymidines on each oligonucleotide were prepared first. 480 µl of kinasing mixture containing 500 µg of kinased oligoncleotide 5'-GAAGCTACGAGC-3' was adjusted to 150 mM NaCl and 10 mM $MgCl_2$. This solution was mixed with 1000 µl irradiation buffer (50 mM TrisHCl, 0.1 mM EDTA, 150 mM NaCl, and 10 mM $MgCl_2$, pH 7.6) containing 400 µg unkinased 5'-TCGTAGCT-3' and then split equally into four 1.5 ml Eppendorf tubes. HMT/EtOH stock solution was added to each tube to a final concentration of 1.2×10^{-4} M HMT and the mixture was irradiated with broad band light (320-380 nm)

for 3 minutes at 4°C. The HMT addition and subsequent irradiation were repeated once. The unreacted and UV damaged HMT were removed by chloroform and ether extractions. The DNA was then EtOH precipitated and electrophoresed on a 20% polyacrymide-7 M urea gel. It was found that during this procedure the oligonucleotide 5'-TCGTAGCT-3' was partially 5'-phosphorylated by the enzyme and ATP in the reaction mixture. A kinased DNA runs differently from its unkinased counterpart on a polyacrylamide gel because of the extra negative charge. Therefore, the two crosslinks (either the furan-end or the pyrone-end attached to 5'-GAAGCTACGAGC-3', see Identification of HMT-DNA Adducts in RESULTS) were not resolved on the gel. Instead, a single broad band, which contained the two crosslinks with either kinased or unkinased 5'-TCGTAGCT-3', was obtained. The crosslinks and unmodified oligonucleotides were isolated and purified as described above.

The crosslinks were photoreversed in order to generate the HMT monoadducted oligonucleotide 5'-GAAGCTACGAGC-3'. About 200 µg of the crosslinks was dissolved in 6 ml of H_2O and photoreversed in a pyrex dish (1 inch diameter) covered with Reynolds Film 910 to cut off light below 240 nm. The dish was placed 2.5 inches below a low pressure 40 watt germicidal lamp with an intensity of about 1.5 mW/cm^2 (estimated with a Black-ray Ultraviolet Meter, Model J-225, Short UV Meter, Ultra-Violet Products, Inc., San Gabriel, CA). The solution was divided into three 2 ml aliquots. Each aliquot was added to the dish and irradiated for 2.5 minutes with continous stirring. After photoreversal the adducts were vacuum dried in a speedvac concentrator and purified by

gel electrophoresis. The furan-side and pyrone-side monoadducted oligonucleotide 5'-GAAGCTACGAGC-3' (about 30 and 15 µg respectively) and the unmodified oligonucleotide 5'-GAAGCTACGAGC-3' were subjected to a second EtOH precipitation, washed with 70% EtOH, and finally dissolved in H_2O and kept refrigerated. The kinase exchange reaction described above was then used to label the DNA-HMT monoadducts, M_{Fu}-A and M_{Py}-A, before they were used.

E) Photoreversal of the Adducts

T-HMT Monoadducts. The photoreversals of the two monoadducts were conducted in a quartz cuvette of 1 cm pathlength at room temperature with monochromatic light. The solution was stirred and the cuvette was covered with Parafilm during irradiation. The furan-side monoadduct (83 nM) was photoreversed in 20 mM NaOAc, 0.4 mM KH_2PO_4, pH 5.0 and the pyrone-side monoadduct (88 nM) was photoreversed in 20 mM NaOAc, 0.1 mM KH_2PO_4, pH 5.0. After photoreversal, the samples were run through a reverse phase HPLC column with a linear 10 mM (pH 2.2) KH_2PO_4-CH_3OH gradient. The products were identified by their retention times on the column and quantified by ^3H scintillation counting.

DNA-HMT Monoadducts. Both the M_{Fu}-A and M_{Py}-A (2 nM) were photoreversed as above, but in 0.1 mM EDTA, pH 5.5. The photoreversed samples were dried in a Speedvac concentrator (Savant Instrument Inc.) without heating, dissolved in 5 M urea, 0.01% bromophenol blue, and 0.01% xylene cyanol FF loading buffer, and then electrophoresed on a 20% polyacrylamide-7 M urea gel (40 cm x 40 cm x 0.05 cm, 35 watts for 3-4 hours). Band positions of the monoadducted and unmodified oligonucleo-

tides were located by autoradiography. The bands were then excised and quantified by Cerenkov counting with a Beckman LS-230 liquid scintillation counter.

The photoreversal of the adducts is first order with respect to the adduct concentrations. The photoreversal kinetics at low adduct concentrations can be analyzed as described in Chapter I to obtain the following relations:

$$C = C^0 \exp[-kt I_3 l / V N_3] \quad (1)$$

$$k = 2.303 \varepsilon \phi \quad (2)$$

where k is the photoreversal rate constant (liters/einstein cm); I_3 is the light intensity (photons/second); V is the reaction volume (liters); N_3 is the Avogadro's number; l is the path length (cm); ε is the extinction coefficient of the adduct; ϕ is the quantum yield of photoreversal; C^0 and C are the concentrations (moles per liter, or M) of the adduct at time zero and at time t, respectively.

3. RESULTS

A) Identification of HMT-DNA Adducts

There are three types of HMT crosslinking sites in the double-stranded DNA formed between oligonucleotides 5'-GAAGCTACGAGC-3' and 5'-TCGTAGCT-3'. These are T-HMT-T, C-HMT-C, and T-HMT-C. Within each type of crosslink, there are two possible orientations of HMT with respect to the oligonucleotide 5'-GAAGCTACGAGC-3', i.e. with the attachment of either the furan-end or the pyrone-end of the HMT. In order to identify the crosslinking site, tritium labelled HMT-DNA crosslinks were prepared essentially as described above. In this pre-

paration, however, both oligonucleotides were 5'-end labelled with ^{32}P. After initial crosslinking and gel electrophoresis, two intense crosslink bands (XLA and XLB) were seen in the autoradiogram. The two crosslinks were isolated and purified. They were then photoreversed by exposure to 254 nm light from a low pressure germicidal lamp and electrophoresed on a 20% polyacrylamide-7 M urea gel. The autoradiogram of the gel is shown in figure 1. It is seen that a different pair of monoadducted oligonucleotides was produced from each of the two crosslinks (XLA and XLB). The crosslinks and monoadducted oligonucleotides were isolated and purified. They were then digested sequentially with DNase II, phosphodiesterase II, and alkaline phophatase (Kanne et al., 1982a) and the digests were analysed by HPLC (Cimino et al., 1986). The HPLC results of the two crosslinks showed that both XLA and XLB contain T-HMT-T diadducts. (Monoadducts, which were probably generated during the digestion, accounted for 5-15% of the ^{3}H.) Since there is only one possible T-HMT-T crosslinking site in the double-stranded DNA formed by the two oligonucleotides, XLA and XLB are HMT-DNA crosslinks formed through the middle thymidine on each oligonucleotide. Similarly it was shown that M_{Fu}-A and M_{Fu}-8mer (see figure 1) are furan-side monoadducted oligonucleotide 5'-GAAGCTACGAGC-3' and furan-side monoadducted oligonucleotide 5'-TCGTAGCT-3', respectively, with the HMT attached to the middle thymidine of each oligonucleotide and that M_{Py}-A and M_{Py}-8mer are the pyrone-side monoadducted counterparts. Thus in XLA HMT is attached to oligonucleotide 5'-GAAGCTACGAGC-3' through its pyrone-end and in XLB it is attached

Figure 1. Isolation and characterization of HMT-oligonucleotide photoadducts by 20% polyacrylamide-7 M urea gel electrophoresis. XLA and XLB were purified on a 20% polyacrylamide-7 M urea gel and then photoreversed as described in the text before applying to this gel. The abbreviations are as follows: 8mer, 5′-TCGTAGCT-3′; M_{Fu}-8mer, 5′-TCG[T(HMT)$_{Fu}$]AGCT-3′; M_{Py}-8mer, 5′-TCG[T(HMT)$_{Py}$]AGCT-3′; A, 5′-GAAGCTACGAGC-3′; M_{Fu}-A, 5′-GAAGC[T(HMT)$_{Fu}$]ACGAGC-3′; M_{Py}-A, 5′-GAAGC[T(HMT)$_{Py}$]ACGAGC-3′; XLA and XLB are HMT crosslinked molecules each containing one molecule of the 8mer and and one molecule of A.

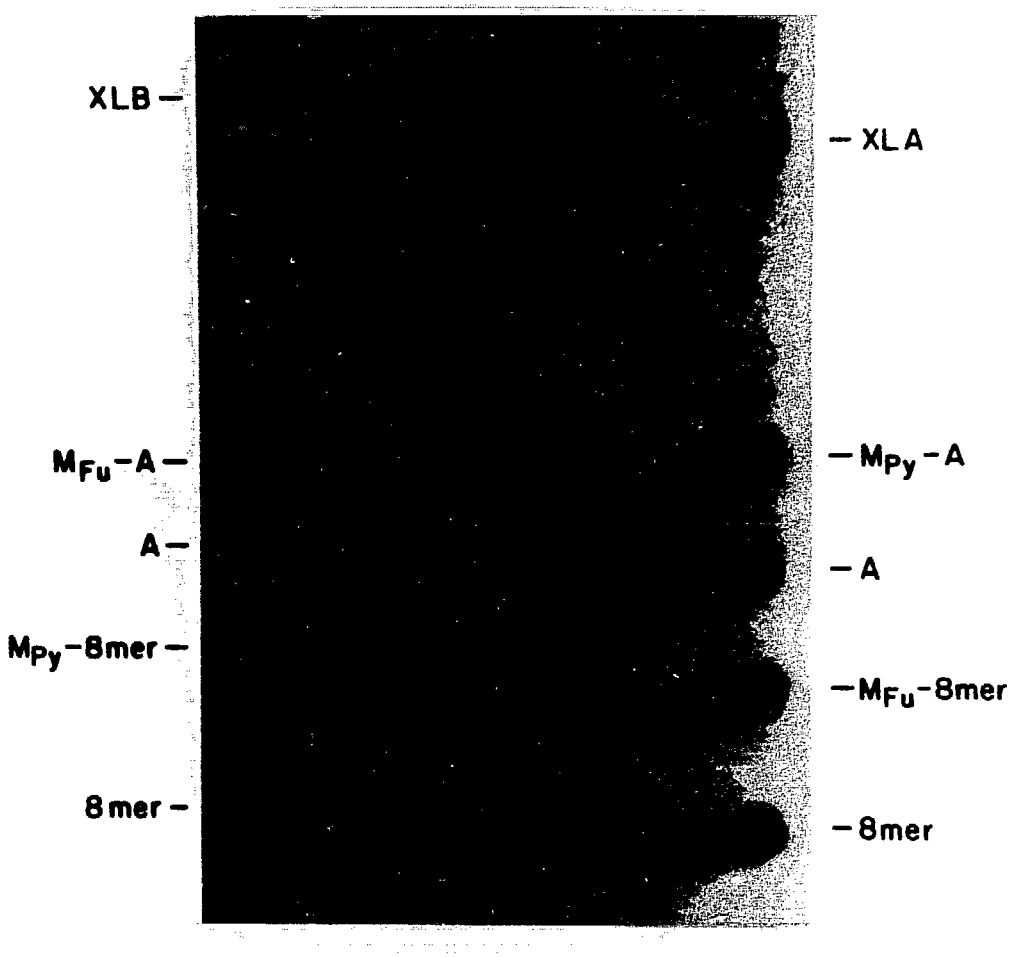
XLB
XLA
M_{Fu}-A
M_{Py}-A
A
A
M_{Py}-8mer
M_{Fu}-8mer
8mer
8mer

through its furan-end. M_{Fu}-A and M_{Py}-A can be then represented as 5'-GAAGC[T(HMT)$_{Fu}$]ACGAGC-3' and 5'-GAAGC[T(HMT)$_{Py}$]ACGAGC-3', respectively. The HMT molecule in each case is at the 3'-side of the thymidine.

B) Photoreversal of the T-HMT Monoadducts

The monoadduct was photoreversed at pH 5.0 and the products were analyzed by HPLC. The photoreversal of T-HMT monoadducts yields thymidine and parent HMT, which can be photo-damaged by UV irradiation. It is known that UV irradiation of aqueous solutions of HMT produces several damaged HMT compounds, including monomeric and dimeric products (Kao, 1984). Since we used T-[^{3}H]HMT, we could detect these damaged HMT compounds following the photoreversal of the monoadducts. In order to obtain the rate constant for the photoreversal of the monoadducts, the amounts of monoadducts remaining after photoreversal were determined by HPLC analysis and the data were analyzed according to equation (1). Figure 2 shows the plots of $\ln(C^0/C)$ vs. irradiation dose for the two monoadducts at three different wavelengths. The rate constant k was calculated from the slope of the lines. The experiments were repeated at different wavelengths from 240 nm to 380 nm to obtain the action spectra for the photoreversals. The action spectrum for the furan-side monoadduct is shown in figure 3. There is no detectible photoreversal at 380 nm. The action spectrum for the photoreversal of the pyrone-side monoadduct is shown in figure 4, the photoreversal extends only to ca. 314 nm.

It is known that psoralen adducts with saturated 3, 4-double bonds

Figure 2. $\ln(C^0/C)$ vs. irradiation dose for the photoreversal of the T-HMT monoadducts. V = 750 µl, l = 1 cm. (A). Photoreversal of T-HMT furan-side monoadduct. The light intensities at 287 nm, 295 nm, and 334.3 nm are 3.80×10^{14}, 1.56×10^{15}, and 1.65×10^{15} photons/second, respectively. (B). Photoreversal of T-HMT pyrone-side monoadduct. The light intensities at 240 nm, 265 nm, and 279 nm are 3.42×10^{14}, 6.1×10^{13}, and 3.62×10^{14} photons/second, respectively.

A

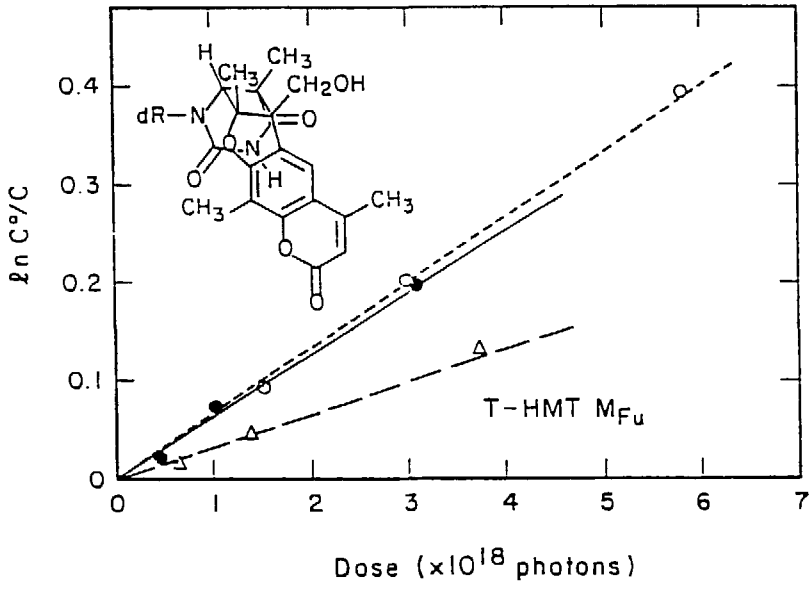
ℓn C°/C
0.4
0.3
0.2
0.1
0
0 1 2 3 4 5 6 7
Dose (x10^18 photons)
T-HMT M_Fu
dR—N
CH3
CH2OH
O
N
H

B.

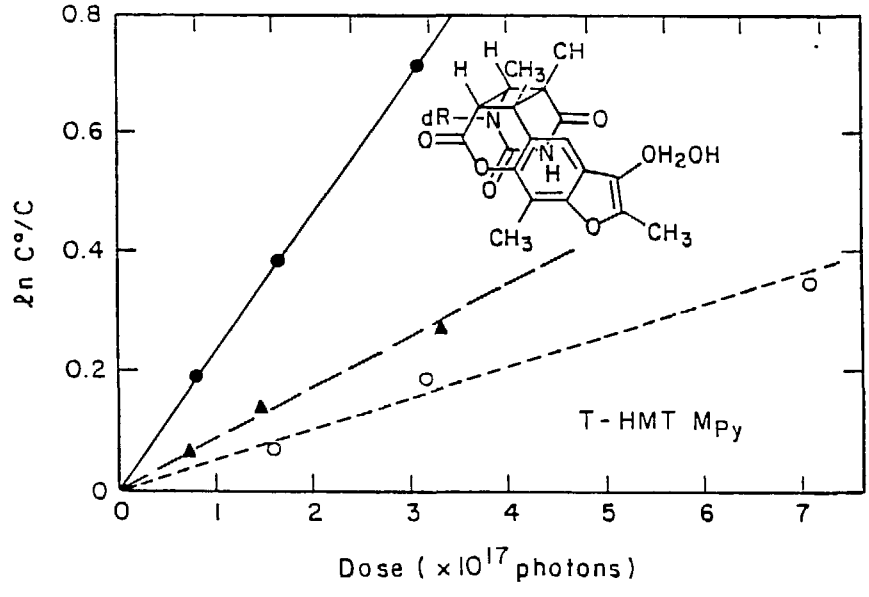
ℓn C°/C
0.8
0.6
0.4
0.2
0
0 1 2 3 4 5 6 7
Dose (x10^17 photons)
T-HMT M_Py
dR—N
CH
CH3
OH2OH
O
N
H

Figure 3. Action spectra for the photoreversal of the T-HMT and DNA-HMT furan-side monoadducts. M_{Fu}-A: see figure 1. At 380 nm, the rate constants for both adducts are 0.

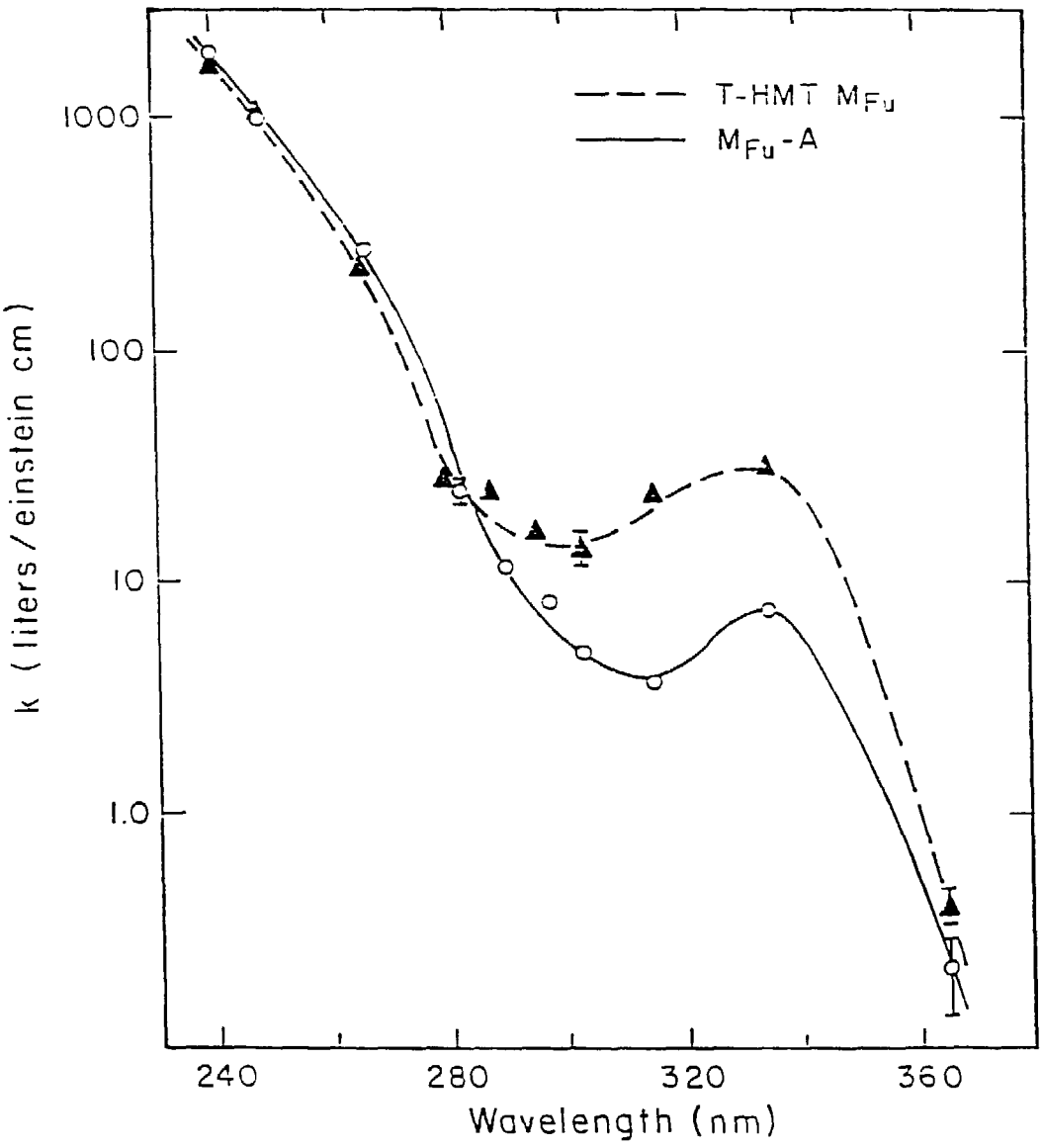
T-HMT M_{Fu}
M_{Fu}-A
1000
100
10
1.0
k (liters / einstein cm)
240
280
320
360
Wavelength (nm)

Figure 4. Action spectra for the photoreversal of the T-HMT and DNA-HMT pyrone-side monoadducts. M_{Py}-A: see figure 1. At 334 nm, the rate constants for both adducts are 0.

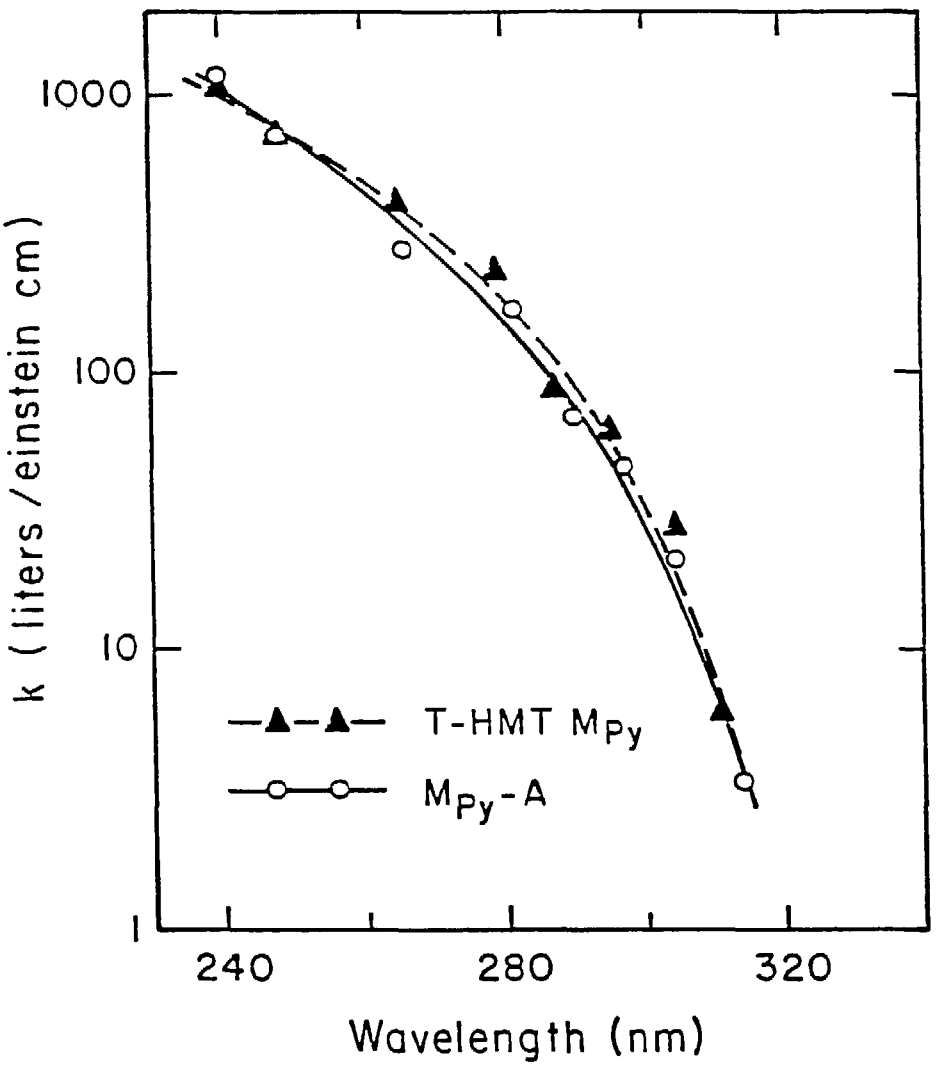
1000
100
10
1
k (liters / einstein cm)
240
280
320
Wavelength (nm)
T-HMT MPy
MPy-A

(in the pyrone-ring) can undergo pyrone-ring opening at high pH (Kanne, et al., 1982; Cimino et al., 1986). It was also observed that at under these conditions the photoreversal of the T-HMT-T diadduct and the same diadduct in a DNA-HMT crosslink is blocked at its pyrone end at wavelengths above 280 nm (see Chapter I). In order to ensure that only the pyrone-ring closed form of the pyrone-side monoadduct existed under the irradiation conditions, samples of the pyrone-side monoadduct in 10 mM KH_2PO_4, pH 2.2 were irradiated at 287 nm and the products were analyzed as described above. The results were identical to those obtained at pH 5.0. Therefore, it is concluded that the action spectrum in figure 4 is that for the pyrone-ring closed form of the monoadduct.

The quantum yield of photoreversal is related to the rate constant and the extinction coefficients of the monoadducts through equation (2). The extinction coefficients of the monoadducts were determined by measuring the absorption of the HPLC purified T-[^{3}H]HMT monoadducts of known concentrations, which were determined by ^{3}H scintillation counting, and the resulting extinction spectra are shown in figure 5. The quantum yield of the photoreversal of the monoadducts could then be calculated from the data in figures 3-5 and the results are plotted in figure 6. It can be seen that the action spectra of the photoreversal of the monoadducts correlate with their corresponding extinction spectra (figures 3-5). The quantum yields, however, are different for different absorption bands. In the case of the pyrone-side monoadduct, two absorption bands contribute to the photoreversal with a quantum yield of 2×10^{-2} at wavelengths below 250 nm and 7×10^{-3} at

Figure 5. Extinction spectra of the T-HMT monoadducts. The absorptions of the monoadducts were measured with a Cary 118 spectrophotometer at room temperature. T-[^{3}H]HMT furan-side monoadduct was in 50 mM NaOAc, 19 mM KH_2PO_4, pH 5.0 and T-[^{3}H]HMT pyrone-side monoadduct was in 50 mM NaOAc, 14 mM KH_2PO_4, pH 5.0. The concentrations of the adducts were determined by ^{3}H liquid scintillation counting.

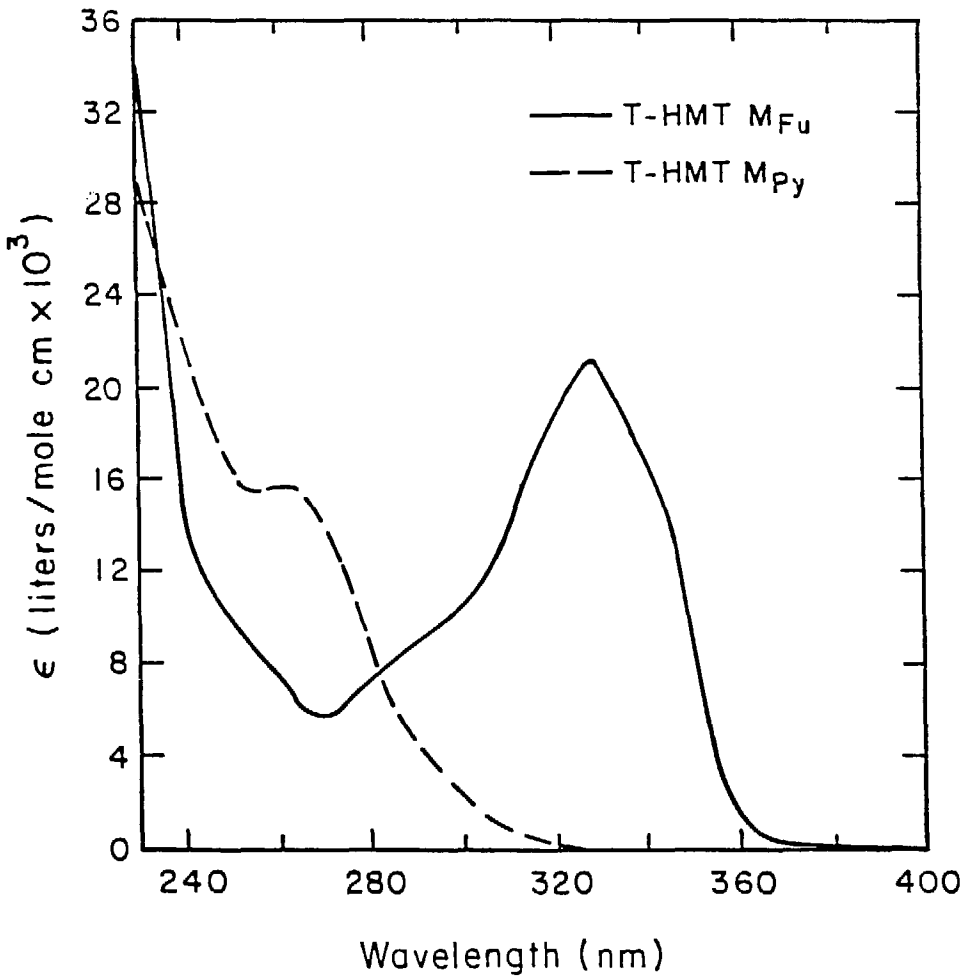
36
32
28
24
20
16
12
8
4
0
240
280
320
360
400
T-HMT M_{Fu}
T-HMT M_{Py}
ϵ (liters/mole cm x 10^3)
Wavelength (nm)

Figure 6. Quantum yields for the photoreversals of the T-HMT-T diadduct and the T-HMT monoadducts. The quantum yield for the photoreversal of the diadduct was estimated from the data of Chapter I.

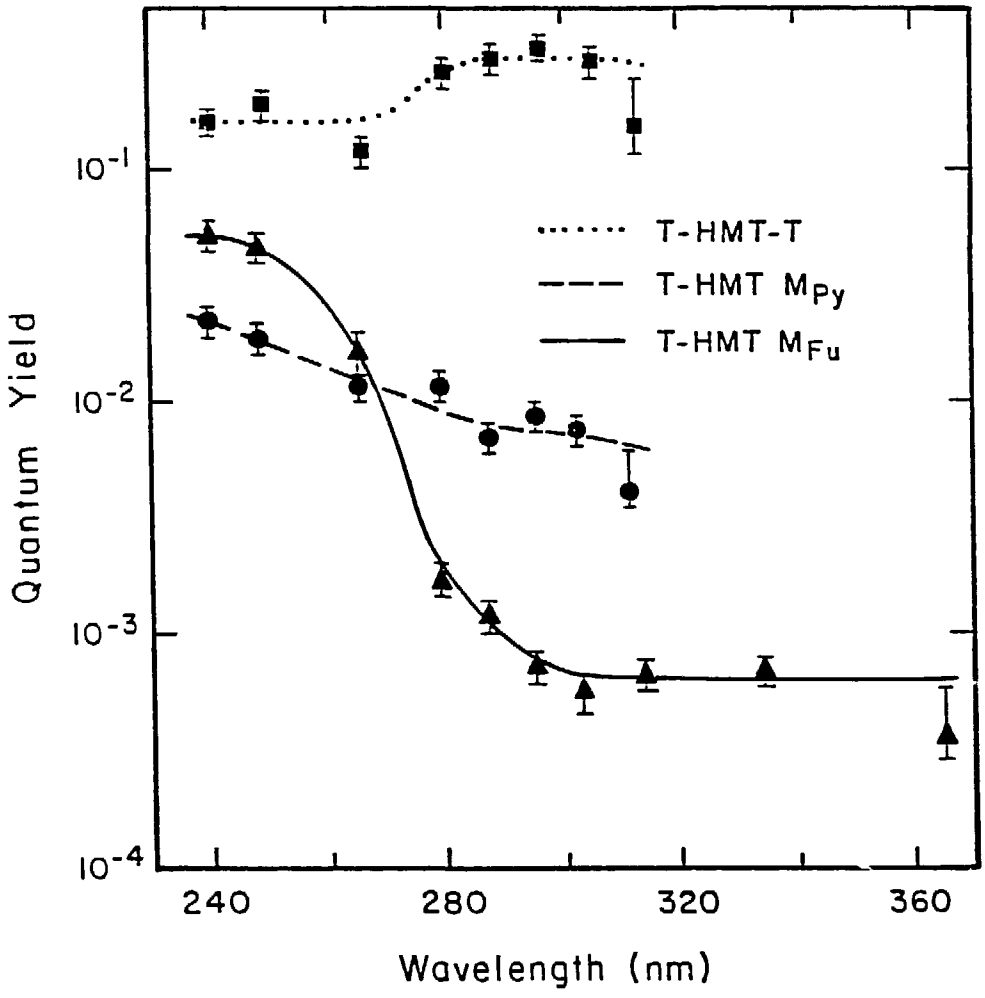
Quantum Yield
10^{-1}
10^{-2}
10^{-3}
10^{-4}
240
280
320
360
Wavelength (nm)
T-HMT-T
T-HMT M_{Py}
T-HMT M_{Fu}

wavelengths from 287 nm to 314 nm. For the furan-side monoadduct, at least three absorption bands contribute to the photoreversal. The quantum yield varies from 5×10^{-2} at wavelengths below 250 nm to 7×10^{-4} at wavelengths between 295 nm and 365 nm.

C) Photoreversal of DNA-HMT monoadducts

The 5'-end labelled single-stranded DNA-HMT monoadducts, M_{Fu}-A and M_{Py}-A, were photoreversed in 0.1 mM EDTA (pH 5.5) with monochromatic light. The products were analyzed by polyacrylamide gel electrophoresis. An autoradiogram of the time course of the photoreversal of M_{Fu}-A at 248 nm and 365 nm is shown in figure 7A. With increasing irradiation dose, the amount of M_{Fu}-A decreased and the amount of the photoreversal product(s) increased. At wavelengths below 314 nm the photoreversal yielded only the unmodified oligonucleotide A. At wavelengths above 314 nm, however, another photoproduct was also produced, as seen in the figure for the irradiation at 365 nm. The product has not been characterized, but we assume that it is some sort of damaged DNA, since irradiating the product (purified from the gel) at 254 nm did not change its mobility on the gel (data not shown), suggesting that it does not contain an HMT moiety. The damage must be due to the absortion of the HMT monoadduct or parent HMT generated during the irradiation because DNA bases do not absorb light above 314 nm. Since there are several absorption bands in the wavelength region (240-380 nm) for both the monoadducted HMT and the parent HMT, the photoreactions at different wavelengths could be quite different. Therefore, the unidentified photoproduct could be generated through either a one pho-

Figure 7. A) Photoreversal of M_{Fu}-A. V = 750 µl, l = 1 cm. M_{Fu}-A: see fugure 1; A = 5'-GAAGCTACGAGC-3'. Lanes 1-5: photoreversal at 365 nm; light intensity was 1.1 x 10^{16} photons/sec.; lane 1, the dark control; lane 2-5, samples exposed to 9.4 x 10^{19}, 1.42 x 10^{20}, 3.16 x 10^{20}, and 5.41 x 10^{20} photons, repectively. lanes 6-10: photoreversal at 248 nm; light intensity was 1.34 x 10^{15} photons/sec.; lane 6, the dark control; lanes 7-10, samples exposed to 8.0 x 10^{16}, 1.60 x 10^{17}, 3.20 x 10^{17}, and 6.40 x 10^{17} photons, respectively. B) Photoreversal of M_{Py}-A. V = 750 µl, l = 1 cm. M_{Py}-A: see figure 1; A: see figure 7. Lane 1, dark control; lanes 2-5, samples exposed to 9.0 x 10^{17}, 1.81 x 10^{18}, 3.60 x 10^{18}, and 7.0 x 10^{18} photons at 302.7 nm, respectively (Light intensity was 7.5 x 10^{15} photons/sec.); lanes 6-9, samples exposed to 7.2 x 10^{16}, 1.34 x 10^{17}, 2.57 x 10^{17}, and 6.9 x 10^{17} photons at 266 nm, respectively (Light intensity was 1.72 x 10^{14} photons/sec.).

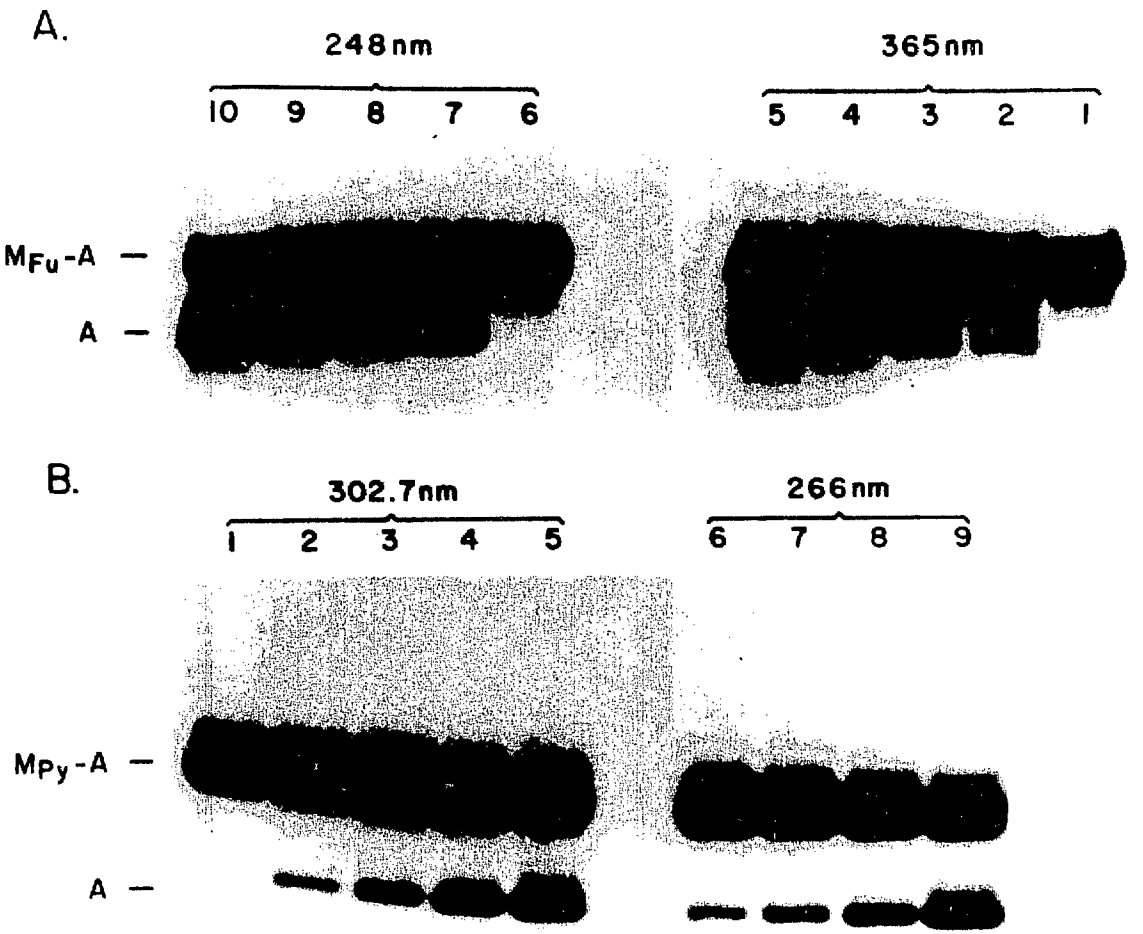
A.
248nm
10 9 8 7 6
365nm
5 4 3 2 1
M_{Fu}-A
A
B.
302.7nm
1 2 3 4 5
266nm
6 7 8 9
M_{Py}-A
A

ton process or a two photon process. In the first case, the excited HMT moiety causes DNA damage upon leaving the DNA. In the second case, the monoadduct is photoreversed first and the parent HMT thus generated acts as a DNA sensitizer, thereby causing damage. No attempt has been made to distinguish between these possibilities.

Figure 7B shows an autoradiogram of the time course of the photoreversal of M_{Py}-A at 266 nm and 302.7 nm. Again, with increasing irradiation dose the photoreversal product(s) increased and M_{Py}-A decreased (this is not easily visible in the figure due to over-exposure of the film). The band moving slower than M_{Py}-A is a damaged product generated during the storage of M_{Py}-A and constituted a few percent of the total ^{32}P counts. Also seen in the figure are products other than the unmodified oligonucleotide A. The amounts of these damaged products varied with wavelength and more damaged products were generated at shorter wavelength. We did not identify these products.

The photoreversal data were analyzed by determining the amount of DNA-HMT monoadducts remaining after photoreversal. This was done by excising the bands and quantifying them by ^{32}P Cerenkov counting. The data were then plotted according to equation (1). The plots of $\ln(C^0/C)$ vs. irradiation dose at three different wavelengths for M_{Fu}-A and M_{Py}-A are shown in figure 8. The photoreversal rate constants were determined from plots such as these. The experiments were repeated at different wavelengths from 240 nm to 380 nm to obtain the action spectra for the photoreversals. Again no photoreversal was detected at 334 nm for M_{Py}-A and at 380 nm for M_{Fu}-A. The action spectra for M_{Fu}-A and M_{Py}-A are

Figure 8. $\ln(C^0/C)$ vs. irradiation dose for the photoreversal of the DNA-HMT monoadducts. V = 750 µl, l = 1 cm. (A). Photoreversal of M_{Fu}-A. The light intensities at 289.5 nm, 297 nm, and 334.3 nm were 3.91 x 10^{15}, 5.76 x 10^{15}, and 1.88 x 10^{15} photons/second, respectively. (B). Photoreversal of M_{Py}-A. The light intensities at 240 nm, 266 nm, and 291.7 nm were 3.57 x 10^{14}, 1.72 x 10^{14}, and 1.72 x 10^{15} photones/sec., respectively.

A.

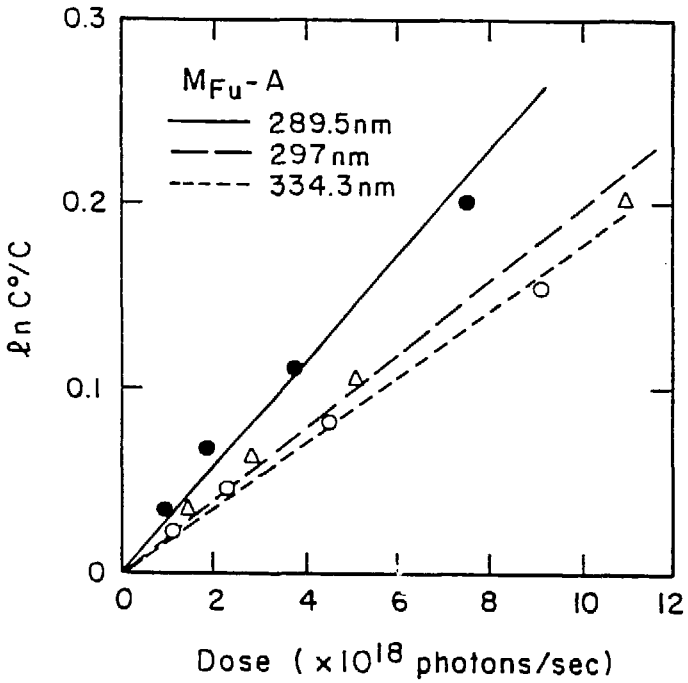
M_{Fu}-A
289.5nm
297nm
334.3nm
ℓn C°/C
0.3
0.2
0.1
0
0
2
4
6
8
10
12
Dose (x 10^{18} photons/sec)

B.

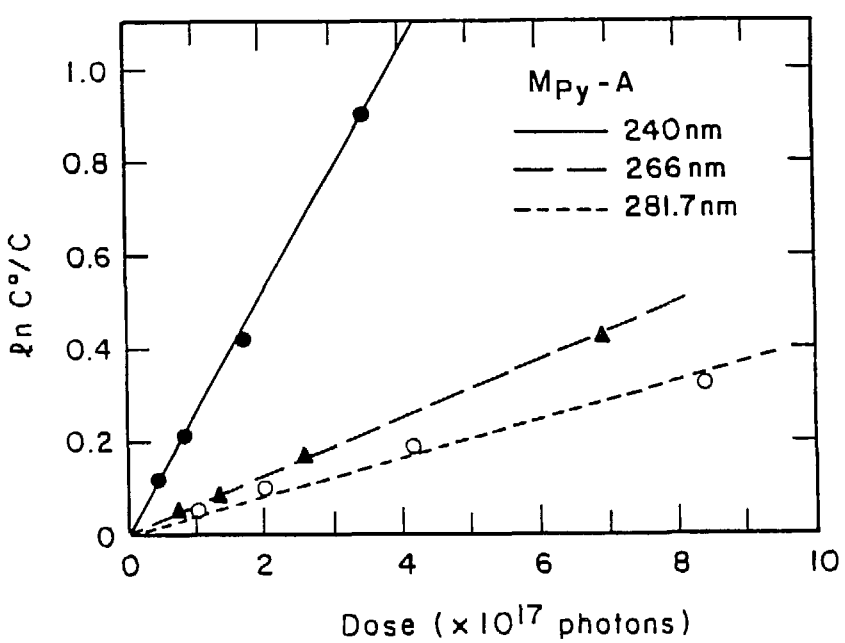
M_{Py}-A
240nm
266nm
281.7nm
ℓn C°/C
1.0
0.8
0.6
0.4
0.2
0
0
2
4
6
8
10
Dose (x 10^{17} photons)

shown in figures 3 and 4 respectively. Compared to the action spectra for the photoreversal of T-HMT monoadducts, it can be seen that the incorporation of the T-HMT pyrone-side monoadduct into the oligonucleotide has little effect upon the photoreversal rate constant. However, the incorporation of the T-HMT furan-side monoadduct into the oligonucleotide reduces the photoreversal rate constant at wavelengths above 285 nm. Below this wavelength the photoreversal rate constant is identical for the T-HMT and DNA-HMT furan-side monoadducts.

The reciprocity of the photoreversal of the M_{Fu}-A was confirmed by exposing identical samples to a constant light dose (5.1×10^{18} photons) at 297 nm. The light intensity seen by each sample was varied by three fold. The irradiation times were varied correspondingly to maintain the constant dose. All irradiated samples photoreversed to an identical extent. Thus under our irradiation conditions, the photoreversal is dependent only on the total irradiation dose and independent of the light intensity. The reaction is, therefore, a one photon process. Similar experiments were done for the photoreversal of M_{Py}-A. Again it was found that the photoreversal was a one photon process.

4. DISCUSSION

A) Quantum Yield of the Photoreversal of the T-HMT Monoadducts

As shown in figure 5, in the wavelength region from 240 nm to 380 nm there are at least three absorption bands for T-HMT furan-side monoadduct and two absorption bands for T-HMT pyrone-side monoadduct. The action spectra for the monoadducts in figures 3 and 4 are clearly similar in shape to the extinction spectra of the corresponding monoad-

ducts. The quantum yields (Figure 6) are different for different absorption bands. For the pyrone-side monoadduct, the photoreversal in the shorter wavelength band is about three times more efficient than the photoreversal in the longer wavelength band. The quantum yield is 2 x 10^{-2} below 250 nm and 7 x 10^{-3} from 287 nm to 314 nm. In the case of the furan-side monoadduct, the quantum yields for different absorption bands differ by up to factor of 70. The quantum yield at wavelengths below 250 nm is 5 x 10^{-2}, wheareas at wavelengths between 295 nm and 365 nm it is only 7 x 10^{-4}.

Also shown in figure 6 is the quantum yield for the photoreversal of T-HMT-T diadduct, which was estimated from the data in Chapter I. It is apparent that the photoreversal of the diadduct is much more efficient than those of the monoadducts at all wavelengths where the diadduct absorbs. This indicates that the electronic properties and/or steric constraints are quite different for the diadduct and the monoadducts. It is known that thymidine dimers can be photoreversed at wavelengths below 260 nm with a quantum yield of about unity (Deering and Setlow, 1963). Therefore, the absorption of the thymidine moieties in the monoadducts can also contribute to the photoreversal of the monoadducts. It has been proposed that the photoreversal of the diadduct below 260 nm is predominantly through the absorption of the thymidine moieties in the diadduct (Chapter I). If this is also true for the photoreversal of the monoadducts, then it is easy to explain the greater quantum yields for the photoreversal of the monoadducts at wavelengths below 250 nm, since the photoreversal through the excita-

tion of the thymidine moiety is very efficient.

B) Effects of DNA Helix and Adjacent DNA Bases on the Photoreversal

Comparison of the photoreversal action spectra of T-HMT and DNA-HMT pyrone side monoadducts in figure 4 indicates that the single-stranded DNA helix and the adjacent DNA bases have no effect upon the photoreversal of the monoadduct. This is in contrast to the photoreversal of the DNA-HMT crosslink (Chapter I), where the photoreversal of the T-HMT-T was dramatically enhanced upon the incorporation of the diadduct into a double-stranded DNA helix at wavelengths below 298 nm. It was proposed that this enhancement was due to energy transfer from excited DNA bases to the psoralen moiety in the crosslink. The fact that the photoreversals of the T-HMT and DNA-HMT pyrone-side monoadducts are identical at all wavelengths suggests that energy transfer from nearby excited DNA bases to the psoralen group is inefficient in the singe-stranded DNA helix. As shown in the next chapter, the photoreversal of the same DNA-HMT pyrone-side monoadduct is enhanced upon addition of the complementary oligonucleotide into the irradiation solution to form double-stranded DNA helix. This suggests that the photoreversal can be enhanced by efficient energy transfer from excited DNA bases in double-stranded but not single-stranded DNA and that the pyrone-side monoadduct is stacked with DNA bases in the double helix.

In the case of furan-side monoadduct, again the DNA helix and the adjacent DNA bases have little effect on the photoreversal of the

monoadduct at wavelengths below 285 nm, indicating that the energy tranfer from DNA bases to the HMT group is inefficient. The photoreversal of the DNA-HMT monoadduct is, however, less efficient than that of the T-HMT furan-side monoadduct at wavelengths above 285 nm. The photoreversal of the furan-side monoadducts could occur via either the singlet excited state or the triplet excited state or both. The exact mechanism has not been established (For review, see Cimino et al., 1985). The triplet characteristics of several psoralen-nucleoside furan-side monoadducts and 4', 5'-dihydropsoralen derivatives have been determined (Blais, et al., 1985; Land and Truscott, 1979). The quantum yields of triplet formation varies form 0.07 to 0.28 for the different adducts. These quantum yields are much larger than the quantum yield of the photoreversal of the furan-side monoadduct. Therefore, it is possible that the photoreversal occurs via the triplet state of the monoadduct. It is also known that thymine quenches the triplet states of psoralen-thymine furan-side monoadducts and 4', 5'-dihydropsoralen efficiently (Bensasson et al., 1980; Land and Truscott, 1979). Other nucleic acid bases can also quench the triplet states of 4', 5'-dihydropsoralen and coumarin, although less efficiently than thymine. Thus the decrease in the photoreversal rate constant above 285 nm upon the incorporation of the T-HMT furan-side monoadduct into oligonucleotide A could be due to the quenching of the triplet state of the monoadduct by adjacent DNA bases.

C) Comparison of the Action Spectra for the Photoreversal of DNA-HMT Monoadducts and Crosslink

The action spectra for the photoreversals of M_{Fu}-A and M_{Py}-A are replotted in figure 9 together with the action spectrum for the photoreversal of a DNA-HMT crosslink (data of Chapter I). The photoreversal action spectra for M_{Fu}-A and M_{Py}-A are quite different due to the differences in both the absorption spectra of the adducts and the quantum yields of the photoreversals. While both M_{Py}-A and the crosslink are transparent to light above 320 nm, M_{Fu}-A can be photoreversed at wavelengths up to 365 nm. Below 320 nm, the photoreversal rate constant of the DNA-HMT crosslink is much larger than the photoreversal rate constants of the DNA-HMT monoadducts.

As described in Chapter I, site specific placement of a psoralen molecule in a nucleic acid should facilitate elucidation of secondary and tertiary interactions in that nucleic acid. This is possible because the thermostability of the psoralen monoadducted double-stranded nucleic acid is similar to that of the unmodified helix (Chapter IV), so the adduct should not perturb the native structure of the nucleic acid. Psoralen monoadduct, if in a double-stranded region, can be driven to a crosslink, which can be analyzed to yield information about the secondary and tertiary interactions in the nucleic acid (Thompson and Hearst, 1983). The results in this paper indicate that site specific placement of a psoralen in a large DNA or RNA can be accomplished by psoralen transfer. As suggested in Chapter I, a monoadducted oligonucleotide containing a site-specific furan-side monoadduct

Figure 9. Action spectra for the photoreversal of DNA-HMT monoadducts and crosslink. The data for the crosslink were from Chapter I.

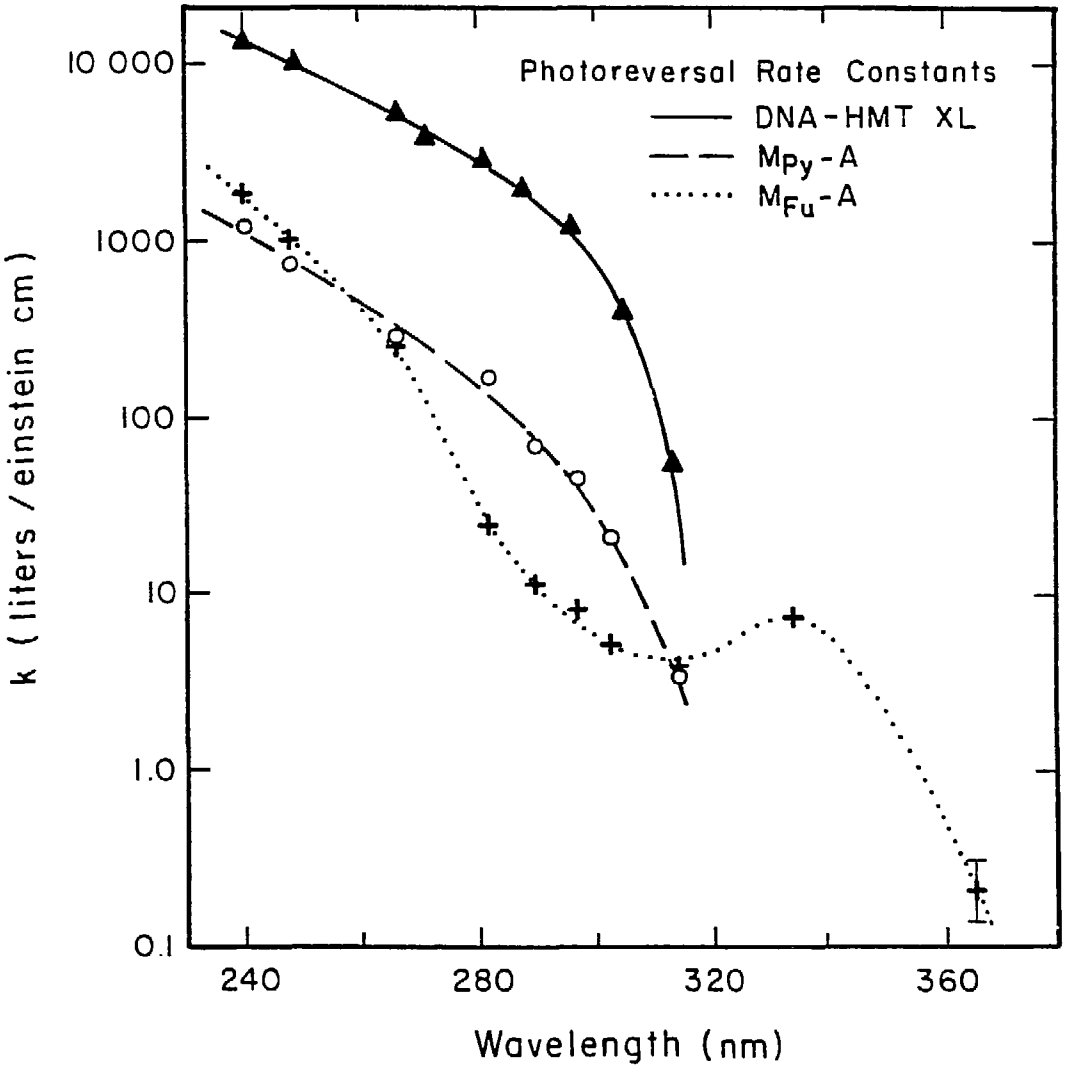
Photoreversal Rate Constants
DNA-HMT XL
M_{Py}-A
M_{Fu}-A
10 000
1000
100
10
1.0
0.1
k (liters / einstein cm)
240
280
320
360
Wavelength (nm)

or pyrone-side monoadduct can be prepared first. The monoadducted oligonucleotide can then be hybridized and crosslinked to its complement in a large nucleic acid. The crosslink can be photoreversed under conditions which favor the retention of the psoralen as a monoadduct on the large nucleic acid. Since the photoreversals of the monoadducts are much slower than that of the crosslink, the photoreversal can be controlled so that only the crosslink is photoreversed while very few monoadducts are photoreversed, allowing the accumulation of the monoadduct in the large nucleic acid. The resultant monoadduct can then function as a probe of local helical structure.

CHAPTER III. WAVELENGTH DEPENDENCE FOR THE PHOTOCROSSLINKING OF PSORALEN-DNA MONOADDUCTS

1. Introduction

The use of psoralens (furocoumarins) in the medical and biological fields is highly dependent upon the ability of these compounds to crosslink double-stranded nucleic acids through photoreactions with adjacent pyrimidine bases on opposite strands as mentioned in the previous two chapters. It has been well established that the furan-side monoadduct can be easily driven to a diadduct in a double-stranded nucleic acid. Gasparro et al. (1984) have reported the action spectrum for the AMT (4'-aminomethyl-4, 5', 8-trimethylpsoralen) crosslinking of pBR322 DNA in the wavelength region from 300 nm to 380 nm. They found that the wavelength dependence for crosslink formation correlates with the absorption spectrum of the furan-side monoadduct. Tessman et al. (1985) have reported the photocrosslinking of another furan-side monoadduct, thymidine-8-methoxypsoralen furan-side monoadduct, in calf thymus DNA. They observed that the monoadduct could be converted to the diadduct at 341.5 nm with a quantum yield of 2.8×10^{-2}. The pyrone-side monoadducts do not absorb light above 320 nm, so they can not be driven to diadducts with 320-380 nm light.

In the preceding chapter, I reported the wavelength dependence for the photoreversals of DNA-HMT monoadducts and isolated T-HMT monoadducts. We found that both the DNA-HMT and the T-HMT pyrone-side monoadducts are photoreversible at wavelengths below 334 nm, which is consistent with the absorption spectrum of the T-HMT pyrone-side

monoadduct. The DNA-HMT and T-HMT furan-side monoadducts can be photoreversed at wavelengths up to 365 nm, which also correlates with the absorption spectrum of the T-HMT furan-side monoadduct. The quantum yield of the photoreversal of the furan-side monoadduct is, however, only 7×10^{-4} at wavelengths above 285 nm, which is much smaller than the photocrosslinking quantum yield of the thymidine-8-methoxypsoralen furan-side monoadduct at 341.5 nm as reported by Tessman et al. (1985). Here we report the complete action spectra for the photoreactions of DNA-HMT monoadducts in a double-stranded helix. We observed that the DNA-HMT pyrone-side monoadduct yielded very little crosslink and was predominantly photoreversed upon UV irradiation in its absorption bands. In the case of the DNA-HMT furan-side monoadduct, UV irradiation at wavelengths ≥313.2 nm yields only crosslink with a quantum yield similar to that observed by Tessman et al. (1985), whereas UV irradiation at wavelengths ≤302.2 nm yields both photocrosslinking and photoreversal products. The results here have been published (Shi and Hearst, 1987b).

2. Materials and Methods

A) Materials

All materials were obtained as described in the preceding chapter.

B) Preparation of 5'-End Labelled DNA Oligonucleotides

The DNA oligonucleotides used in this study are: 5'-GAAGCTACGAGC-3', 5'-GCTCGTAGCTTC-3', and 5'-TCGTAGCT-3', respectively called oligonucleotide A, B, C. The furan-side DNA-HMT monoadduct, 5'-GAAGC[T(HMT)$_{Fu}$]ACGAGC-3' (M_{Fu}-A) and the pyrone-side DNA-HMT monoad-

duct, 5'-GAAGC[T(HMT)$_{Py}$]ACGAGC-3' (M_{Py}-A), were prepared as described in the preceding chapter. All unmodified and HMT monoadducted oligonucleotides were 5'-phosphorylated. Oligonucleotides with 5'-CH were labelled with [γ-^{32}P]ATP and T4 polynucleotide kinase and subsequently chased with cold ATP. The kinase exchange reaction described in the preceding chapter was used to label oligonucleotides with 5'-phosphate (see Chapter II).

The concentrations of the unmodified and HMT monoadducted DNA oligonucleotides were determined by absorption measurements at 260 nm. The extinction coefficients for oligonucleotides A, B, C, M_{Fu}-A, and M_{Py}-A are 1.2×10^5, 1.1×10^5, 7.4×10^4, 1.3×10^5, and 1.3×10^5, respectively (Chapter IV).

C) Photocrosslinking of the DNA-HMT Monoadducts

Monochromatic irradiations were done using the apparatus as described in Chapter I. The band width was maintained constant at 5.0 nm. The light intensity was monitored continuously with an in-line photodiode, which was calibrated by actinometry with $K_3Fe(C_2O_4)_3$. The photocrosslinking of the DNA-HMT monoadducts, both M_{Fu}-A and M_{Py}-A, was done in the presence of the cold 5'-phosphorylated complementary oligonucleotides B or C. The solutions were irradiated with monochromatic light in a stirred cuvette, which was covered with parafilm, at 4°C in 100 mM NaOAc, 10 mM $MgCl_2$, 0.1 mM EDTA, pH 6.0, or as otherwise indicated. 16 µg of carrier tRNA was added to each sample after irradiation and the sample was then concentrated in a speedvac concentrator (Savant Instrument Inc.) to 400 µl (irradiation volume was 750 µl) and EtOH

precipitated overnight (2.5 v/v EtOH) at -20°C. The sample pellets were then dissolved in 8 M urea, 0.02% bromophenol blue, and 0.02% xylene cyanol FF loading buffer and electrophoresed on a 20% polyacrylamide-7 M urea gel (40 cm x 40 cm x 0.05 cm, 35 watts for 3-4 hours). Band positions of the photoproducts and the reactants were located by autoradiography. The bands were then excised and quantified by ^{32}P Cerenkov counting with a Beckman LS-230 liquid scintillation counter.

D) Kinetics of the Photoreactions

The photoreactions of DNA-HMT monoadducts in double-stranded DNA are relatively complicated. Figure 1 shows the possible reactions of a double-stranded DNA formed between oligonucleotides A and B, with an HMT monoadduct attached to A. The initial reactions are the photoreversal and the photocrosslinking of the monoadduct. Photocrosslinking yields a crosslink which links A and B together. Upon absorbing a second photon, the crosslink can be photoreversed to yield a DNA-HMT monoadduct with the HMT attached to either B or A. Photoreversal of the monoadduct gives a complex with the HMT molecule intercalated in the double-stranded helix A:B. This complex can either undergo a photoreaction to yield a DNA-HMT monoadduct or a reversible dark dissociation to yield a free HMT molecule, which can be subsequently photodamaged.

Instead of relying upon the complicated kinetic equations, we used initial rate analysis to obtain the rate constants for the photoreversal and photocrosslinking of the monoadducts. The photoreaction kinetics at very low reactant concentrations can be analyzed as described in Chapter I to obtain the following initial rate equations:

Figure 1. Photoreaction kinetics of HMT monoadducts in double-stranded DNA.

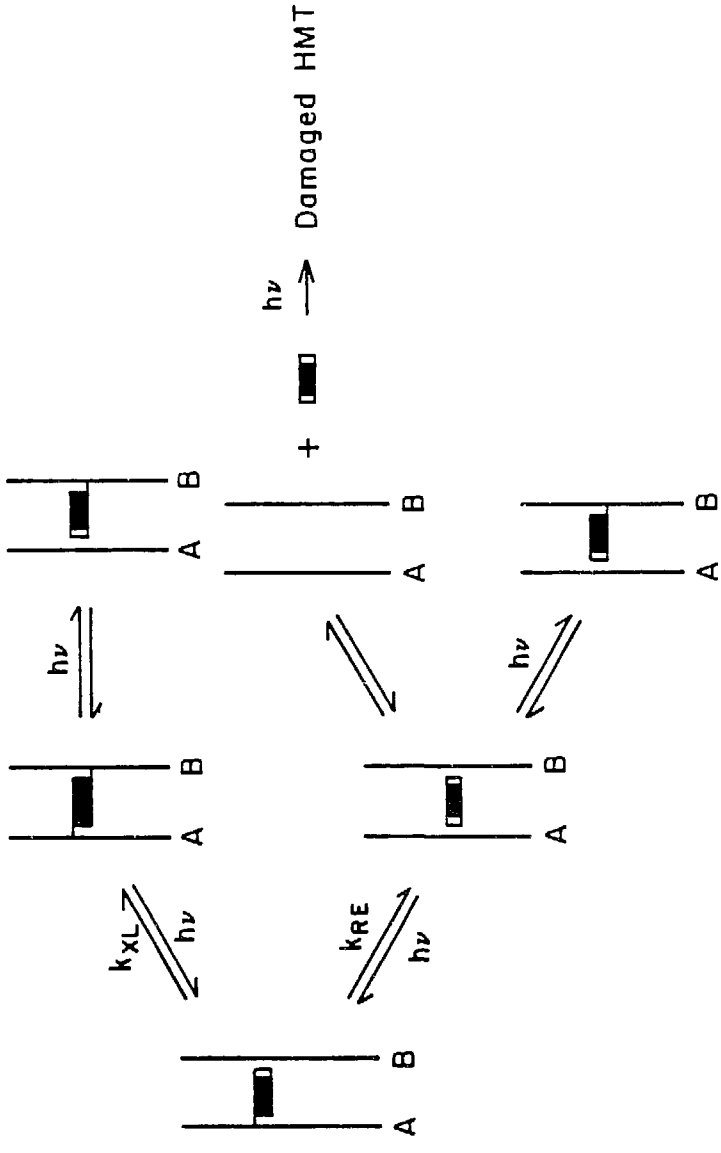
hν
Damaged HMT
+
B
A
hν
hν
hν
k_{XL}
k_{RE}

$$-d(C/C^0)/d(I_0t) = 1k_t/VN_0 \quad (1)$$

$$d(P/C^0)/d(I_0t) = 1k/VN_0 \quad (2)$$

$$k = 2.303\varepsilon\phi \quad (3)$$

where k_t is the total photoreaction rate constant of the DNA-HMT monoadduct (liters/einstein cm); I_0 is the light intensity (photons/second); I_0t is the irradiation dose (photons); V is the reaction volume (liters); N_0 is the Avogadro's number; 1 is the path length (cm); ε is the extinction coefficient of the monoadduct; P is the concentration of a product; k and ϕ are the rate constant (liters/einstein cm) and the quantum yield for the formation of P, respectively; and C^0 and C are the concentrations (moles per liter, or M) of the DNA-HMT monoadduct at time zero and at time t, respectively.

3. RESULTS

A) Photocrosslinking of 5'-GAAGC[T(HMT)$_{Fu}$]ACGAGC-3'

The photocrosslinking of M_{Fu}-A (2 nM) was done in the presence of a 10 fold excess (20 nM) of its unlabelled complementary oligonucleotide B (5'-GCTCGTAGCTTC-3') at 4°C in 100 mM NaOAc, 10 mM $MgCl_2$, 0.1 mM EDTA, pH 6.0. Under these conditions, M_{Fu}-A and its complement B exist in the double-stranded state (Shi and Hearst, 1986). The photocrosslinking samples were irradiated with monochromatic light followed by EtOH precipitation in the presence of carrier tRNA. The samples were then electrophoresed on a 20% polyacrylamide gel to separate the photoproducts. An autoradiogram of the time course of the irradiation at three wavelengths is shown in figure 2. With increasing irradiation dose, the amount of M_{Fu}-A decreased at all wavelengths. Product forma-

Figure 2. Photocrosslinking of double-stranded M_{Fu}-A:B. V = 750 µl, l = 1 cm. Abbreviations: A = 5′-GAAGCTACGAGC-3′; M_{Fu}-A = 5′-GAAGC[T(HMT)$_{Fu}$]ACGAGC-3′; B = 5′-GCTCGTAGCTTC-3′; XL = crosslink formed between M_{Fu}-A and B through the addition of the pyrone end of the HMT to the middle thymidine in B; D_1, D_2, and D_3 = XL with DNA damage(s) (see text). Lane 1: dark control. Lanes 2-6: samples exposed to 2.37 x 10^{16}, 5.28 x 10^{16}, 1.06 x 10^{17}, 3.20 x 10^{17}, and 1.07 x 10^{18} photons at 334 nm, repectively; light intensity was 1.58 x 10^{15} photons/sec. for lane 2 and 3.56 x 10^{15} photons/sec. for the other lanes; Lanes 7-11: samples exposed to 5.52 x 10^{16}, 1.29 x 10^{17}, 3.43 x 10^{17}, 1.03 x 10^{18}, and 3.54 x 10^{18} photons at 302.2 nm, repectively; light intensity was 3.68 x 10^{15} photons/sec. for lane 7 and 8.58 x 10^{15} photons/sec. for the other lanes; Lanes 12-16: samples exposed to 1.49 x 10^{16}, 2.99 x 10^{16}, 7.97 x 10^{16}, 2.49 x 10^{17}, and 7.97 x 10^{17} photons at 266 nm, repectively; light intensity was 1.66 x 10^{14} photons/sec.

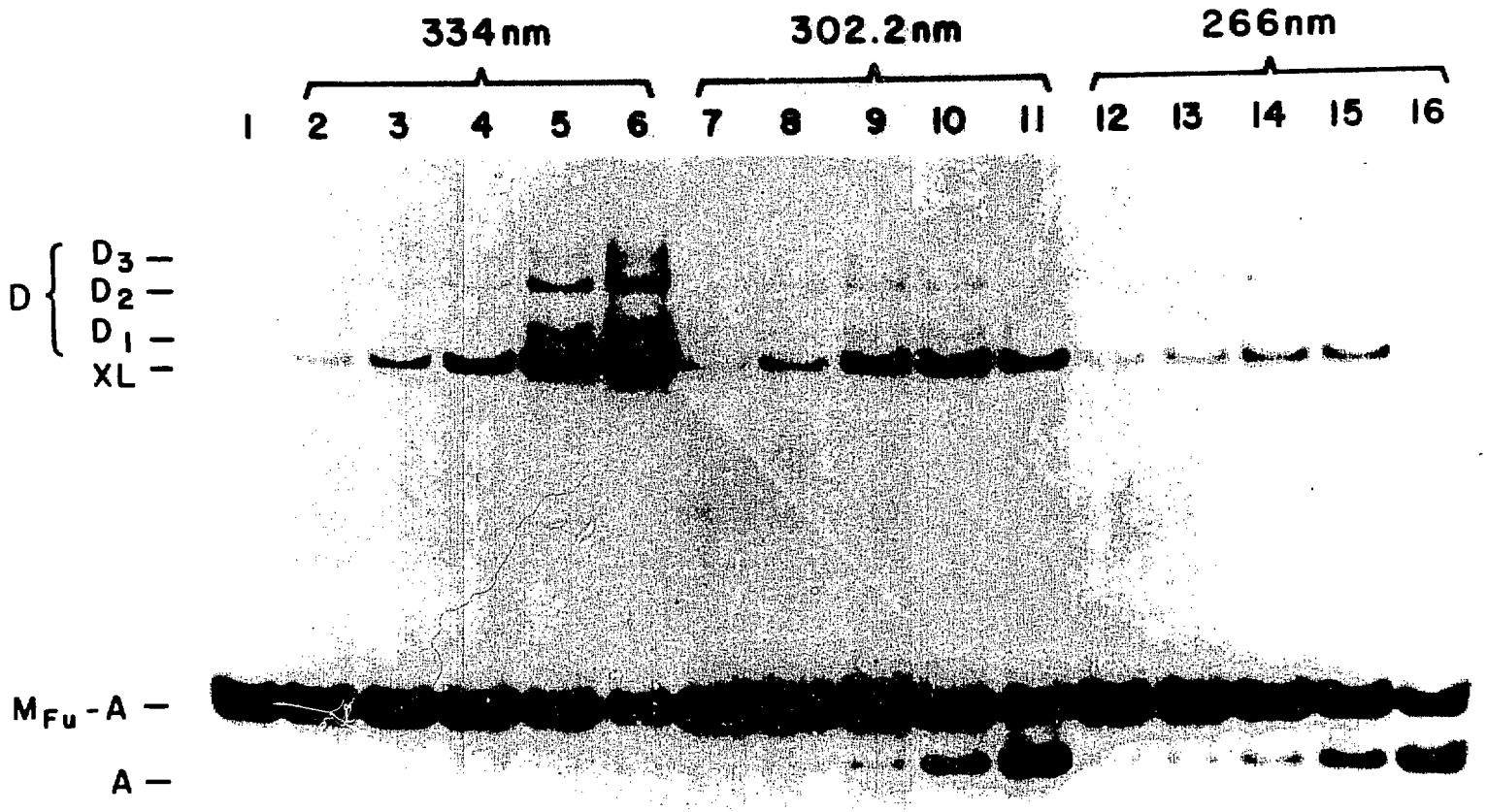
334nm
302.2nm
266nm
1 2 3 4 5 6 7 8 9 10 11 12 13 14 15 16
D
D3
D2
D1
XL
MFu-A
A

tion is very dependent on the irradiation wavelength. The three wavelengths in the figure are in three different absorption bands of the isolated T-HMT furan-side monoadduct (see figure 5 of Chapter II). More photoreversal product (A) was produced at shorter wavelengths. No photoreversal occurred at 334 nm. More crosslink(s), which links the oligonucleotides A and B together through the middle thymidine on each strand, was produced at longer wavelengths. The bands moving slower than the crosslink XL, ie., D_1, D_2, D_3, were identified as crosslinks with photodamage(s) on oligonucleotide B and/or A (See below). At 334 nm, XL and D (including D_1, D_2, and D_3) increased with increasing dose, whereas at shorter wavelength(s), XL and D increased first and then decreased with increasing dose. This is attributed to the competing photoreversal of the crosslinks at the shorter wavelengths since it is known that crosslinks can be photoreversed at wavelengths ≤313 nm (Chapter I). It is also apparent that the damaged crosslink formation is dependent upon the wavelength and that more damaged bands were seen at 266 nm.

The identities of the photoproducts were tested by the following experiments. Unlabelled M_{Fu}-A and ^{32}P-labelled B were irridiated under the same conditions as above and then analyzed by gel electrophoresis. Again, the crosslinking yielded XL, D_1, D_2, and D_3. Upon photoreversal at 254 nm, these purified adducts yielded, as expected, M_{Py}-B and B as analyzed by gel electrophoresis. These and above results indicate that XL, D_1, D_2, and D_3 are DNA-HMT crosslinks. In addition, photoreversal of D_2 and D_3 yielded bands running slightly slower than B. When similar

photoreversal was performed on XL, D_1, D_2, and D_3 using labelled A strand, only A and M_{Fu}-A were produced in all crosslinks. These results suggest that there is photodamage on the B strand in D_2 and D_3. But the possibility that damage on the A strand, especially in the case of D_1 where photoreversal yielded no damaged DNA when the label was on either A strand or B strand, cannot be ruled out because of the possibility of photoreversal of the damage at 254 nm, especially pyrimidine dimers, and the limited resolution by gel electrophoresis. The mechanism of the damaged product formation is unknown. These products could be produced by direct absorption of the DNA bases or more probably by energy tranfer from the excited psoralen moiety to the pyrimidine bases, especially at wavelengths ≥334 nm, where DNA bases have little absorption. It has been shown that the triplet states of the furan-side monoadducts of several psoralen derivatives with thymine as well as those of coumarin and 4', 5'-dihydropsoralen can be quenched by nucleic acid bases (Bensasson et al., 1980; Land and Truscott, 1979; Blais, et al., 1985), suggesting that energy transfer between these adducts and nucleic acid bases can occur.

The bands of the reactant and the products, such as those in figure 2, were excised and quantified by ^{32}P Cerenkov counting in order to determine the concentration of each reactant and product. The plots of the concentrations as a function of irradiation dose at 302.2 nm and 334 nm are shown in figure 3, where D stands for the total damaged crosslinks running slower than XL on the gel. Again, it can be seen that only XL and D were produced at 334 nm, whereas photoreversal of

Figure 3. C/C^0 vs. irradiation dose for the photocrosslinking of M_{Fu}-A. All the irradiation conditions and abbreviations are identical to those described in figure 2. The ratios of concentrations of the reactant (M_{Fu}-A) and the products (A, XL, and D) to the initial concentration of M_{Fu}-A plotted in this figure were determined by excising the bands from the photocrosslinking gel and measuring the ^{32}P counts of each band with a scintillation counter. The relative concentrations of A, XL, and D shown in figure 4B are the actual value for each product multiplied, respectively, by 2, 4, and 4 as indicated in the figure for the convenience of presentation.

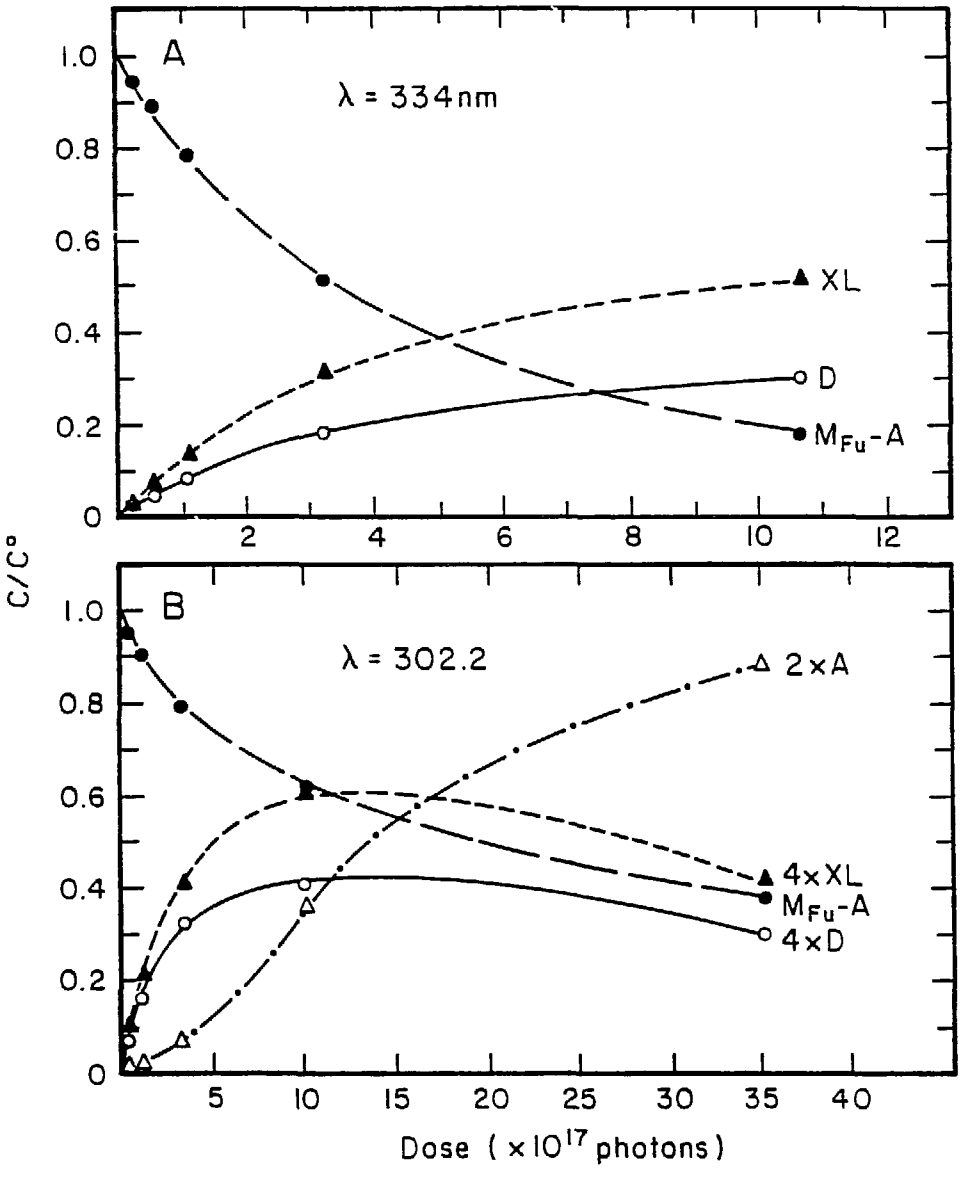
A
λ = 334nm
XL
D
M_{Fu}-A
B
λ = 302.2
2×A
4×XL
M_{Fu}-A
4×D
C/C°
Dose (×10^17 photons)

M_{Fu}-A to yield A was a competing process at 302.2 nm. With increasing irradiation dose at 302.2 nm, XL and D initially increased and then decreased due to the photoreversal of the crosslinks. The production of A was sigmoidal. Initially A was produced only from the photoreversal of M_{Fu}-A. As more XL and D were formed, a significant amount of A was produced from the photoreversal of XL and D, since it is known that about 30% of the time photoreversal of crosslinks at this wavelength occurs at the furan end (Chapter I), which in our case yields A. Consequently, the rate of A formation is increased. The initial rate constants for the photoreversal (k_{RE}), and XL and D formation (k_{XL} and k_D, respectively) were determined from these plots. The experiments were repeated at wavelengths ranging from 248 nm to 379 nm to obtain the action spectra for the photoreversal and photocrosslinking. Figure 4 shows the initial rate constants for the photoreversal (k_{RE}) and the total crosslink formation ($k^t_{XL} = k_{XL} + k_D$) as a function of wavelength. Essentially no photoreversal occurs at wavelengths ≥313 nm, although a detectible amount of A was produced after prolonged irradiation at 313.2 nm, which was due to photoreversal of the crosslink (Chapter I).

Two series of experiments were done to determine the dependence of the reaction rate on the stability of the double helix. In the first, the irradiation temperature was raised from 4°C to 25°C and in the second, the oligonucleotide C was used as the complement of M_{Fu}-A. The photoreaction data were analyzed as described above and the results are presented in table I. When the irradiation temperature was changed from

Figure 4. The action spectra for the photoreversal and photocrosslinking of T-HMT furan-side monoadduct in double-stranded M_{Fu}-A:B. k^{t}_{XL} is the initial rate constant for the total crosslink formation and k_{RE} is the initial rate constant for the formation of the unmodified oligonucleotide A, ie., the photoreversal. k_{RE} is zero at wavelengths ≥313 nm.

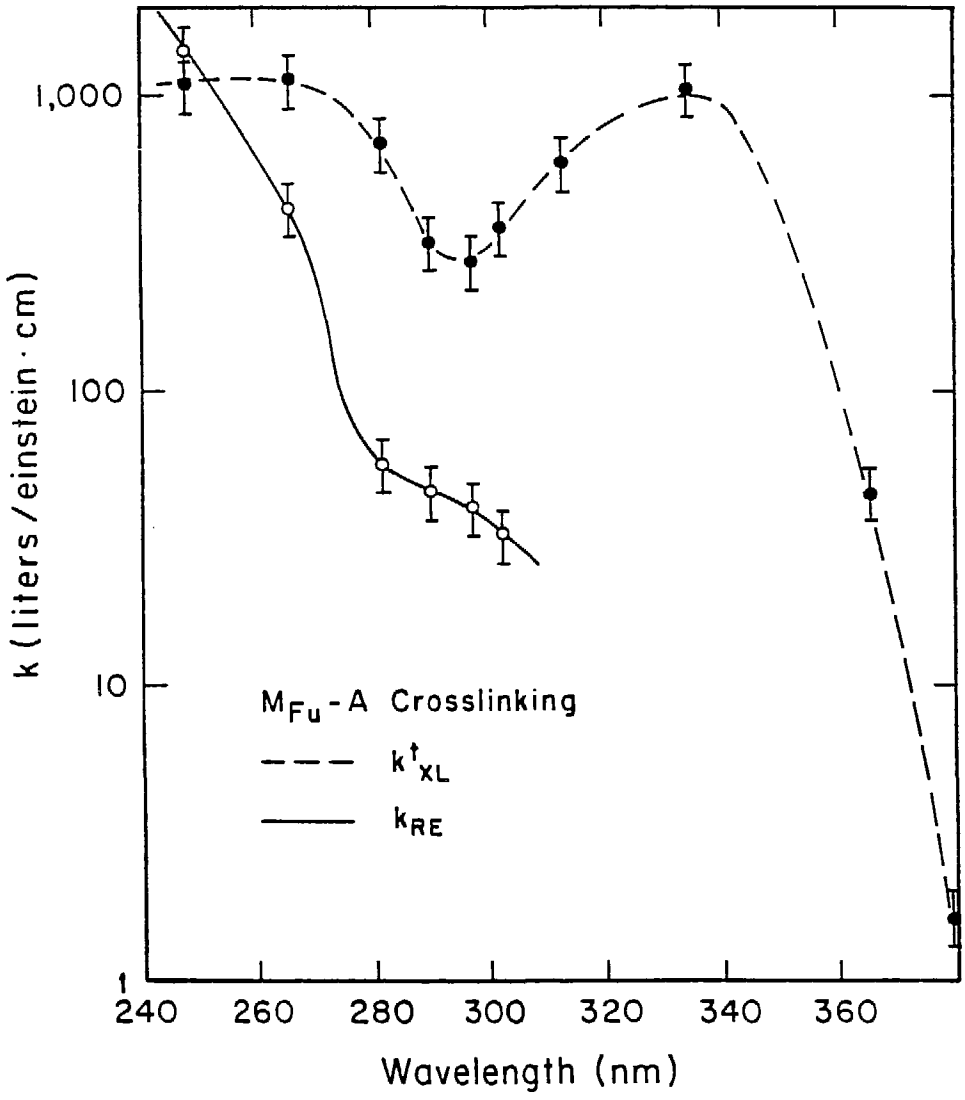
1,000
100
10
1
k (liters / einstein · cm)
240
260
280
300
320
340
360
Wavelength (nm)
M_{Fu}-A Crosslinking
k^t_{XL}
k_{RE}

Table I. Initial Rate Constants of M_{Fu}-A Crosslinking*

λ (nm)	248			297			334		
T (°C)	25	4		25	4		25	4	
Complement	B	B	C	B	B	C	B	B	C
k^t	2020	2530	2010	295	321	212	680	1050	529
k^t_{XL}	870	1090	740	266	290	173	680	1050	529
k_{RE}	1150	1440	1270	19	41	39	0	0	0
k_D/k^t_{XL}	0.43	0.51	0	0.37	0.54	0	0.29	0.44	0

* Abbreviations: M_{Fu}-A = 5'-GAAGC[T(HMT)$_{Fu}$]ACGAGC-3'

B = 5'-GCTCGTAGCTTC-3'

C = 5'-TCGTAGCT-3'

Irradiation Buffer: 100 mM NaOAc, 10 mM $MgCl_2$, 0.1 mM EDTA, pH 6.0.

Concentrations: [M_{Fu}-A] = 2 nM, [B] = 20 nM, [C] = 6 nM.

k^t: Total photoreaction rate constant of M_{Fu}-A (liters/einstein cm).

k^t_{XL}: Total photocrosslinking rate constant (liters/einstein cm).

k_{RE}: photoreversal rate constant (liters/einstein cm).

k_D: rate constant of damaged crosslink formation (liters/einstein cm).

Estimated precision in rate constants: ±20%.

4°C to 25°C without altering other conditions, the photoreaction rate constants were slightly decreased, though the differences were not significant compared to the experimental error (see data in the first and second columns for each wavelength). The ratio of k_D/k_{XL}^t at 25°C was also smaller than that at 4°C at all wavelengths, indicating that fewer damaged crosslinks (D) were produced at the higher temperature. Data in the second and third columns for each wavelength show that the rate constants when using C as the complement were smaller than those obtained using B as the complement. The results from these two series of experiments indicate that the photoreactions are less efficient in less stable helices. Also shown by these experiments is that the ratio of k_D/k_{XL}^t was 0, or no damaged crosslinks (D) were produced, at all wavelengths when C was used as the complement.

To ensure that all the M_{Fu}-A were in the double-stranded state under the conditions used to obtain the action spectra shown in figure 4, the salt concentration of the irradiation buffer and/or the DNA concentrations were increased and the samples were irradiated at 334 nm and analyzed as described above. The results are shown in table II. Upon changing the $MgCl_2$ concentration in the irradiation buffer from 10 mM to 20 mM, or increasing the DNA concentrations by a factor of five, or both, the photoreversal rate constants as well as the ratio of k_D/k_{XL}^t remained the same. Since these changes favor double-stranded DNA formation, the results indicate that under the original conditions, all the M_{Fu}-A was double-stranded.

Tessman et al. (1985) have reported that a

Table II. Initial Rate Constants at 334 nm and 4°C*

Sample Set	1	2	3	4
$[M_{Fu}\text{-}A]$ (nM)	2	10	2	10
[B] (nM)	20	100	20	100
Buffer	B1	B1	B2	B2
$k^t = k^t_{XL}$	1050	1010	1040	1000
k_D/k^t_{XL}	0.44	0.44	0.37	0.42

* Abbreviations: See table I.

Buffers: B1 = 100 mM NaOAc, 10 mM $MgCl_2$, 0.1 mM EDTA, pH 6.0.

B2 = 100 mM NaOAc, 20 mM $MgCl_2$, 0.1 mM EDTA, pH 6.0.

Estimated precision in rate constants: ±20%.

thymidine-8-methoxypsoralen furan-side monoadduct in double-stranded calf thymus DNA can be converted to a pyrone-side monoadduct by direct photoisomerization upon irradiation at 341.5 nm. To test whether the T-HMT furan-side monoadduct in a double helix can photoisomerize to the pyrone-side monoadduct, 5'-^{32}P labelled oligonucleotide C was used as the complement of M_{Fu}-A in photocrosslinking experiments. Any production of pyrone-side monoadducted C could be detected as a unique band on a polyacrylamide gel (Chapter IV). These experiments showed that no pyrone-side monoadducted C was produced at 334 nm, although detectable amounts were generated at 297 nm and 248 nm. Formation of M_{Py}-C at lower wavelengths was probably due to the photoreversal of the crosslink formed in the forward crosslinking reaction. Therefore, it is conclude that the T-HMT furan-side monoadduct cannot undergo direct photoisomerization. The difference between this adduct and the thymidine-8-methoxypsoralen furan-side monoadduct is probably due to the properties of the two psoralen derivatives.

The reciprocity of the photoreactions was confirmed by exposing several identical samples to a constant light dose (1.08×10^{17} photons) at 334 nm. The light intensity seen by each sample was varied by up to a factor of ten and the irradiation time was varied correspondingly to maintain the constant dose. The photoreactions in all samples occurred to the same extent. They are, therefore, dependent only on the irradiation dose and not on the light intensity, and are one photon processes. The initial rate constants determined above should also be independent of light intensity.

The quantum yield of initial crosslink formation was estimated based on k_{XL}^{t} and the extinction coefficient of the isolated T-HMT furan-side monoadduct (figure 5 of Chapter II) according to equation (3). The result is shown in table III. The quantum yield in the shorter wavelength region is slightly larger than that in the longer wavelength region. The quantum yield above 300 nm is 2.4×10^{-2}, which is similar to that reported by Tessman et al. (1985) for the crosslinking of thymidine-8-methoxypsoralen furan-side moncadduct in calf thymus DNA. The uncertainty in quantum yield is not known due to the unknown effects that the DNA helix and bases may have on the absorption of the T-HMT furan-side monoadduct in the double-stranded M_{Fu}-A:B helix, especially in the wavelength regions where DNA bases absorb. Energy transfer from excited DNA bases to the HMT group may also contribute to the crosslinking, which may explain the bigger quantum yield around 260 nm.

B) Photocrosslinking of 5'-GAAGC[T(HMT)$_{Py}$]ACGAGC-3'

The photocrosslinking of M_{Py}-A (2 nM) was performed under the same conditions used for M_{Fu}-A. All of the M_{Py}-A should be double-stranded under these conditions based on the thermodynamic parameters for the double helix formation by M_{Py}-A and B (Chapter IV). The photocrosslinking samples were treated as above and an autoradiogram of the time courses of the irradiation at 297 nm is shown in figrue 5. With increasing irradiation dose, the amount of M_{Py}-A decreased. The loss of M_{Py}-A was predominantly photoreversal. The amount of XL formed was only a few percent and it decreased after prolonged irradiation (compare lane 5 to lanes 2, 3, and 4). When this XL was isolated and photore-

Table III. Quantum Yield of M_{Pu}-A Crosslinking*

λ (nm)	248	266	281.7	289.5	297	302.2	313.2	334	365.4
ϕ (10^{-2})	5	8	4	2	1.2	1.4	1.7	2.4	4

* Oligonucleotide B was used as the complement in the photoreaction (4°C). See Table I for abbreviations and other reaction conditions.

Figure 5. Photocrosslinking of double-stranded M_{Py}-A:B. V = 750 µl, l = 1 cm. Abbreviations: M_{Py}-A = 5'-GAAGC[T(HMT)$_{Py}$]ACGAGC-3'; XL = crosslink formed between M_{Py}-A and B through the addition of the furan end of the HMT to the middle thymidine in B. Lane 1: dark control. Lanes 2-5: samples exposed to 2.33×10^{17}, 7.0×10^{17}, 2.10×10^{18}, and 7.0×10^{18} photons at 297 nm, repectively; light intensity was 5.83×10^{15} photons/sec.

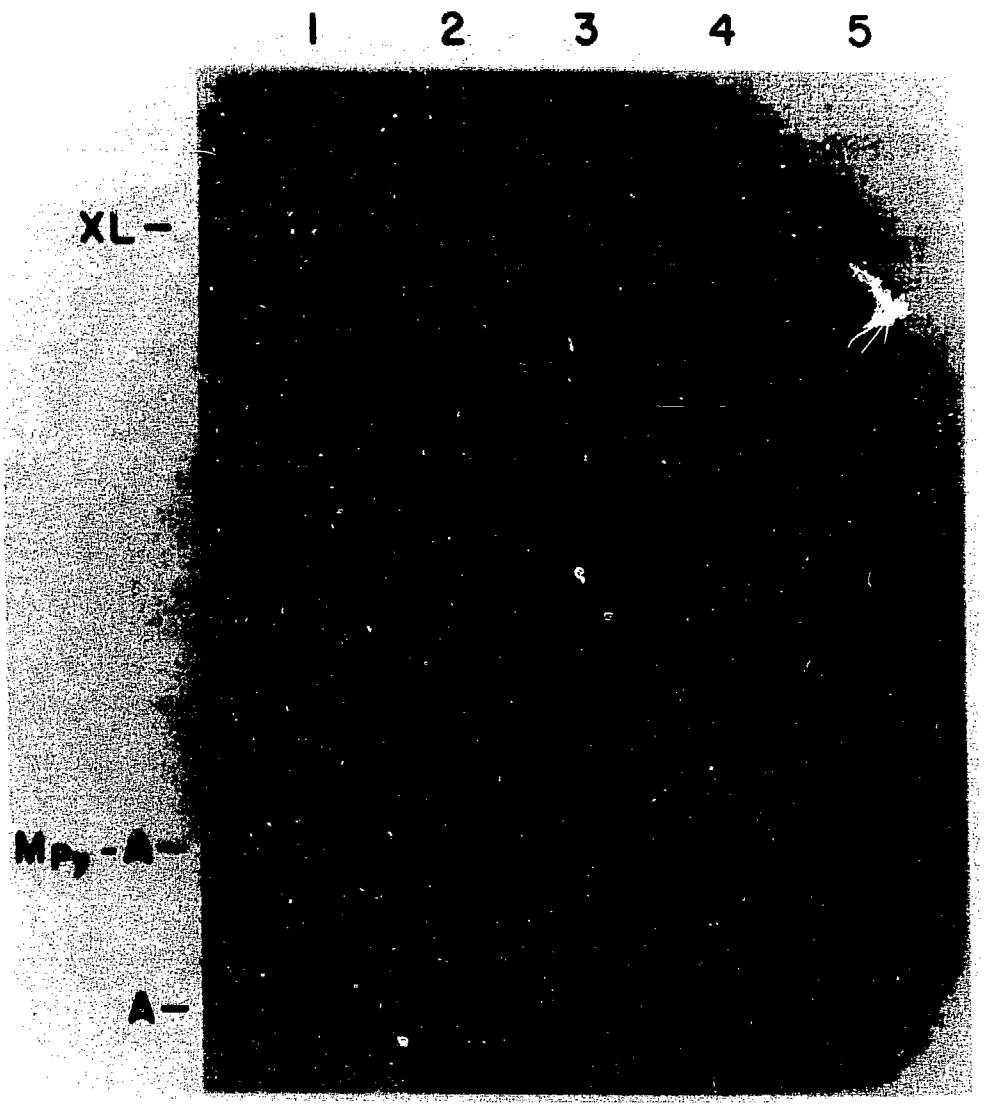
1
2
3
4
5
XL –
M_{ρ_1} - A –
A –

versed at 254 nm, it gave M_{Py}-A and A, indicating that in XL the HMT is attached to A through its pyrone end and attached to B through its furan end and that the formation of XL was not due to contamination of M_{Py}-A with M_{Fu}-A. The bands migrating slightly slower than A represent damaged DNA. These same bands were also observed in the photoreversal of M_{Py}-A in its single-stranded state (see Chapter II). The amount of material in each band was quantified by excising the band from the gel and counting it in a scintillation counter. The photoreaction rate constant(s) could then be determined. The experiments were repeated at different wavelengths in both absorption bands of the T-HMT pyrone-side monoadduct (see figure 5 of Chapter II). It was found that photoreversal was the predominant reaction and that only a few percent of XL was formed at all wavelengths. Thus the total photoreaction rate constant (i.e. the rate constant for the consumption of M_{Py}-A) is approximately equal to the photoreversal rate constant of M_{Py}-A in the double-stranded helix. The photoreaction rate constants at 248 nm and 297 nm under these conditions are listed in the first column for each wavelength in table IV. Compared to the photoreversal rate constants of the single-stranded M_{Py}-A in the fourth column for each wavelength, the photoreversal rate in a double-stranded helix is about twice as fast as in a single-stranded helix. The enhancement of photoreversal under the photocrosslinking conditions could be due to: 1) photoreversal through a transient photocrosslinking, i.e., through formation and photoreversal of XL, which would give mostly oligonucleotide A and M_{Fu}-B (Chapter I); 2) direct photoisomerization, i.e., the excited HMT group pho-

Table IV. Photoreaction Rate Constant of M_{Py}-A*

λ (nm)	248				297			
T (°C)	4			24	4			24
Buffer	B1			B3	B1			B3
Complement	B	C	none	none	B	C	none	none
k^t	1980 ±270	1640 ±180	917 ±92	731[a] ±73	116 ±19	97 ±21	52 ±5	45[a] ±5

* Abbreviations: M_{Py}-A = 5'-GAAGC[T(HMT)$_{Py}$]ACGAGC-3' and see Table I.

Buffers: B1 = 100 mM NaCAc, 10 mM $MgCl_2$, 0.1 mM EDTA, pH 6.0.

B3 = 0.1 mM EDTA, pH 5.5.

Concentrations: [M_{Py}-A] = 2 nM, [B] = 20 nM, [C] = 10 nM.

k^t: Total photoreaction rate constant of M_{Py}-A (liters/einstein cm).

a. Data from the preceding paper, Shi and Hearst.

toreverses at its pyrone end and simultaneously attaches to the thymidine residue in B through its furan end; 3) the irradiation buffer and/or temperature; 4) the electronic properties and steric constraints of the pyrone-side monoadduct in the double-stranded DNA; and 5) energy transfer from excited DNA bases in double-stranded DNA to the HMT group.

The first two possibilities were investigated by irradiating samples of M_{Py}-A in the presence of ^{32}P labelled complementary oligonucleotide C under the same conditions as above. The furan-side monoadducted C, if generated by either one of these, could be detected as a unique band on a polyacrylamide gel (Chapter IV). These experiments showed that the furan-side monoadducted C was generated at only a few percent even when most of the M_{Py}-A had been photoreversed. The photoreaction rate constants at 248 nm and 297 nm and the amount of XL formed were similar to those obtained when oligonucleotide B was used as the complement and the rate constants are shown in the second column for each wavelength in table IV. Based on all these results it is concluded that the photoreversal through transient crosslinking and direct photoisomerization may contribute to the enhancement of the photoreversal, but they have only a small effect and cannot explain the two fold enhancement. To test the third possibility, samples of M_{Py}-A were irradiated under the same conditions as above except no complement was added and the irradiated samples were analyzed to obtain the photoreversal rate constant. These results, shown in the third column for each wavelength in table IV, show that the photoreversal rate constant of

single-stranded M_{Py}-A in the buffer at 4°C is identical to that in 0.1 mM EDTA at 24°C. Thus the enhancement of photoreversal is dependent on double helix formation and independent of the irradiation temperature and buffer conditions. The effects of double-stranded DNA formation on the electronic properties and the steric constraints of the pyrone-side monoadduct and the possibility of energy transfer from excited DNA bases to the HMT group cannot be directly tested.

4. DISCUSSION

A) Effects of Double Helix Formation on the Photoreactions of M_{Fu}-A

Photoreversal is the only reaction which occurs when single-stranded M_{Fu}-A is irradiated with UV light as described in the preceding paper. In the presence of the complement B (5'-GCTCGTAGCTTC-3') or C (5'-TCGTAGCT-3'), the photoreactions of M_{Fu}-A become more complicated. Initially, there are two parallel reactions: photoreversal and photocrosslinking of M_{Fu}-A to its complement. The relative rate of photoreversal vs. photocrosslinking is dependent on irradiation wavelength. As shown in figure 4, except at wavelengths below 250 nm, photocrosslinking is the favored reaction for the double-stranded M_{Fu}-A:B and the ratio of k^t_{XL}/k_{RE} increases as the irradiation wavelength increases. At wavelengths ≥ 313 nm, only photocrosslinking occurs. Photocrosslinking is still detectible at 379 nm, although no detectible photoreversal occurs at this wavelength. Due to the photoreversibility of the crosslink(s), unmodified oligonucleotide A will be the major product after prolonged irradiation at wavelength

≤313 nm.

The initial photoreversal rate constant k_{RE} is larger than that for the single-stranded M_{Fu}-A as reported in the preceding paper. As for M_{Py}-A in double-stranded M_{Py}-A:B, there are several possible causes for this enhanced photoreversal, which have not been tested. The k_{RE} in figure 4 overestimates the actual photoreversal rate constant, since crosslink formation and subsequent photoreversal are fast and 30% of this photoreversal yields unmodified oligonucleotide A (Chapter I), which contributes to the apparent photoreversal rate.

The efficient photocrosslinking of DNA-HMT furan-side monoadducts at wavelengths above 313 nm , where DNA bases do not absorb, enhances the usefulness of oligonucleotide hybridization probes. Crosslinkable HMT monoadducted oligonucleotide probes facilitate solution hybridization formats, which are much more rapid and convenient than traditional hybridization methods. These same probes can be used to study hybridization kinetics and thermodynamics of the interactions between oligonucleotides and large nucleic acids (Gamper et al., 1986 and 1987).

B) Quantum Yield of Photocrosslinking of M_{Fu}-A

The accurate quantum yield for photocrosslinking is difficult to determine due to the difficulty in measuring the extinction coefficient of the T-HMT furan-side monoadduct in the double-stranded M_{Fu}-A:B. The quantum yield can be estimated approximately by the using photocrosslinking rate constant k^{t}_{XL} and the extinction coefficient of the isolated T-HMT furan-side monoadduct. Though the error in the quantum

yield so calculated is unknown, the data in table III clearly indicate that the quantum yield for photocrosslinking of M_{Fu}-A at wavelengths above 300 nm (2.4×10^{-2}) is much larger than the corresponding value for the photoreversal of the T-HMT furan-side monoadduct (7×10^{-4}, Chapter II). The photoreversal of the single-stranded M_{Fu}-A above 300 nm is even less efficient than that of the T-HMT furan-side monoadduct (see the preceding Chapter). This explains why at wavelengths $\geq$ 313 nm only photocrosslinking was observed.

The quantum yields of photocrosslinking of M_{Fu}-A at wavelengths $\leq$ 281.7 nm are slightly larger than those at longer wavelengths. This difference could be due to either more efficient crosslinking of the monoadduct at these wavelengths or energy transfer from excited DNA bases to the HMT group in the monoadduct, especially around 260 nm, where DNA bases absorb efficiently. At wavelengths above 300 nm, DNA bases absorb little light and only the absorption of the T-HMT furan-side monoadduct in the helix contributes to the photocrosslinking. The quantum yield at wavelengths above 300 nm is similar to that observed for the photocrosslinking of the thymidine-8-methoxypsoralen furan-side monoadduct in calf thymus DNA (Tessman et al., 1985).

C) Enhanced Photoreversal of M_{Py}-A in the double-stranded DNA

In contrast to M_{Fu}-A:B, UV irradiation of double-stranded M_{Py}-A:B results mostly in photoreversal of M_{Py}-A. Consequently the photoreaction rate constant approximates the value of the photoreversal rate constant of M_{Py}-A in the double helix. Results show that photoreversal of M_{Py}-A in the double helix is more efficient than that in the

single-stranded helix. Upon the formation of the double-stranded M_{Py}-A:B, the electronic and steric constraints of the T-HMT pyrone-side monoadduct may change, thereby affecting the photoreversal of the monoadduct. As described above, energy transfer from the excited DNA bases in the double-stranded DNA to the HMT group may also play a role in the enhancement of photoreversal. Two other mechanisms, though having only a small effect as described above, can also contribute to the enhanced photoreversal. These are photoreversal through a transient crosslink formation and direct photoisomerization. In the first case the crosslink is formed initially and then photoreversed. Approximately 70% of the photoreversal of the crosslink will produce the furan-side monoadducted B and unmodified oligonucleotide A (Chapter I), consequently increasing the apparent photoreversal rate constant of M_{Py}-A. In the second case the excited HMT group photoreverses at the pyrone end and simultaneously attaches to B through its furan end. This yields the same products as in the first case.

PART II

BIOLOGICAL EFFECTS OF PSORALEN-DNA ADDUCTS

CHAPTER IV. EFFECTS OF COVALENT ADDITIONS OF A PSORALEN ON THE THERMOSTABILITY OF DOUBLE-STRANDED DEOXYRIBONUCLEIC ACIDS

1. Introduction

Double-stranded nucleic acid intercalators, such as ethidium and proflavine, stabilize the double helix through favorable stacking interactions with adjacent bases upon intercalation. The intercalation is associated with a favorable enthalpy change and an unfavorable entropy change (Nelson and Tinoco, 1984; Baba et al., 1981). Similarly, the intercalation of a psoralen into a double-stranded nucleic acid also provides a favorable ΔH^0 and an unfavorable ΔS^0, resulting in a net stabilization of the helix (Kao, 1984). However, the effects of covalent additions of a psoralen on the thermostability of double-stranded nucleic acids are essentially unknown. In this chapter, we present a thermodynamic study of the effects of several well defined adducts of the psoralen derivative, HMT (4'-hydroxymethyl-4, 5', 8-trimethylpsoralen), on the stability of two double-stranded DNA oligonucleotides. HMT was used in this study because 1) HMT and its pyrimidine adducts are neutral, and therefore do not have the added complications associated with charged intercalators; 2) the adducts are well characterized; and 3) the different HMT adducted oligonucleotides can be resolved by a polyacrylamide gel system.

Our results showed that: 1) monoaddition of HMT does not destabilize the double-stranded DNA, but stabilizes the helix to some extent; 2) HMT crosslinking of the two strands of a double-stranded DNA, as expected, remarkably stabilizes the double helix; 3) the

double-stranded helix formed by a self complementary oligonucleotide containing in the center a thymidine-HMT furan-side monoadduct is, however, dramatically destabilized compared to the unmodified double-stranded helix. The results in this chapter have been published (Shi and Hearst, 1986).

2. Materials and Methods

A) Materials

See Chapters I and II.

B) Preparation of HMT-crosslinked Double-stranded 5'-GGGTACCC-3'

The crosslink was prepared following the precedures described in Chapter I. 400 µg 5'-GGGTACCC-3' was dissolved in 700 µl irradiation buffer (50 mM TrisHCl, 0.1 mM EDTA, 150 mM NaCl, 10 mM $MgCl_2$, pH 7.6) after kinasing and EtOH precipitation. The solution was split into two 1.5 ml Eppendorf tubes, each containing 350 µl, and 15 µl concentrated HMT/EtOH solution was added to each tube (final HMT concentration was 1.5×10^{-4} M). Each mixture was irradiated for 3 minutes at 4 °C with broad-band light from a 2.5 kW Hg/Xe lamp, whose output was filtered through pyrex glass and an aqueous cobaltous nitrate solution (1.7% $Co(NO_3)_2$, 2% NaCl, 9 cm pathlength) (320-380 nm, 1 watt/cm^2, Chapter I). The HMT addition and subsequent irradiation were repeated three times for each tube. Unreacted and photodamaged HMT were removed by chloroform and ether extractions. The irradiated DNA was EtOH precipitated and electrophoresed on a 20% polyacrylamide-7 M urea gel (40 cm x 40 cm x 0.05 cm, 35 watts for 3-4 hours). The crosslink and the unmodified DNA bands were located by autoradiography, excised, and eluted

from the gel with a solution of 50 mM NaCl, 1 mM EDTA. The unmodified DNA and crosslink were finally EtOH precipitated, washed, and dissolved each in 200 µl H_2O. The unmodified DNA was stored at -20°C and the crosslink at 4°C.

C) Preparation of HMT Furan-side Monoadducted 5'-GGGTACCC-3'

About 140 µg of the crosslink prepared as above was dissolved in 9 ml H_2O. The crosslink solution was photoreversed with 297 nm monochromatic light in 3 ml aliquots. Under these conditions, the photoreversal produces a four to one ratio of the furan-side monoadducted oligonucleotide to the pyrone-side counterpart (Chapter I). Each aliquot was irradiated for 65 minutes at a light intensity of 7 X 10^{14} photons per second [determined by actinometry with $K_3Fe(C_2O_4)_3$], vacuum dried in a Speedvac concentrator (Savant Instrument Inc.) without heating, and electrophoresed on a 20% polyacrylamide-7 M urea gel. The unmodified and furan-side monoadducted DNA bands and the crosslink band were isolated as described above, EtOH precipitated, washed, and dissolved in water. About 35 µg of furan-side monoadducted 5'-GGGTACCC-3' was obtained. The unmodified DNA was frozen, and the crosslink and the monoadducted DNA were refrigerated.

D) Preparation of HMT Monoadducted 5'-GAAGCTACGAGC-3'

The monoadducted oligonucleotides were prepared as described in Chapter II.

E) Concentration Measurement

The extinction coefficients per mole of single-stranded oligonucleotide at 260 nm, 25°C, and neutral pH were calculated from the

extinction coefficients of mononucleotide and dinucleotide phosphates (Fasman, 1975). The values for 5'-GGGTACCC-3' (oligonucleotide C), 5'-GAAGCTACGAGC-3' (oligonucleotide A), and its complement 5'-GCTCGTAGCTTC-3' (oligonucleotide B) are 7.5 x 10^4, 12 x 10^4, and 11 x 10^4 M^{-1} cm^{-1}, respectively. The specific activities (5'-end labelled ^{32}P counts per minute per mole of single-stranded oligonucleotde, typically 10^{14} cpm/mole) for these oligonucleotides were thus measured based on the absorption at 260 nm, the extinction coefficients above, and ^{32}P Cerenkov counting. [The extinction coefficients of the furan-side monoadducted and pyrone-side monoadducted 5'-GAAGCTACGAGC-3' (i.e., M_{Fu}-A and M_{Py}-A, respectively) are both equal to 13 x 10^4 M^{-1} cm^{-1} as determined based on the specific activity and the absorption of the HMT-modified oligonucleotides]. The concentrations of the oligonucleotide(s) and the psoralen modified derivative(s) could then be determined by ^{32}P Cerenkov counting.

F) Melting Curve Measurement and Data Analysis

Melting curves were obtained using a Gilford model 250 UV-Vis spectrophotometer with a Gilford model 2527 thermoprogrammer as described earlier (Aboul-ela et al., 1985; Borer et al., 1974). The buffer used for the melting curves of double-stranded 5'-GGGTACCC-3' and its HMT modified derivatives was 1 M NaCl, 10 mM phosphate, and 1 mM EDTA in H_2O at pH 7.0, unless otherwise indicated. The buffer used for melting curves of double-stranded DNA formed by unmodified or monoadducted 5'-GAAGCTACGAGC-3' and its complement was 50 mM NaCl, 10 mM phosphate, and 2 mM EDTA at pH 7.0 because of the high stability of the

double-stranded DNA helices formed in this system. The rate of temperature increase was $1^{o}C$/min. Thus, the melting curves were measured at essentially equilibrium conditions, since the relaxation times of the double-stranded vs. single-stranded oligonucleotide equilibria at our conditions are much smaller than 1 s as estimated on the basis of kinetic data of oligonucleotides (Riesner and Romer, 1973; Craig et al., 1971; Porschke and Eigen, 1971).

The data were analyzed using the van't Hoff method to obtain thermodynamic parameters for double-stranded DNA formation (Martin et al., 1971; Aboul-ela et al, 1985). The melting curves (for example, see figure 1) were analyzed based on a two state model to obtain the melting temperature (the temperature at which 50% of the strands are single-stranded). The equilibrium constant for the double-stranded helix formation by a self complementary oligonucleotide is:

$$K = f/[2(1-f)^{2}C_{T}] \qquad (1)$$

where C_T is the total strand concentration (moles/liter or M) and f is the fraction of strands in double-stranded state. The values of f were obtained by using the method described by Aboul-ela et al. (1985). Since the equilibrium constant is related to the thermodynamic parameters ΔH^{o}, ΔS^{o}, and ΔG^{o} through the equation

$$\Delta G^{o} = -RT\ln(K) = \Delta H^{o} - T\Delta S^{o} \qquad (2)$$

the following equations can be derived at the melting temperature, T_m, at which f = 1/2:

$$\ln(C_T) = \Delta H^{o}/RT_m - \Delta S^{o}/R \qquad (3)$$

$$\Delta G^{o}(T_m) = RT_m\ln(C_T) \qquad (4)$$

Figure 1. Melting curves of the double-stranded DNA formed by 5′-GAAGC[T(HMT)$_{Py}$]ACGAGC-3′ (M_{Py}-A) and 5′-GCTCGTAGCTTC-3′ (B) at different total strand concentrations (C_T) in 50 mM NaCl, 10 mM Na_2HPO_4, 2 mM EDTA, pH 7.0. The absorptions were normalized at 67°C. The data above 68°C were cut off by the plotting program. The base line slopes for determination of melting temperatures were, however, deduced from the complete melting curves, which extended up to 75°C.

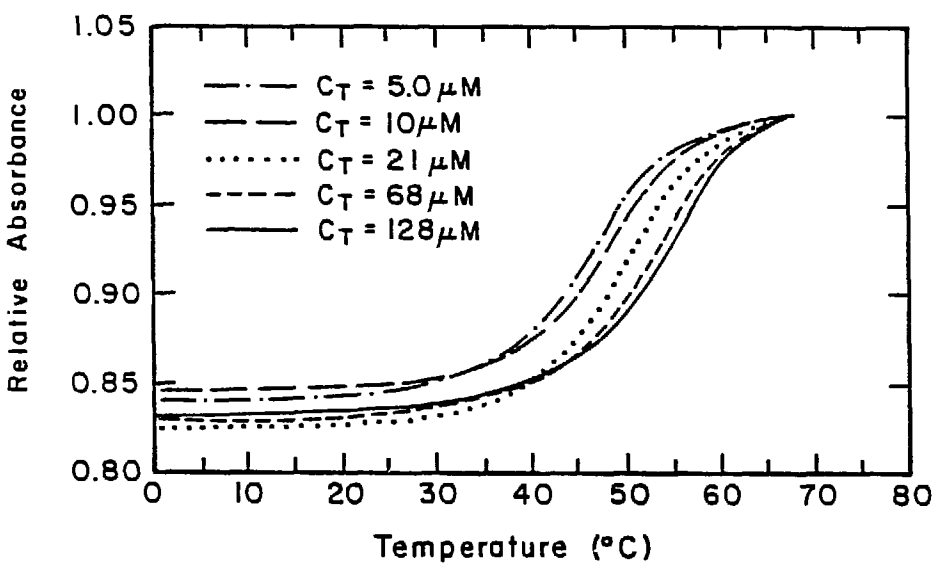
1.05
1.00
0.95
0.90
0.85
0.80
Relative Absorbance
C_T = 5.0 μM
C_T = 10μM
C_T = 21 μM
C_T = 68μM
C_T = 128μM
0
10
20
30
40
50
60
70
80
Temperature (°C)

The formulae corresponding to (1), (3), and (4) for double-stranded DNA formation from non-self complementary oligonucleotides are respectively (5), (6), and (7) (see Aboul-ela et al., 1985):

$$K = 2f/[(1-f)^2 C_T] \quad (5)$$

$$\ln(C_T/4) = \Delta H^c/RT_m - \Delta S^o/R \quad (6)$$

$$\Delta G^o(T_m) = RT_m \ln(C_T/4) \quad (7)$$

Hypochromicity or diminution of absorbance at 260 nm for double-stranded DNA formation is caused by stacking interactions between base pairs. It is temperature dependent because the temperature dependence of the absorption of the single-stranded and double-stranded DNA are different. We therefore chose 50°C as a standard temperature to calculate the hypochromicity since it is around the T_m of most of the oligonucleotides studied here. The hypochromicity was calculated using the following formula as described (Martin et al., 1971):

$$\%H = 100[A_s(50^oC) - A_d(50^oC)]/A_s(50^oC) \quad (8)$$

where %H is the percent hypochromicity and $A_s(50^oC)$ and $A_d(50^oC)$ are the absorbances of the single-stranded and double-stranded species at 50°C respectively, which were obtained by extrapolating the absorbances from the temperature region in which all the strands are single-stranded or double-stranded to 50°C.

3. RESULTS

A) Identification of HMT-DNA adducts

As shown in Chapter II, the HMT is attached through its furan end to the the thymidine residue in 5'-GAAGCTACGAGC-3' (oligonucleotide A) in M_{Fu}-A and through its pyrone end to the thymidine residue in

5′-GAAGCTACGAGC-3′ in M_{Py}-A. The two monoadducted DNA can be represented as 5′-GAAGC[T(HMT)$_{Fu}$]ACGAGC-3′ and 5′-GAAGC[T(HMT)$_{Py}$]ACGAGC-3′, respectively.

The HMT crosslinking site in the 5′-GGGTACCC-3′ crosslink is the thymidine base on each strand (Gamper et al., 1984; also see Chapter I). The site of HMT monoaddition in the furan-side monoadducted 5′-GGGTACCC-3′ is the thymidine base of the DNA strand since it is generated from the photoreversal of the crosslink. Therefore, this monoadducted oligonucleotide can be represented as 5′-GGG[T(HMT)$_{Fu}$]ACCC-3′ and the HMT molecule is at the 3′-side of the thymidine.

B) Stability of the HMT Adducts

It is known that both crosslinks and monoadducted oligonucleotides are photoreversible (Chapters I and II). Therefore, it is important to know whether the HMT adducts are photoreversed during the UV melting curve measurements (at 260 nm). To investigate this the oligonucleotides were recovered by EtOH precipitation after melting curve measurements and then analyzed by gel electrophoresis. The results are shown in figure 2. It is seen that the unmodified oligonucleotide 5′-GAAGCTACGAGC-3′ is separated from its complement 5′-GCTCGTAGCTTC-3′ on this gel (compare Lanes 2, 3, and 4). Therefore, any photoreversal could be monitored by the appearance of an unmodified oligonucleotide 5′-GAAGCTACGAGC-3′ band in the mixture of HMT monoadducted 5′-GAAGCTACGAGC-3′ and its unmodified complement. The results showed that no detectible photoreversal of the monoadducted oligonucleotides

Figure 2. Analysis of oligonucleotides after melting curve measurements. Abbreviations: The abbreviations are as follows: B, 5′-GCTCGTAGCTTC-3′; A, 5′-GAAGCTACGAGC-3′; M_{Fu}-A, 5′-GAAGC[T(HMT)$_{Fu}$]ACGAGC-3′; M_{Py}-A, 5′-GAAGC[T(HMT)$_{Py}$]ACGAGC-3′; XLA and XLB are HMT crosslinked molecules each containing one molecule of the 8mer and one molecule of A (see Chapter II, 8mer is 5′-TCGTAGCT-3′). Lane 1: Mixture of oligonucleotides A and B after melting curve measurements; the ^{32}P specific activity of A is about 6 times larger than that of B. Lane 2: Mixture of B and M_{Fu}-A. Lane 3: Mixture of B and M_{Py}-A. Lane 4: A sample of the crosslinks used to generate the M_{Fu}-A and M_{Py}-A (see chapter II) after an exposure to 254 nm light from a low pressure 40 watt germicidal lamp (3 min. at a distance of about 6 cm). The two crosslinks were not resolved because of the partial kinasing of the complementary 8mer (see the method section in Chapter II).

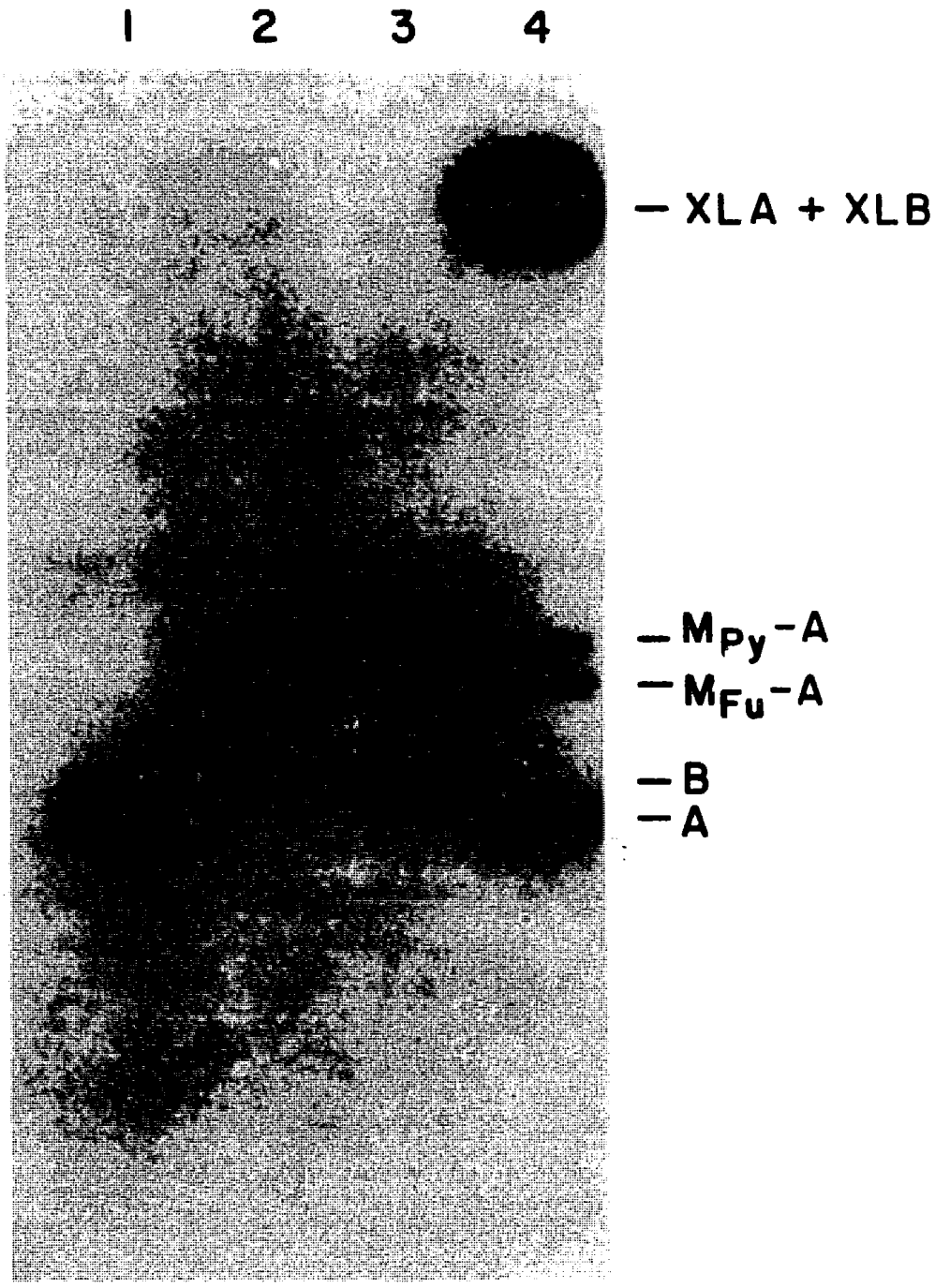
1
2
3
4
— XLA + XLB
— M_{Py}-A
— M_{Fu}-A
— B
— A

occurred during the melting curve measurements (see lanes 2 and 3). Similarly, it was shown that the crosslinked and furan-side monoadducted 5'-GGGTACCC-3' are photochemically stable under the conditions used for the melting curve measurement (data not shown). These data also shows that these adducts are thermally stable under these conditions.

C) Thermostability of Double-stranded DNA Formed from Oligonucleotide 5'-GCTCGTAGCTTC-3' and Unmodified or HMT Monoadducted Oligonucleotide 5'-GAAGCTACGAGC-3'

The effects of HMT monoaddition on the thermostability of double-stranded oligonucleotides were investigated by studying the melting properties of the helices formed between oligonucleotide 5'-GCTCGTAGCTTC-3' and unmodified or HMT monoadducted oligonucleotide 5'-GAAGCTACGAGC-3'. The psoralen was site specifically placed on the thymidine residue of oligonucleotide 5'-GAAGCTACGAGC-3'. The melting curves for the helix formed between 5'-GCTCGTAGCTTC-3' and 5'-GAAGC[T(HMT)$_{Py}$]ACGAGC-3' are shown in figure 1. Similar melting curves were obtained for the helices formed by 5'-GCTCGTAGCTTC-3' and 5'-GAAGCTACGAGC-3' or 5'-GAAGC[T(HMT)$_{Fu}$]ACGAGC-3'. The melting data were analyzed by the van't Hoff method. The van't Hoff plots for the helices with or without a psoralen are shown in figure 3. The thermodynamic parameters thus obtained are listed in Table I. Two sets of free energy values are shown in the table, one at 25°C, which is the commonly used standard temperature, and one at 50°C, which is close to the melting temperatures of the helices. Shown in Table II are the excess thermodynamic parameters due to the HMT additions, which are the

Figure 3. Van't Hoff plots of $\ln(C_T/4)$ vs. $1/T_m$ for the double-stranded helices formed by (Δ): B + M_{Fu}-A, (o): B + M_{Py}-A, and (x): B + A (see Figure 2 for abbreviations) in 50 mM NaCl, 10 mM Na_2HPO_4, 2 mM EDTA, pH 7.0, where C_T is the total strand concentration (M) and T_m is the melting temperature (^oK).

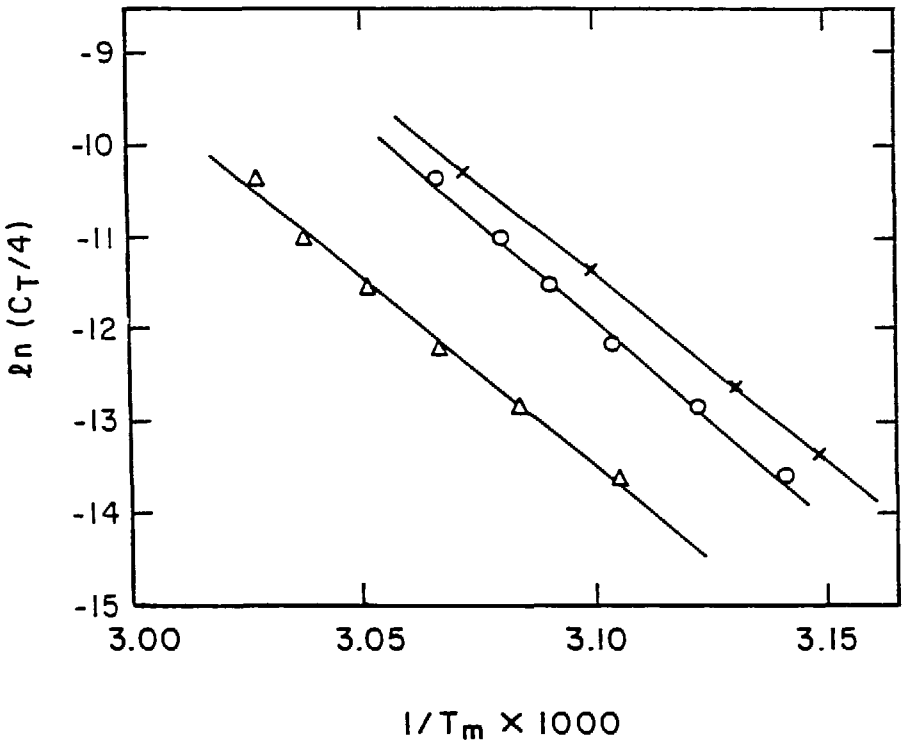
-9
-10
-11
-12
-13
-14
-15
3.00
3.05
3.10
3.15
ℓn (C_T/4)
1/T_m X 1000

Table 1. Thermodynamic Parameters of Double-Stranded DNA Helix Formation.*

Double-Stranded DNA	ΔH° (Kcal/mole)[a]	ΔS° (Cal/°K mole)[b]	ΔG°(25°C) (Kcal/mole)[c]	ΔG°(50°C) (Kcal/mole)[c]	T_m(C_T=100μM) (°C)[d]	Buffer
C:C	-44.5	-119	-9.0	-6.0	51	1M NaCl 10mM Na_2HPO_4 1mM EDTA pH 7.0
M_{Fu}-C: M_{Fu}-C	-35.9	-96	-7.2	-4.8	41	
A:B	-80.9	-228	-12.9	-7.2	51	50mM NaCl
M_{Fu}-A:B	-81.9	-227	-14.2	-8.5	57	10mM Na_2HPO_4
M_{Py}-A:B	-86.3	-244	-13.6	-7.5	53	2mM EDTA, pH 7.0

*Abbreviations: C = 5'-GCGTACCC-3'

M_{Fu}-C = 5'-GGG[T(HMT)$_{Fu}$]ACCC-3'

A = 5'-GAAGCTACGAGC-3'

B = 5'-GCTCGTAGCTTC-3'

M_{Fu}-A = 5'-GAAGC[T(HMT)$_{Fu}$]ACGAGC-3'

M_{Py}-A = 5'-GAAGC[T(HMT)$_{Py}$]ACGAGC-3'

: Indicates a double-stranded DNA formed by the two components.

a. Precision in ΔH° ± 3.5 Kcal/mole.
b. Precision in ΔS° ± 10 Cal/°K mole.
c. Precision in ΔG° ± 0.2 Kcal/mole.
d. Precision in T_m ± 1°C.

Table II. Excess Thermodynamic Parameters due to HMT Additions*

HMT Adducts in	Δ ΔH° (Kcal/mole)	Δ ΔS° (Cal/°K mole)	Δ ΔG°(25°C) (Kcal/mole)	Δ ΔG°(50°C) (Kcal/mole)
M_{Fu}-C: M_{Fu}-C	+8.6	+23	+1.8	+1.2
M_{Fu}-A:B	-1.0	+1	-1.3	-1.3
M_{Py}-A:B	-5.4	-16	-0.7	-0.3

*See Table I for abbreviations and buffer conditions.

Table III. Hypochromicity of Double-Stranded DNA Helices*

Double-Stranded DNA	C:C	M_{Fu}-C:M_{Fu}-C	A:B	M_{Fu}-A:B	M_{Py}-A:B
%H (50°C)	12.0	7.6	14.3	14.7	14.2

*See Table I for abbreviations and buffer conditions. Precision in %H: ± 0.8.

differences between the thermodynamic parameters of the modified and unmodified helices. Results in Tables I and II show that the HMT monoaddition does not destabilize the double helix. Instead, it stabilizes the helices, especially in the case of furan-side monoaddition. The free energy of helix formation at 25°C is changed by -1.3 Kcal/mole for the furan-side monoaddition and by -0.7 Kcal/mole for the pyrone-side monoaddition. Due to the large experimental uncertainties in ΔH° and ΔS°, it is difficult to separate the entropic and enthalpic contributions. It is likely that pyrone-side monoaddition of HMT slightly favors double helix formation through a negative enthalpy contribution, which is -5.4 ± 7.0 Kcal/mole.

When double-stranded DNA is formed from complementary single-stranded DNAs, the stacking interactions between bases increase and consequently the absorption at 260 nm decreases. This is known as the hypochromicity of double-stranded DNA formation. The hypochromicities shown in Table III for the unmodified and the HMT monoadducted double helices described above at 260 nm and 50°C are the same within experimental error. This indicates that stacking interactions between base pairs are only very slightly, if at all, perturbed. It also suggests that the psoralen moiety is stacked with adjacent base pairs. These conclusions are confirmed by the ΔH° of the formation of the monoadducted helices, which are about the same as or slightly more negative than that of the unmodified helix, since stacking interactions are the dominant contributor to ΔH°.

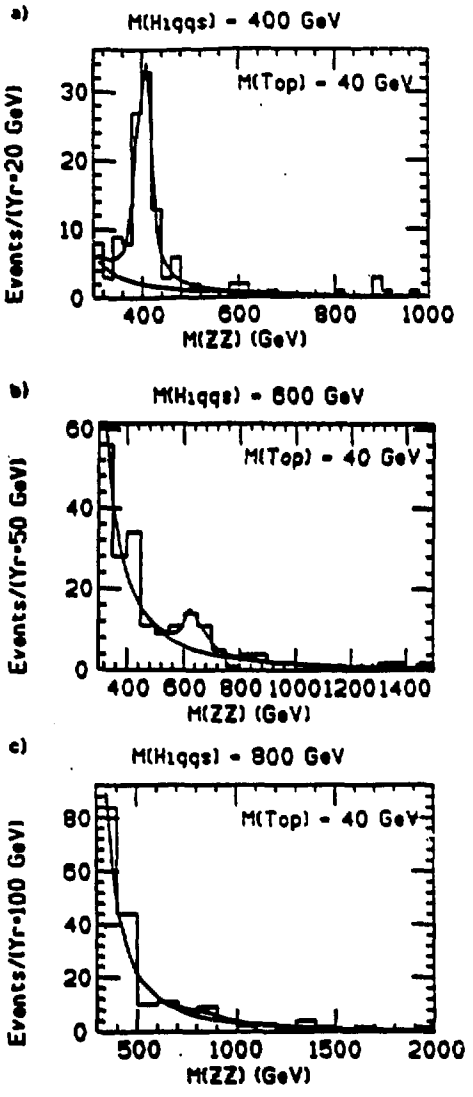

Figure 3: Monte Carlo results for the ZZ invariant mass distribution from the continuum background and the Higgs boson for SSC parameters. The t quark mass is set to 40 GeV. The figure is taken from Ref. [11].

Figure 4. Melting curves of the double helices formed by the unmodified and HMT-modified oligonucleotide 5'-GGGTACCC-3' in 1 M NaCl, 10 mM Na_2HPO_4, 1 mM EDTA, pH 7.0 (except XL1, see below). M_{Fu}-C and C are 5'-GGG[T(HMT)$_{Fu}$]ACCC-3' and 5'-GGGTACCC-3', respectively. M_{Fu}-C:M_{Fu}-C and C:C are the double-stranded DNA formed by these oligonucleotides. XL1, XL2, and XL3 are samples of HMT crosslinked C:C at different concentrations. The total strand concentrations are: [M_{Fu}-C] = 100 μM; [C] = 77 μM; [XL2] = 20 μM; [XL3] = 10 μM; [XL1] = 2 μM in 1 mM TrisHCl, 0.1 mM EDTA, ca. 2 mM NaCl, pH 7.5. The absorptions were normalized at 0°C.

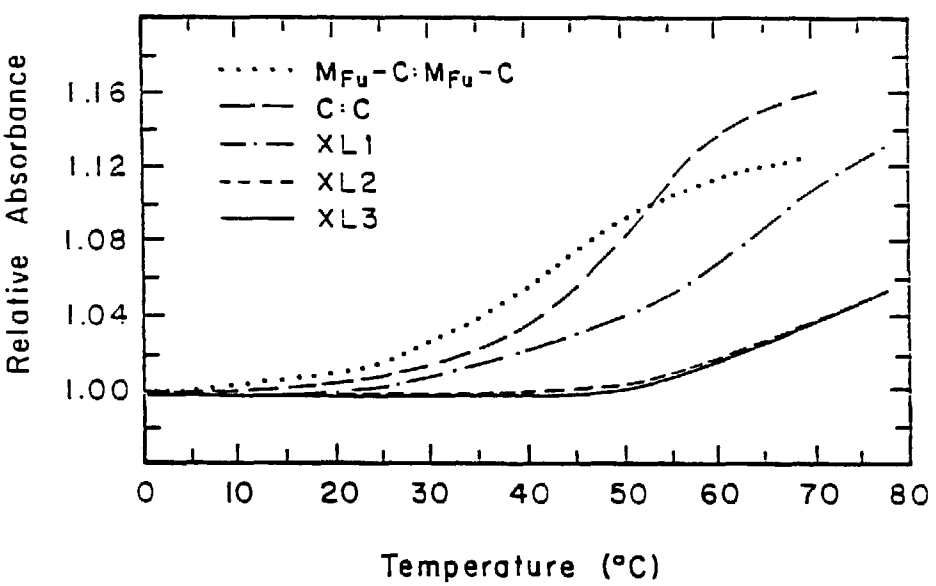
Relative Absorbance
1.16
1.12
1.08
1.04
1.00
0
10
20
30
40
50
60
70
80
Temperature (°C)
M_{Fu}-C:M_{Fu}-C
C:C
XL1
XL2
XL3

Figure 5. Van't Hoff plots of $\ln(C_T)$ vs. $1/T_m$ for the double-stranded helices formed by (Δ): 5'-GGG[T(HMT)$_{Fu}$]ACCC-3', and (x): 5'-GGGTACCC-3' in 1 M NaCl, 10 mM Na_2HPO_4, 1 mM EDTA, pH 7.0, where C_T is the total strand concentration (M) and T_m is the melting temperature (^{0}K).

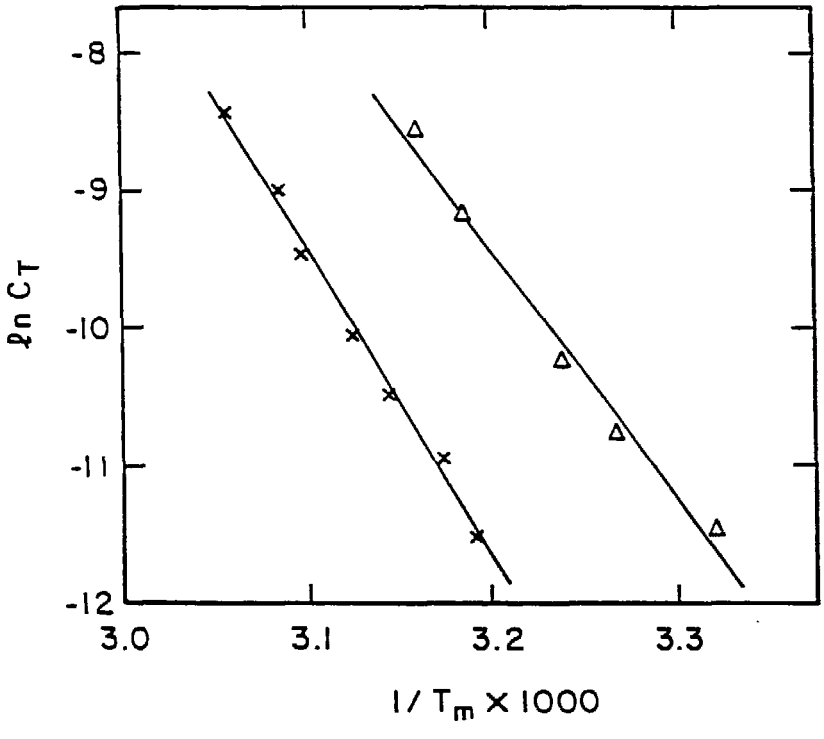
-8
-9
-10
-11
-12
ln C_T
3.0
3.1
3.2
3.3
$1/T_m \times 1000$

tion between the base pairs, probably near the thymidine bulged outside of the helix. This is also supported by a positive increase in ΔS^0, which is +23 Cal/^{0}K mole, and a decrease in hypochromicity upon the monoaddition of two HMT molecule (see Tables II and III).

When the two strands of the double helix formed by 5'-GGGTACCC-3' are crosslinked together by a HMT molecule via the thymidine base on each strand, the helix is remarkably stabilized. As shown in figure 4, the melting of the crosslinked double helix is independent of concentration as expected for a unimolecular process. The crosslinked helix is so stable that it is essentially double-stranded in 1 M NaCl at 51^{0}C, which is the melting temperature of the unmodified helix at a total strand concentration of 100 μM. In a buffer containing only 2 mM NaCl, 1 mM TrisHCl, and 0.1 mM EDTA, at pH 7.5, the melting is broad and the DNA is double-stranded at room temperature. This high stability of a crosslinked double-stranded DNA and the unimolecular nature of the single-stranded to double-stranded DNA transition made possible the kinetic studies of psoralen-DNA photochemistry by Johnston et al. (1977 and 1981).

4. DISCUSSION

The thermodynamic data for the unmodified and HMT-modified double helices formed between oligonucleotide 5'-GAAGCTACGAGC-3' and and its complement 5'-GCTCGTAGCTTC-3' demonstrate that HMT monoaddition to the thymidine residue in 5'-GAAGCTACGAGC-3' stabilizes the helix by 0.7 and 1.3 Kcal/mole at 25^{0}C in 50 mM NaCl for pyrone-side and furan-side monoaddition, respectively. X-ray crystallographic study has shown that

in the monoadduct formed between thymine and 8-methoxypsoralen the thymine and psoralen moieties remain planar and the interplanar angle is about 50° (Peckler et al., 1982). The hypochromicity and enthalpy results reported here indicate that the stacking interactions between the psoralen and adjacent bases are strong enough to compensate for the possible distortions caused by HMT photoaddition. Though the results can not definitely determine whether the stabilizing effect of psoralen monoaddition on the double helix is enthalpic or entropic, the excess thermodynamic values of ΔH° and ΔS° due to pyrone-side monoaddition (Table II) suggest that change in ΔH° may be the dominant factor. Our results do not address whether or not these effects are dependent on the DNA sequence around the psoralen.

Double-stranded DNA melting is known to be dependent on counterion concentration because different amounts of counterions associate with double-stranded and single-stranded DNA. Covalent addition of a psoralen molecule to a DNA helix results in an increase in the separation between phosphates around the psoralen, especially in a double-stranded helix. The negative charge density is altered and the counterion condensation is consequently changed. In order to determine the effect of psoralen monoadditon on the salt dependence of double-stranded DNA stability, the NaCl concentration of the buffer used in the melting curve measurements was increased from 50 mM to 1 M without altering other components of the buffer. The melting temperatures of both the unmodified helix and the two HMT monoadducted double helices were increased by about 11°C at a total strand concentration of 10 μM. No difference

was observed within experimental error (data not shown).

The thermodynamic parameters of double-stranded helix formation by the unmodified or the HMT-monoadducted self complementary oligonucleotide 5'-GGGTACCC-3' demonstrate that upon covalent addition of a HMT molecule to each of the two thymidine bases in the double helix as a furan-side monoadduct, stacking interactions are dramatically reduced as reflected in the decreased hypochromicity and the excess thermodynamic parameters (Table III and II). Since it is impossible for the two HMT moieties to be accommodated between the same two A:T base pairs, this destabilizing effect may be caused by forcing one of the thymidines and its attached psoralen out of the helix. This thymidine and its attached psoralen moiety could be moved out of the helix by rotating the P-O bonds around the thymidine residue. Morden et al. (1983) have reported that the unpaired cytosine in the DNA helix formed by 5'-CA_3CA_3G-3' and 5'-CT_6G-3' is outside of the helix, and this extrahelical cytosine causes a 15°C decrease in the helix melting temperature and a positive increase in ΔG^0 of helix formation at 25°C of 2.9 Kcal/mole in 1 M NaCl buffer at a total strand concentration of 200 μM. This destabilizing effect is the result of an unfavorable change in enthalpy and a possibly favorable change in entropy. Their proton NMR results indicate that there is a change in the stacking interactions between adjacent bases around the extrahelical cytosine. In the case of the double-stranded DNA formed by 5'-GGG[$T(HMT)_{Fu}$]ACCC-3' the free energy of helix formation is changed by +1.8 Kcal/mole at 25°C and the melting point is decreased by 10°C at a total strand concentration of

100 μM as compared to the unmodified helix. The addition of the psoralen molecules is associated with an unfavorable enthalpy change and a favorable entropy change for the helix formation. The monoaddition of a HMT molecule as a furan-side monoadduct in the double helix formed by oligonucleotides 5'-GAAGCTACGAGC-3' and 5'-GCTCGTAGCTTC-3' decreases the ΔG° of the helix formation by 1.3 Kcal/mole at 25°C and increases the melting temperature by about 6°C in 50 mM NaCl (see Tables I and II). The effects due to the exclusion of one of the two HMT-thymidine groups from the helix formed by 5'-GGG[T(HMT)$_{Fu}$]ACCC-3' is similar to the effects of the extrahelical cytosine if one assumes that the other HMT-thymidine group remains inside the helix, and stabilizes the helix to about the same extent as in the case where only one psoralen is attached to the helix as a furan-side monoadduct.

Adenosine is the base with strongest stacking tendency (Morden et al., 1983); it prefers to stack inside the helix even if it cannot form a base pair. Patel et al., (1982) have reported that the extra adenosines stack into the helix formed by the nearly self complementary deoxyoligonucleotide 5'-CGCAGAATTCGCG-3'. In the double helix formed by 5'-GGG[T(HMT)$_{Fu}$]ACCC-3', the adenosine opposite the HMT-thymidine which is outside the helix would be expected to remain inside the helix, though it cannot form hydrogen bonds with that thymidine. The other adenosine may be base paired as usual with the HMT-thymidine group opposing it and the psoralen moiety is probably stacked onto the base pair.

The fact that psoralen monoaddition does not destabilize the dou-

ble-stranded DNA helix suggests that psoralen monoaddition can be very useful in nucleic acid secondary and tertiary structure determination. Psoralens have been widely used as nucleic acid structure probes (Cimino et al., 1985). Traditionally, single-stranded nucleic acids are irradiated in the presence of psoralens with light of 320-400 nm in order to determine possible secondary or even tertiary structures. Double-stranded regions in these nucleic acids are thus crosslinked by psoralen molecules. The crosslinked regions can then be analyzed using the method described by Thompson and Hearst (1983). In these kinds of experiments all the double-stranded regions can be crosslinked by psoralen molecules. This makes the product analysis very difficult. In con- trast, the product analysis can be enormously simplified if one uses a psoralen transfer technology. As described in Chapters I and II, this method allows one to place a psoralen molecule site specifically in a nucleic acid as either a furan-side monoadduct or a pyrone-side monoadduct. Subsequent reconstitution will allow secondary and tertiary structures to reform. Because the stability of monoadducted double helices is similar to that of the unmodified helices, the secondary and tertiary structures reformed should be very close to the structures of the unmodified nucleic acid and they can be determined by irradiating the reconstituted nucleic acid to crosslink possible double-stranded region(s) containing the psoralen monoadduct. The analysis of the crosslinks should be easy since the sequence of the site to which the psoralen was initially transferred is known. The degree of stabilization of psoralen monoaddition on double-stranded nucleic acids should

be dependent on the substitutions on psoralen molecules, since it is known that different psoralen derivatives have different binding constants to nucleic acids (Isaacs et al., 1977, 1982). Different psoralen derivatives can be used in structure determination if one needs to minimize the stabilization effect.

CHAPTER V. EFFECTS OF PSORALEN-DNA ADDUCTS ON TRANSCRIPTION BY T7 AND *E. COLI* RNA POLYMERASES

1. INTRODUCTION

The photoreactivity of psoralens with nucleic acids has found application in the medical and biological fields. Psoralens are used in the treatment of human skin diseases (Fitzpatrick et al., 1982; Parrish et al., 1982) and for probing nucleic structure (Cimino et al., 1985; Rinke et al., 1985; Calvet et al., 1982; Setyono and Pederson, 1984) and nucleic acid-protein interactions (Shi et al., 1987 a, b). The nucleic acid lesions formed by psoralen plus near UV (320-400 nm) have both mutagenic and lethal effects (Fujuta, 1984; Cassier et al., 1984; Piette et al., 1985). It has been shown that psoralen-DNA adducts can be recognized by repair systems (Saffran and Cantor, 1984; Bohr and Nielsen, 1984; Zhen, et al., 1986; van Houten et al., 1986a, b). Ou et al. (1978) and Piette and Hearst (1983) have shown that psoralen interstrand diadducts block replication by *E. coli* DNA polymerase I, whereas psoralen monoadducts act as kinetic attenuators when located on the template strand and have no effect when located on the nick translated strand. However, psoralen monoadducts on a single-stranded DNA template terminate DNA synthesis by *E. coli* DNA polymerase I large fragment, T4 DNA polymerase, and AMV reverse transcriptase (Piette and Hearst, 1985).

I report here the effects of HMT-DNA adducts on transcription by both T7 and *E. coli* RNA polymerases. The psoralen derivative was site specifically placed in two double-stranded synthetic DNA fragments con-

taining a T7 RNA polymerase promoter at one end and an *E. coli* RNA polymerase promoter at the other end as either a diadduct or a furan-side monoadduct. Transcription on the psoralen modified templates indicate that the diadduct blocks transcription by either polymerase as would be expected by preventing strand separation of the template by the polymerase. The furan-side monoadduct also terminates transcription when located on the coding strand but has no effect when attached to the noncoding strand for the two RNA polymerases. The results have been published (Shi et al., 1987, 1988 a, b).

2. Materials and Methods

A) Materials

E. coli RNA polymerase holoenzyme (40-50% active) was a gift from M. Chamberlin. T7 RNA polymerase (185 units/μg) was gift from P. Schultz. All oligonucleotides were synthesized on an automated DNA synthesizer. After synthesis, the oligonucleotides were deprotected and purified by electrophoresis on polyacrylamide-urea gels followed by extraction and EtOH precipitation. T4 DNA ligase and ^{32}P labelled ribonucleotides were purchased from Amersham. T4 polynucleotide kinase was obtained from New England Biolabs. 3'-OCH_3 nucleoside triphosphate derivatives were acquired from Pharmacia Molecular Biologicals. The concentration of double-stranded DNA was measured by absorption using an extinction coefficient of 1.2×10^4 M^{-1} cm^{-1}/bp (van Dyke and Derven, 1983). For the rest, see previous chapters.

B) Preparation of Double-stranded 138mer Templates

The double-stranded 138mer shown in figure 1 contains an *E. coli*

Figure 1. Sequence of the double-stranded 138mer and the oligonucleotides from which the 138mer was synthesized. The numbers with and without prime are relative to the transcription start sites by *E. coli* RNA polymerase and T7 RNA polymerase, respectively. The arrow denotes the thymidine residue on the bottom strand to which an HMT furan-side monoadduct is attached in the M_{Fu}-138mer. The solid triangle denotes the thymidine residue on the top strand which is additionally modified in the XL-138mer.

Bottom Strand: 5'-51mer-18mer-12mer-14mer-43mer-3'

12mer: 5'-GAAGCTACGAGC-3'
14mer: 5'-TGAGGCCATCGATA-3'
18mer: 5'-CAGACTCAGTACGAATTC-3'
43mer: 5'-AAGGTCTAGATCTCCCTATAGTGAGTCGTATTAATTTCGACGT-3'
51mer: 5'-CCCATCCCCCTGTTGACAATTAATCATCGGCTCGTATAATGTGTGGAATTG-3'

Top Strand: 5'-40mer-52mer-46mer-3'

40mer: 5'-TACGTCGAAATTAATACGACTCACTATAGGGAGATCTAGA-3'
46mer: 5'-TCCACACATTATACGAGCCGATGATTAATTGTCAACAGGGGGATGG-3'
52mer: 5'-CCTTTATCGATGGCCTCAGCTCGTAGCTTCGAATTCGTACTGAGTCTGCAAT-3'

DS 138mer:

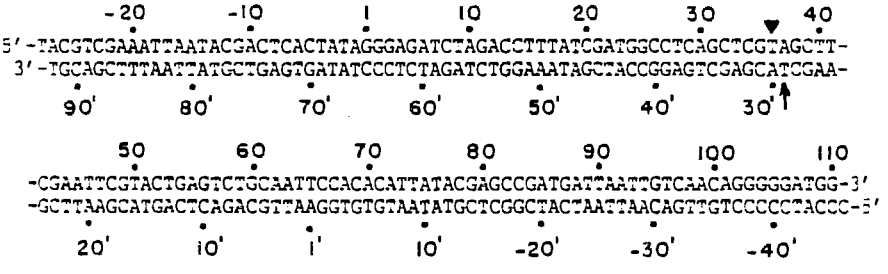

RNA polymerase *tac* promoter (de Boer et al., 1983) at the right end and a T7 RNA polymerase class III promoter (Chamberlin and Ryan, 1982) at the left end with an HMT molecule attached to the site indicated as either an interstrand diadduct (XL-138mer) or a furan-side monoadduct (M_{Fu}-138mer). The unmodified (UM-138mer) and the psoralen modified 138mer templates were prepared as follows.

UM-138mer. The double-stranded UM-138mer was prepared with ^{32}P-label at the 5'-end of either the top strand or the bottom strand. For the top strand labelled DNA, 6 µg of the 40mer (the oligonucleotide at the 5'-end of the top strand, see figure 1) was end-labelled with ^{32}P in 50 µl 1X kinase buffer (50 mM TrisHCl, 10 mM $MgCl_2$, 0.1 mM spermidine, 0.1 mM EDTA, and 5 mM DTT, pH 7.5) containing 0.8 mCi [γ-^{32}P]ATP (3000 Ci/mmole, lyophilyzed to dryness and dissolved back in H_2O) and 20 units of T4 polynucleotide kinase at 37°C for 18 hours. The 46mer (1.6 µg) and 52mer (2.9 µg) of the top strand and the 43mer (6 µg), 18mer (4 µg), 14mer (4.5 µg), and 12mer (3 µg) of the bottom strand were 5'-phosphorylated in 25 µl 1X kinase buffer containing 4.8 mM ATP and 20 units T4 polynucleotide kinase at 37°C for 18 hours. Both kinased samples were then extracted with phenol and precipitated with EtOH. All the phenol extractions in this chapter include two equal volume phenol extractions, pH 7.8, followed by one back extraction of the phenol phase with water to recover any DNA in the phenol phase, and then two ether extractions of the combined aqueous phase. Half of the labelled 40mer (the other half was used in the preparation of M_{Fu}-138mer, see below) was combined with the other phosphorylated oli-

gonucleotides and 2.5 µg of the bottom strand 51mer in ligation buffer. The mixture was heated at 65°C for 10 min. and then incubated at room temperature for at least 20 min. to allow the oligonucleotides to hybridize. BSA (to 200 µg/ml), ATP (to 1.6 mM), and 6 units of T4 DNA ligase were added to the mixture (final volume of 50 µl in 50 mM TrisHCl, 10 mM $MgCl_2$, 8 mM EDTA, and 10 mM DTT, pH 7.5). The DNA was ligated at room temperature (22-24°C) for 1-2 hours and then at 4°C for 18 hours. The product was extracted with phenol, vacuum dried in a Speedvac concentrator (Savant Instrument Inc.) and purified by electrophoresis on an 8% polyacrylamide-8 M urea gel (40 cm x 20 cm x 0.05 cm, 20 W for 2-3 hours; see figure 2A). The mobilities of the two strands were identical and consequently both strands (only one was labelled) were isolated from the gel as a single band. The DNA was then electro-eluted out of the gel and purified by EtOH precipitation. To ensure that all labelled strands were double-stranded, the DNA was further purified by non-denaturing 8% polyacrylamide gel electrophoresis. The top strand labelled UM-138mer was prepared following the same procedures as above except that the 51mer of the top strand instead of the 40mer of the bottom strand was ^{32}P labelled in the kinase reaction. The overall yield was about 40%.

M_{Fu}-138mer. An HMT furan-side monoadduct was site specifically placed on the thymidine residue of the bottom strand 12mer as previously described in Chapter II. This monoadducted 12mer was substituted for the 12mer of the bottom strand during a ligation reaction like that above to produce end labelled double-stranded 138mer with a site spec-

Figure 2. Preparation of double-stranded 138mer templates. A) 8% polyacrylamide-8 M urea gel purification of the ligation products with ^{32}P-label on the 5'-end of the top strand 40mer. B) Preparation of XL-138mer from end-labeled M_{Fu}-138mer. The M_{Fu}-138mer was irradiated with 320-380 nm light and electrophoresed on an 8% polyacrylamide-8 M urea gel to separate it from the XL-138mer.

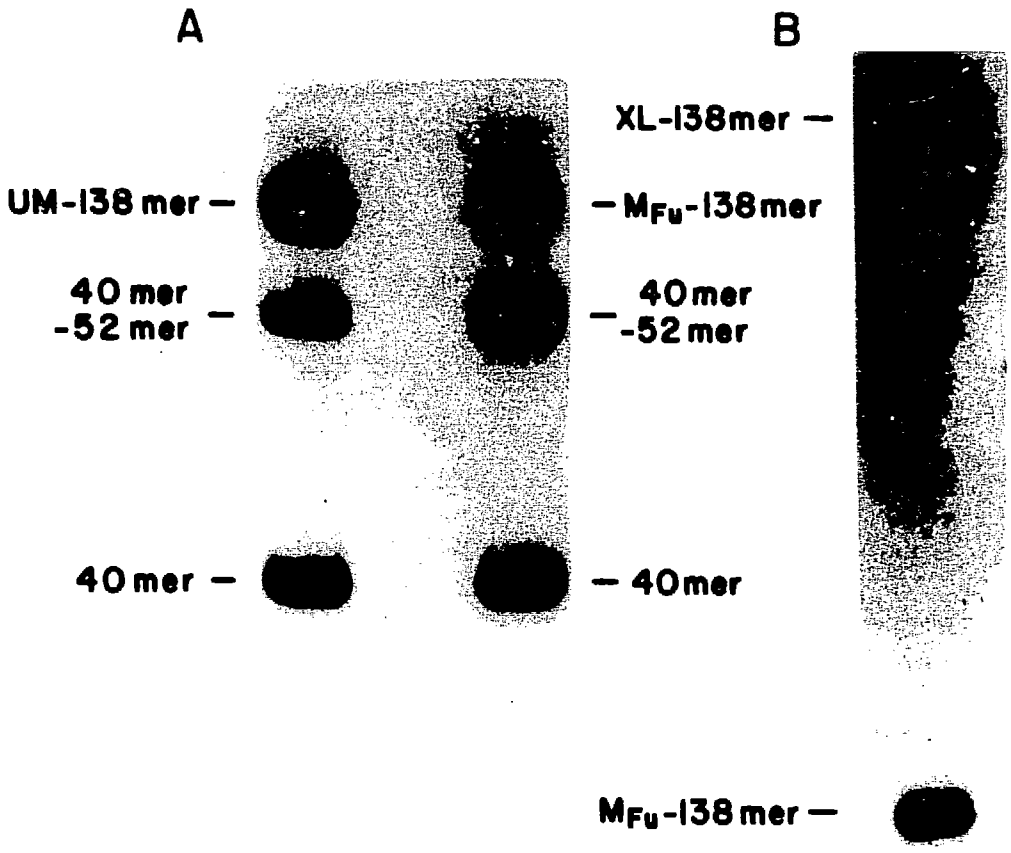
A
B
UM-138 mer
40 mer
-52 mer
40 mer
XL-138mer
M_{Fu}-138mer
40mer
-52 mer
40mer
M_{Fu}-138 mer

ific HMT monoadduct (M_{Fu}-138mer). Though psoralen monoadducted short oligonucleotides run slower than the corresponding unmodified oligonucleotides (Gamper et al., 1984; and previous chapters), it was observed that incorporation of a psoralen monoadduct into oligonucleotides longer than 60 bases did not alter their electrophoretic mobility (data not shown and see figure 2A). Therefore, the component strands of the M_{Fu}-138mer could be isolated as a single band in a denaturing gel. The M_{Fu}-138mer was purified as above with a 25% overall yield.

XL-138mer. The purified M_{Fu}-138mer (in 10 mM TrisHCl, 1 mM EDTA, and 10 mM NaCl, pH 7.4) was heated at 65°C for 5 min, cooled at room temperature for 20 min, and then irradiated at room temperature for 3 min with 0.4 W/cm^2 320-380 nm light from a 2.5 kW Hg/Xe lamp whose output was filtered through a pyrex glass and an aqueous cobaltous nitrate solution [1.7% $Co(NO_3)_2$, 2% NaCl, 9 cm pathlength] (Chapter I), which resulted in 80% conversion of the M_{Fu}-138mer to XL-138mer. The XL-138mer was separated from the M_{Fu}-138mer by electrophoresis on an 8% polyacrylamide-8 M urea gel (see figure 2B). The crosslink band was isolated from the gel and purified as above.

C) Preparation of Double-stranded 140mer templates

The double-stranded 140mer shown in figure 3 is similar to the double-stranded 138mer. The psoralen modified 140mer contains an HMT molecule attached to the site indicated as either an interstrand diadduct (XL-140mer) or a furan-side monoadduct (M_{Fu}-140mer). The 140mer templates were prepared similarly as described above.

Figure 3. Sequence of the double-stranded 140mer and the oligonucleotides from which the 140mer was synthesized. The numbers with and without prime are relative to the transcription start sites by *E. coli* RNA polymerase and T7 RNA polymerase, respectively. The arrow denotes the thymidine residue on the bottom strand to which an HMT furan-side monoadduct is attached in the M_{Fu}-140mer. The solid triangle denotes the thymidine residue on the top strand which is additionally modified in the XL-140mer.

Bottom Strand: 5'-58mer-12mer-70mer-3'

12mer: 5'-GAAGCTACGAGC-3'
58mer: 5'-TACGTCGAAATTAATACGACTCACTATAGGGAGATCTAGACCTTTATCGATGGCCTCA-3'
70mer: 5'-GAATGTTCGTACTCACTCTCCAATTCCACACATTATACGAGCCGATGATTAATTGTCAAC-
-AGGGGGATGG-3'

Top Strand: 5'-65mer-75mer-3'

65mer: 5'-CCCATCCCCCTGTTGACAATTAATCATCGGCTCGTATAATGTGTGGAATTGGAGAGTGAG-
-TACGA-3'
75mer: 5'-ACATTCGCTCGTAGCTTCTGAGGCCATCGATAAAGGTCTAGATCTCCCTATAGTGAGTCG-
-TATTAATTTCGACGT-3'

DS 140MER:

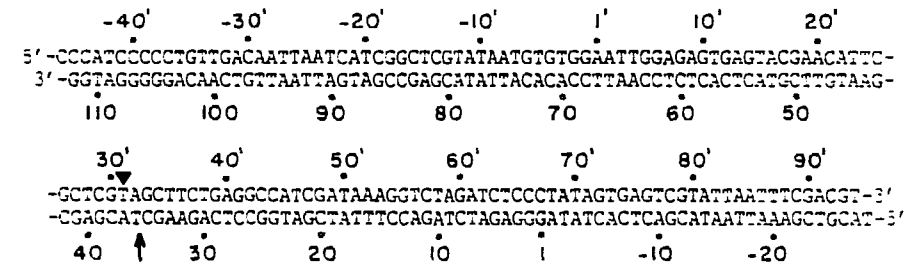

D) Transcription and RNA Sequencing by *E. coli* RNA Polymerase

The DNA template (1 nM) and *E. coli* RNA polymerase holoenzyme (30 nM) were preincubated together at 37°C for 5 min in transcription buffer (40 mM TrisHCl, 10 mM $MgCl_2$, 100 mM KCl, 0.1 mM EDTA, and 0.1 mM DTT, pH 8.0). Transcription was initiated by the addition of 0.2 mM ATP, 0.2 mM GTP, 0.2 mM CTP, and 10 µM [α-^{32}P]UTP (100 Ci/mmol) (final concentrations in 25 µl of transcription buffer). After incubation at 37°C for additional 10 min., the reaction was stopped by adding 100 µl stop buffer (3.75 mM EDTA, 125 mM LiCl, 3 µg carrier tRNA, and 0.05% SDS) followed by EtOH precipitation (3 fold EtOH at -20°C for overnight). The precipitated RNA transcripts were dissolved in 95% deionized formamide containing 10 mM TrisHCl, 1 mM EDTA, and 10 mM NaCl, pH 7.4 and marker dyes and analyzed on a 20% polyacrylamide-7 M urea gel.

RNA sequencing was modeled after the protocol described by Reisbig and Hearst (1981). The reactions were performed as above except for the concentration of the nucleotide being analyzed, which was 13.4 µM for ATP, 6.7-13.4 µM for GTP, 10 µM for UTP, or 13.4 µM for CTP, respectively. The corresponding 3'-OCH_3 nucleoside triphosphate analog concentrations were 0.48 mM A, 0.4 mM G, 0.48 mM U, or 0.2 mM C, respectively. The sequencing samples were treated and analyzed as described above.

E) Transcription and RNA Sequencing by T7 RNA Polymerase

Transcription was modeled after the protocol described by Ikeda and Richardson (1986). The template (0.5 nM) was incubated with T7 RNA

polymerase (0.9 μM) in 25 μl T7-trans buffer (50 mM TrisHCl, 10 mM $MgCl_2$, pH 8.0) in the presence of 0.2 mM ATP, 0.2 mM GTP, 0.2 mM CTP, and 10 μM [α-^{32}P]UTP (100 Ci/mmole) at 37°C for 10 min. The reaction was stopped by adding 100 μl stop buffer (3.75 mM EDTA, 125 mM LiCl, 25 mM KCl, 3 μg carrier tRNA, and 0.05% SDS) followed by EtOH precipitation (3 fold EtOH at -20°C for overnight). The precipitated RNA transcripts were then dissolved in 95% deionized formamide containing 10 mM TrisHCl, 1 mM EDTA, and 10 mM NaCl, pH 7.4 and analyzed on an 8% polyacrylamide-8 M urea gel.

RNA sequencing reactions were performed as above except for the concentration of the nucleotide being analyzed. When [α-^{32}P]UTP was used as the labelled nucleotide, it was maintained at 10 μM (100 Ci/mmole) for all samples. The concentration of the nucleotide being analyzed was 6.7 μM ATP, 17 μM GTP, 10 μM UTP, or 13.4 μM CTP. The corresponding 3'-OCH_3-NTP concentrations were 0.24 mM A, 0.2 mM G, 0.24 mM U, or 0.2 mM C, respectively. When [α-^{32}P]CTP was used as the labelled nucleotide, it was maintained at 10 μM (100 Ci/mmole) for all samples. The UTP concentration was 0.2 mM for analyzing A, G, C, and 6.7 μM for analyzing U. Other conditions were identical as when [α-^{32}P]UTP was used as the labelled nucleotide. Sequencing reaction samples were treated and analyzed the same as above.

3. RESULTS

A synthetic double-stranded 138mer with or without an HMT adduct at a specific site was constructed from eight oligonucleotides as shown in figure 1. First, an unmodified double-stranded 138mer (UM-138mer)

was constructed with an *E. coli* RNA polymerase tac promoter (de Boer et al., 1983) at the right end and a T7 RNA polymerase class III promoter (Chamberlin and Ryan, 1982) at the left end by hybridizing and ligating the oligonucleotides together. The UM-138mer thus produced contained a 5'-^{32}P label on either the top strand or the bottom strand. The product was purified by denaturing polyacrylamide gel electrophoresis. An autoradiogram of a purification gel is shown in figure 2. To insure that all labelled strands were in the double-stranded state, the DNA was further purified by non-denaturing polyacrylamide gel electrophoresis to remove single-stranded DNA.

To prepare the psoralen modified 138mers (M_{Fu}-138mer and XL-138mer), the psoralen derivative, HMT (4'-hydroxymethyl-4, 5', 8-trimethylpsoralen) was first site specifically placed at the thymidine residue in the bottom strand 12mer as a furan-side monoadduct (Chapter II). This modified oligonucleotide was then hybridized and ligated with the rest of the oligonucleotides to obtain M_{Fu}-138mer (see figure 2). The product was purified as above and irradiated with broad band near UV light (320-380 nm) to produce the XL-138mer. The XL-138mer was purified by denaturing 8% polyacrylamide-8 M urea gel electrophoresis. As shown in figure 2, the XL-138mer ran very slowly as a diffuse band. We believe that the diffuse character of the band reflects the high stability of the duplex form of the XL-138mer (Chapter IV) such that even in the presence of 8 M urea it was not completely denatured and consequently ran inhomogeneously in the gel. This interpretation is supported by the fact that the band ran faster and

was more diffuse in a 7 M urea gel compared to an 8 M urea gel and the observation that upon photorevesal at 254 nm only one sharp product band, corresponding to the 138mer, was generated.

Relative to *E. coli* RNA polymerase promoter, the HMT molecule was attached to T-29 of the noncoding strand as a furan-side monoadduct in the M_{Fu}-138mer and to both T-29 of the noncoding strand and T-30 of the coding strand as an interstrand diadduct in the XL-138mer. The effects of these HMT additions on transcription by *E. coli* RNA polymerase was investigated by analyzing the RNA transcripts produced from the unmodified and HMT-adducted templates. 3'-OCH_3 RNA sequencing on the unmodified template was used to determine the exact termination sites. It is known that during transcription the RNA polymerase transiently unwinds the DNA template and that a newly incorporated RNA chain forms a short RNA-DNA hybrid with the coding strand (Von Hippel et al., 1984). Consequently, the covalent interstrand HMT diadduct in the XL-138mer blocks forward movement of RNA polymerase by preventing DNA unwinding and strand separation. As expected, figure 4 shows that the HMT diadduct efficiently blocked elongation thus yielding a transcript terminated with U-29, i.e., one base before the adducted thymidine (T-30) on the coding strand (lanes 3 and 4). In contrast, the furan-side monoadduct on the noncoding strand had no effect on transcription (compare lanes 1 and 2). Both the UM-138mer and the M_{Fu}-138mer yielded runoff transcript (the slowest moving band). The band running slightly faster than the runoff transcript corresponds to transcription termination in the AT rich region at the right end of the

Figure 4. Analysis of *E. coli* transcripts from UM-138mer, M_{Fu}-138mer, and XL-138mer. Lanes A, G, U, and C are the corresponding 3'-OCH_3 RNA sequencing reactions. Lane 1: UM-138mer; Lane 2: M_{Fu}-138mer; Lanes 3 and 4: XL-138mer.

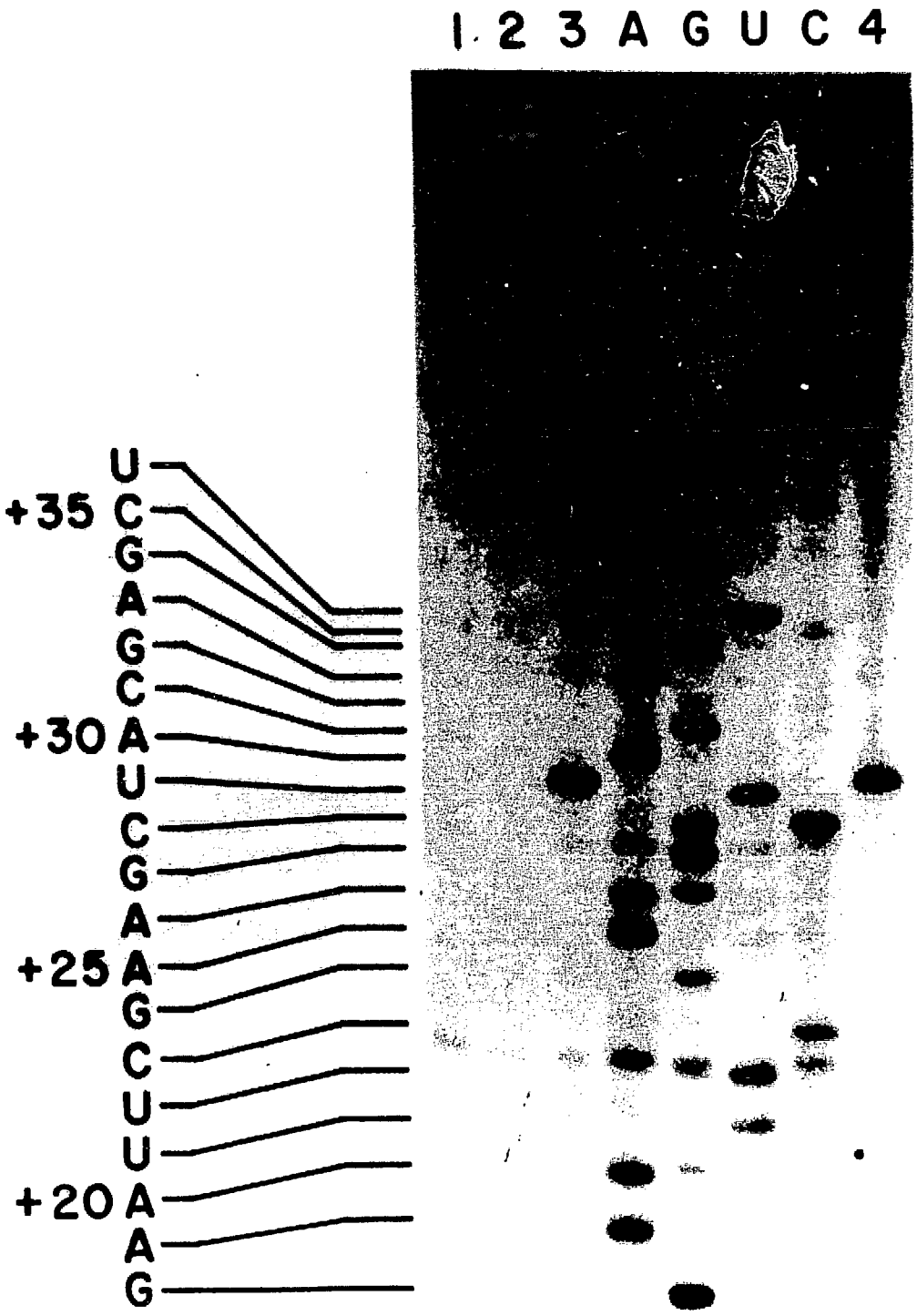
1 2 3 A G U C 4
+35
+30
+25
+20
U
C
G
A
G
C
A
U
C
G
A
A
G
C
U
U
A
A
G

template and it decreased when higher UTP concentration was used (data not shown).

The double-stranded 138mer templates also contains a T7 RNA polymerase promoter and consequently the effects of psoralen addition on transcription by T7 RNA polymerase could be examined. As shown in figure 1, the HMT molecule was attached to T-37 of the coding strand in M_{Fu}-138mer and both T-36 of the non-coding strand and T-37 of the coding strand in XL-138mer relative to T7 RNA polymerase promoter.

3'-OCH_3-NTP analogs are efficient chain terminators of *E. coli* RNA polymerase and have been used to sequence *E. coli* RNA polymerase transcripts (Axelrod et al., 1978; Reisbig and Hearst, 1981; and above). We used these analogs to sequence T7 RNA polymerase transcripts. As shown in figure 5, 3'-OCH_3-UTP and 3'-OCH_3-CTP were efficiently used by the polymerase to produce the respective terminated transcripts. 3'-OCH_3-ATP and 3'-OCH_3-GTP did not yield efficient termination at the A and G positions, respectively. At high concentrations of 3'-OCH_3-ATP and 3'-OCH_3-GTP, transcription was completely blocked, whereas at low concentrations, transcript reactions yielded full length runoff transcript (110 bases long). Since the DNA sequence was known, the RNA sequence could be easily determined from the U and C sequencing lanes.

Results in figure 5 indicate that transcription on the UM-138mer yielded full length runoff transcript (lane 5) while the furan-side monoadduct on the coding strand and the diadduct (lanes 4 and 3, respectively) blocked transcription by T7 RNA polymerase to yield identical aborted transcripts. The major transcript for both the

Figure 5. Analysis of T7 transcripts from UM-138mer, M_{Fu}-138mer, and XL-138mer. The transcription and sequencing samples were electrophoresed on an 8% polyacrylamide-8 M urea gel. 138mer: 5'-end labelled template, which is not visible in lanes 4 (M_{Fu}-138mer) and 5 (UM-138mer) because much less template was loaded in these lanes and in lane 3 (XL-138mer) because the XL-138mer ran much slower and is not shown here. 110mer: runoff transcript from UM-138mer. Lanes 1 and 2: 3'-OCH_3 RNA sequencing for U and C, respectively; [α-^{32}P]CTP was used as the label. Lanes 3-5: transcripts from the XL-138mer, M_{Fu}-138mer, and UM-138mer, respectively. Lanes 6-9: 3'-OCH_3 RNA sequencing for C, U, G, and A, respectively; [α-^{32}P]UTP was used as the label. All samples had equal amounts of template but the amount of the transcripts loaded for the XL-138mer, M_{Fu}-138mer, and UM-138mer was, respectively, 1/6, 1/6, and 1/30 of the rest of the lanes.

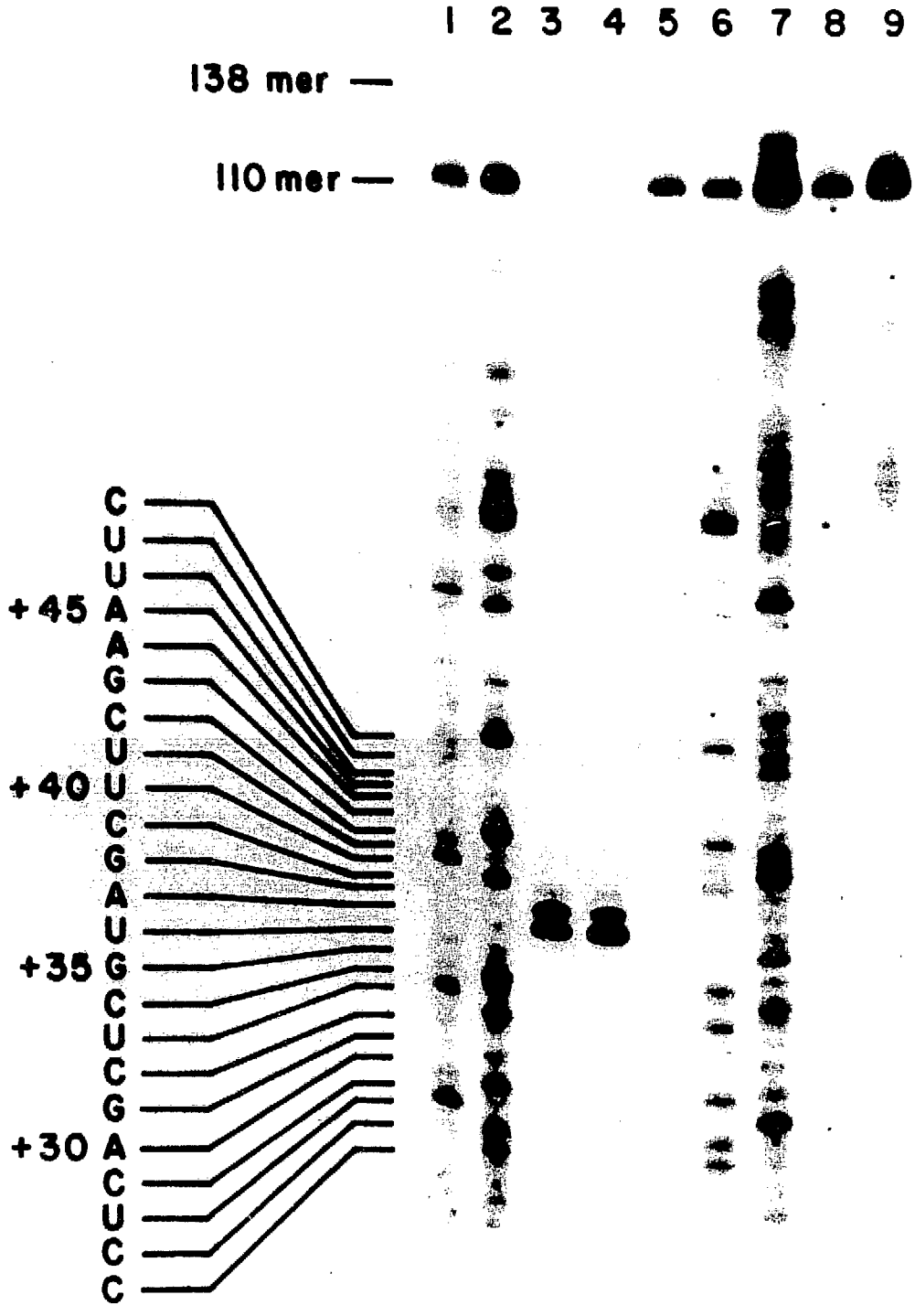
1 2 3 4 5 6 7 8 9
138 mer
110 mer
+45
+40
+35
+30
C
U
U
A
A
G
C
U
U
C
G
A
U
G
C
U
C
G
A
C
U
C
C

M_{Fu}-138mer and the XL-138mer was the product of transcription termination at the HMT adducts, i.e., termination at U(+36). There were also two minor transcripts, corresponding to the addition of, respectively, one or two more bases after U(+36). Lowary et al. (1986) have observed that T7 RNA polymerase can insert a randomly selected residue to the 3'-end of the RNA chain before terminating, thus yielding a transcript longer than the expected runoff transcript. Our data suggest that this same phenomenon may occur in T7 elongation complexes blocked by a psoralen adduct. In the case of the UM-138mer, transcripts containing one or two additional bases could not be resolved from the expected runoff transcript. However, we did observe transcripts running slower than the runoff transcript; the origin of these products is not clear.

These results show that the HMT diadduct blocks transcription by both T7 and *E. coli* RNA polymerases. The furan-side monoadduct has totally different effects depending on which strand it is located. When it is located on the coding strand as for the T7 RNA polymerase, it blocks transcription. However, when it is located on the noncoding strand as for the *E. coli* RNA polymerase, it does not affect transcription. These results thus suggest that a monoadduct on a coding strand might also block transcription by *E. coli* RNA polymerase. To test this hypothesis, a double-stranded 140mer was constructed.

As shown in figure 3, the double-stranded 140mer consists of five oligonucleotides, three on the bottom strand and two on the top strand. These oligonucleotides were hybridized together and ligated to produce the unmodified 140mer (UM-140mer). To make the HMT modified templates,

a bottom strand 12mer which contained an HMT furan-side monoadduct on the thymidine residue was used in the hybridization and ligation reaction to produce M_{Fu}-140mer with an HMT furan-side monoadduct attached to T-32 of the coding strand relative to *E. coli* RNA polymerase promoter. The M_{Fu}-140mer was then irradiated with 320-380 nm light to generate the XL-140mer with an HMT attached to both T-32 of the coding strand and T-31 of the noncoding strand relative to *E. coli* promoter.

Figure 6 shows the results of transcription on the double-stranded 140mer templates. The UM-140mer yielded runoff transcript and some shorter transcripts (lane 1), which were reduced upon increasing the UTP concentration during transcription (data not shown). The HMT diadduct in the XL-140, as expected, stopped transcription by the polymerase (lane 2). Similar to the result obtained with T7 RNA polymerase, the HMT furan-side monoadduct on the coding strand blocked elongation by *E. coli* RNA polymerase (lane 3). Both the XL-140mer and M_{Fu}-140mer templates yielded a transcript 31 bases long, i.e., terminated one base before the HMT adducted thymidine residue (T-32) on the coding strand.

These 140mer templates also contain a T7 RNA polymerase promoter as indicated in figure 3. Due to an error most likely generated during oligonucleotide synthesis, the promoter in the 140mer template did not serve as a efficient promoter for T7 RNA polymerase and very few transcripts were produced (data not shown). However, the data obtained does suggest that the diadduct blocks transcription as expected and the furan-side monoadduct on the noncoding strand seems to have no effect

Figure 6. Analysis of *E. coli* transcripts from UM-140mer, M_{Fu}-140mer, and XL-140mer. Lanes A, G, U, and C are the corresponding 3'-OCH_3 RNA sequencing reactions. Lane 1: UM-140mer; Lane 2: XL-140mer; Lane 3: M_{Fu}-140mer.

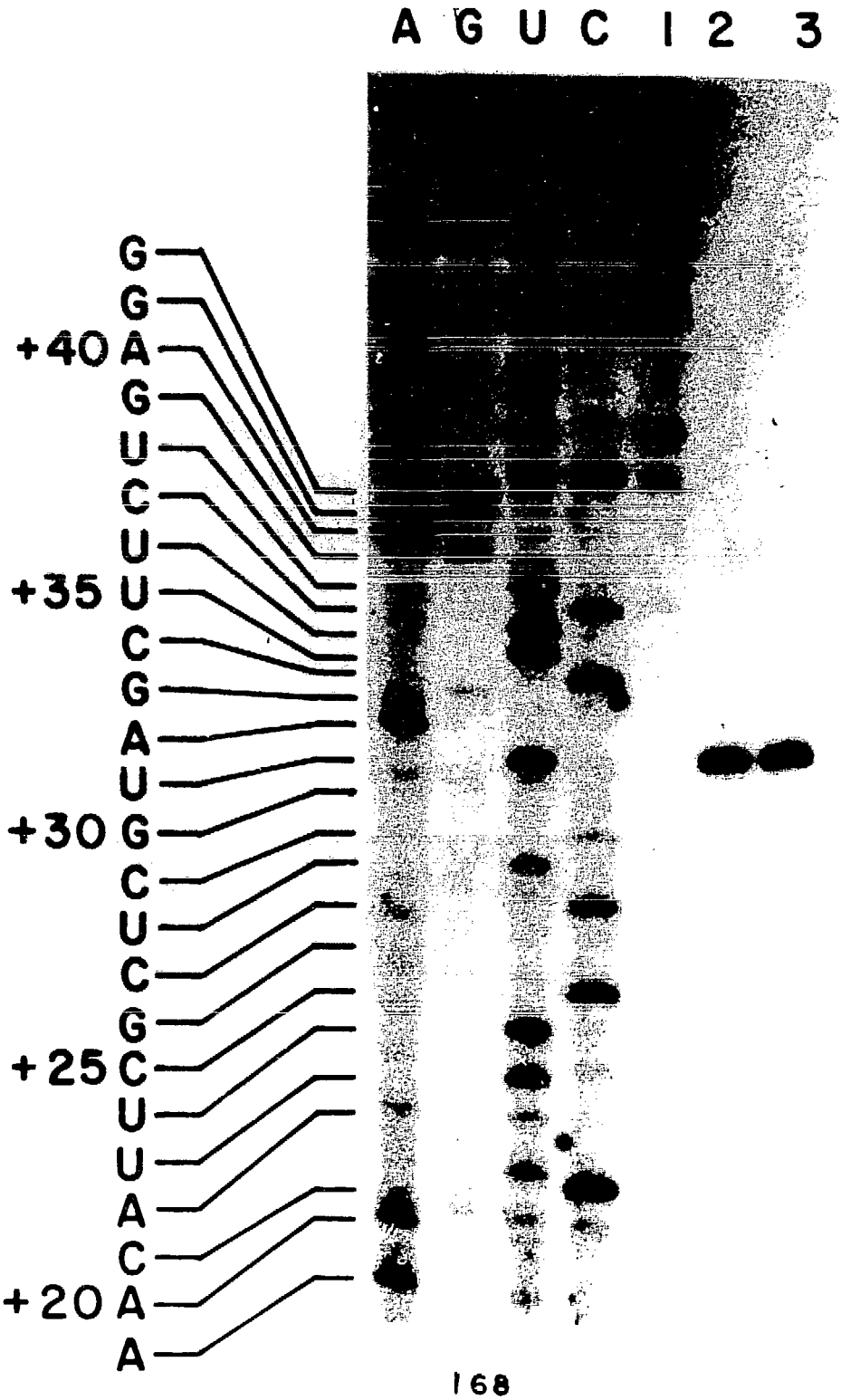
A G U C 1 2 3
G
G
+40 A
G
U
C
U
+35 U
C
G
A
U
+30 G
C
U
C
G
+25 C
U
U
A
C
+20 A
A

on transcription by the polymerase.

4. Discussion

DNA damages, such as thymidine glycols (Clark and Beardsley, 1986; Ide et al., 1985), abasic sites (Sagher and Strauss, 1985), UV photoproducts (Chan et al., 1985; Piette and Moore, 1982; Moore et al., 1981), and chemical lesions (Moore et al., 1981, 1982), often block DNA synthesis. Psoralen interstrand diadducts in double-stranded DNA (Piette and Hearst, 1983) and psoralen monoadductes in single-stranded DNA (Piette and Hearst, 1985) have been shown to arrest replication. In contrast, psoralen monoadducts in double-stranded DNA have a negligible effect on DNA synthesis by *E. coli* DNA polymerase I (Piette and Hearst, 1983). Little is known about the effects of psoralen adducts on transcription. We have determined, using a double-stranded DNA substrate, that either orientational isomer of an HMT diadduct effectively blocks transcription by *E. coli* and T7 RNA polymerases whereas a furan-side HMT monoadduct arrests transcription only when on the template strand. The mechanism of transcription termination may be fundamentally different for the two lesions. While the monoadducted thymidine is no longer able to function as a template for RNA synthesis, the diadduct blocks elongation either due to the noncoding character of the adducted thymidine or by preventing DNA unwinding and strand separation. A similar pattern of inhibition has been observed for DNA synthesis by T4 DNA polymerase (Kodadek and Gamper, 1987). These results indicate that a psoralen monoadducted thymidine is usually noncoding and that the ability of *E. coli* DNA polymerase I to synthesize past such a modified base

may be an example of error-prone synthesis. Although we have not examined the effects of a psoralen pyrone-side monoadduct on transcription, its structural similarity to the furan side monoadduct would imply a similar mode of action.

Though the results reported here are the *in vitro* effects of psoralen adducts on transcription, analyses of cellular RNA in cells treated with psoralen and near UV have also shown that these adducts block RNA synthesis (Prager et al., 1983; Shames et al., 1983; Nocentini, 1978). Hanawalt (1986) has suggested that the blockage of transcription, i.e., the arrested elongation complex, could act as a signal of DNA repair. If this is true, our data would suggest that monoadducts on a coding strand would be repaired efficiently, whereas those on a noncoding strand would not. Recent data by Vos and Hanawalt (1987) supports such a prediction.

Using 3'-OCH_3 RNA sequencing the exact transcription termination sites induced by the HMT diadduct and the HMT furan-side monoadduct on the coding strand have been determined. In both cases, RNA synthesis by the T7 and *E. coli* RNA polymerases proceeds to the 5' neighboring base of the HMT adducted thymidine residue on the coding strand. It is known that during the elongation process, *E. coli* RNA polymerase opens approximately 12-17 base pairs of DNA template (Von Hippel et al., 1984; Gamper and Hearst, 1982). Based on an unwinding angle analysis of *E. coli* RNA polymerase complexes at different stages of transcription, Gamper and Hearst (1982) have proposed a topological model for transcription elongation, in which they suggest the existence of unwindase

and rewindase activities on the polymerase. During elongation, the unwindase opens the DNA helix while the rewindase, lagging by 17 base pairs, displaces the RNA transcript and reseals the DNA helix. If the model is correct, our results suggest that the unwindase and the catalytic sites of the enzyme are located very close to each other since RNA synthesis proceeds up to the diadduct site in both the XL-138mer and XL-140mer templates, where the unwinding site is assumed to be arrested by the interstrand crosslink. Using an in vitro transcription assay, Phillips and Crothers (1986) have found that RNA synthesis by *E. coli* RNA polymerase proceeds up to bases adjacent to preferred intercalation sites of the drug actinomycin D. Since drug intercalation requires a double-stranded helix, this result also suggests that strand separation does not extend more than one or two bases ahead of the catalytic site of the enzyme. If the same arguement about the unwinding site and catalytic site is true for T7 RNA polymerase, our results would suggest that the two sites of the T7 enzyme are very close to each other.

CHAPTER VI. EFFECTS OF COVALENT ADDITIONS OF A PSORALEN ON THE STRUCTURE OF DOUBLE-STRANDED NUCLEIC ACIDS

1. Introduction

As shown in the previous chapter, psoralen-thymidine adducts (di-adducts and coding strand monoadducts) block transcription by *E. coli* and T7 RNA polymerases. Similar effects have been observed for DNA polymerases (Ou et al., 1978; Piette and Hearst, 1983 and 1985; Kodadek and Gamper, 1987). X-ray crystallographic study has shown that in the monoadduct formed between thymidine and 8-methoxypsoralen the thymidine and psoralen moieties remain planar and the interplanar angle is about 50^0 (Peckler et al., 1982). A flow linear dichroism study of furan-side monoadducts of several psoralen derivatives in DNA has also suggested that the plane of a psoralen in a adduct is deviated from normal to the helix axis (Vigny et al., 1987). Thermadynamically, however, the stacking interactions between the psoralen in a monoadduct and the adjacent bases are strong enough to compensate for the possible distortions of the DNA helix caused by the psoralen addition (see Chapter IV).

Based on the X-ray crystallographic data on the psoralen-thymidine monoadduct, a theoretical molecular structure of a DNA helix containing a psoralen diadduct has been proposed and a sharp kink at the diadduct site has been predicted (Kim et al., 1983). The kink caused by a psoralen diadduct was predicted to be greater than that caused by a pyrimidine dimer (Pearlman, et al., 1985). However, no appreciable bends in DNA by psoralen diadducts could be detected based on non-denaturing polyacrylamide gel electrophoresis and differential

decay of birefringence in solution (Sinden and Hagerman, 1984).

RecA protein from *E. coli* has been shown to be involved in SOS repair and mutagenesis by first binding to damaged DNA to initiate the SOS processes (Witkin and Kogoma, 1984; Little and Mount, 1982; Ennis et al., 1985). Lu et al. (1986) have recently shown that RecA protein binds preferentially to double-stranded DNA with UV lesions. I have used their this to analyze the effects of psoralen addition on the binding of double-stranded DNA by recA protein. Our results showed that the addition of one psoralen inter-strand diadduct in a double-stranded 138mer enhanced the binding of recA whereas the addition of one psoralen furan-side monoadduct had no effect, thus suggesting that the diadduct causes deformation of the helix but the monoadduct does not have a big effect. Consistent with this, we have also shown in collaboration with Dr. Jack Griffith (Univ. of North Carolina at Chapel Hill) that the crosslinked 138mer appeared to be preferentially bent at the diadduct site and the monoadducted 138mer appeared to be similar to the unmodified 138mer under an electron microscope.

2. Materials and Methods

A) Materials

Rec A protein from *E. coli* was a gift from Chi Lu. The stock recA solution was diluted with 20 mM TrisHCl, 10% glycerol, 0.1 mM EDAT, 1 mM DTT, pH 7.5. ATP-γ-S was obtained from Boehringer Mannheim Biochemicals. For the rest see previous chapters.

B) Nitrocellulose Filter Binding Experiment

The minifold from Schleicher and Schuell, Inc. was used for the

experiment. The nitrocellulose filters (BA85, 8.2 mm diameter) were presoaked in 1 mM ATP for at least 30 min. before use.

The binding of recA to double-stranded 138mers (UM-138mer, M_{Fu}-138mer, and XL-138mer as described in Chapter V) was quantified by nitrocellulose filter binding following the precedures of Lu et al. (1986). 5'-end labeled double-stranded 138mer (3.3 nM) and recA (0-6 μM) in 10 μl reaction buffer (20 mM TrisHCl, 10 mM $MgCl_2$, 1 mM EDTA, 30 mM NaCl, 1 mM DTT at indicated pH) was incubated at 37°C for 5 min followed by the addition of 1 μl 2 mM ATP-γ-S in the reaction buffer and incubation at the 37°C for additional 10 min. The binding reaction was stopped by adding 100 μl reaction buffer (4°C). The solution was then filtered through nitrocellulose filter (BA85, 8.2 mm diameter) at a flow rate of 2 ml/min. The filter was washed twice with 200 μl the reaction buffer (4°C) at the same flow rate. The filter was then dissolved in 5 ml scintillation fluid (mixture of 12 g PPO-BisMSB from ICN Radiochemicals, 2 l toluene, 1 l triton X-100, and 333 ml H_2O) and counted. A sample for each reaction set counted without filtration was used as the control. The background binding of DNA to the filter was determined by the counts from samples without recA. The binding was expressed as percentage of the total counts retained on the filter. Most of the data were averages of two independent experimental results.

3. Results

A) Binding of Psoralen Modified 138mers by RecA Protein

RecA protein binds to both single-stranded and double-stranded DNA. It has been shown that recA binds preferentially to damaged

double-stranded DNA, such as UV irradiated DNA (Lu et al., 1986), due to structural destortion of the DNA. The binding of recA protein to psoralen modified 138mer was followed by nitrocellulose filter binding experiments. The unmodified and psoralen modified 138mers were prepared as described in Chapter V. A single HMT molecule was attached as either a furan-side monoadduct (M_{Fu}-138mer) or an inter-strand diadduct (XL-138mer) at a specific site in a double-stranded 138mer. As shown in figure 1A, recA binded to UM-138mer with a saturation retention of about 30%. Irradiation of the UM-138mer with 254 nm light increased the retention of the DNA by recA, consistent with the results of Lu et al. (1986). Addition of a furan-side monoadduct in the double-stranded 138mer had little effect on the recA binding to the DNA. (In fact, we consistently observed a slight reduced binding of recA to M_{Fu}-138mer as compared to UM-138mer.) In contrast, addition of a psoralen as a diadduct in the 138mer increases the retention by approximately two fold.

The pH dependence of the recA binding to 138mers was also investigated. Figure 1B shows the pH dependence at 3 μM recA and similar behavior was observed at other recA concentrations. In general increasing pH decreased both the binding to unmodified double-stranded DNA and the damaged DNA. The preferential binding to XL-138mer was observed at all pH tested. At pH ≥ 9.0, the binding could not be determined due to the high background binding of DNA to nitrocellulose filter in the absence of protein.

B) Electron Micrographic Examination of the 138mers

Electron microscopy has been proven to be very powerful in inves-

Figure 1. A) Binding of recA to 138mers at pH 7.5 as assayed by nitrocellulose filter binding. UM: UM-138mer; UM + hv: UM-138mer irradiated with 254 nm light (3 kJ/m^2); M_{Fu}: M_{Fu}-138mer; XL: XL-138mer.B) Binding of recA (3 μM) to 138mers at different pH as assayed by nitrocellulose filter binding.

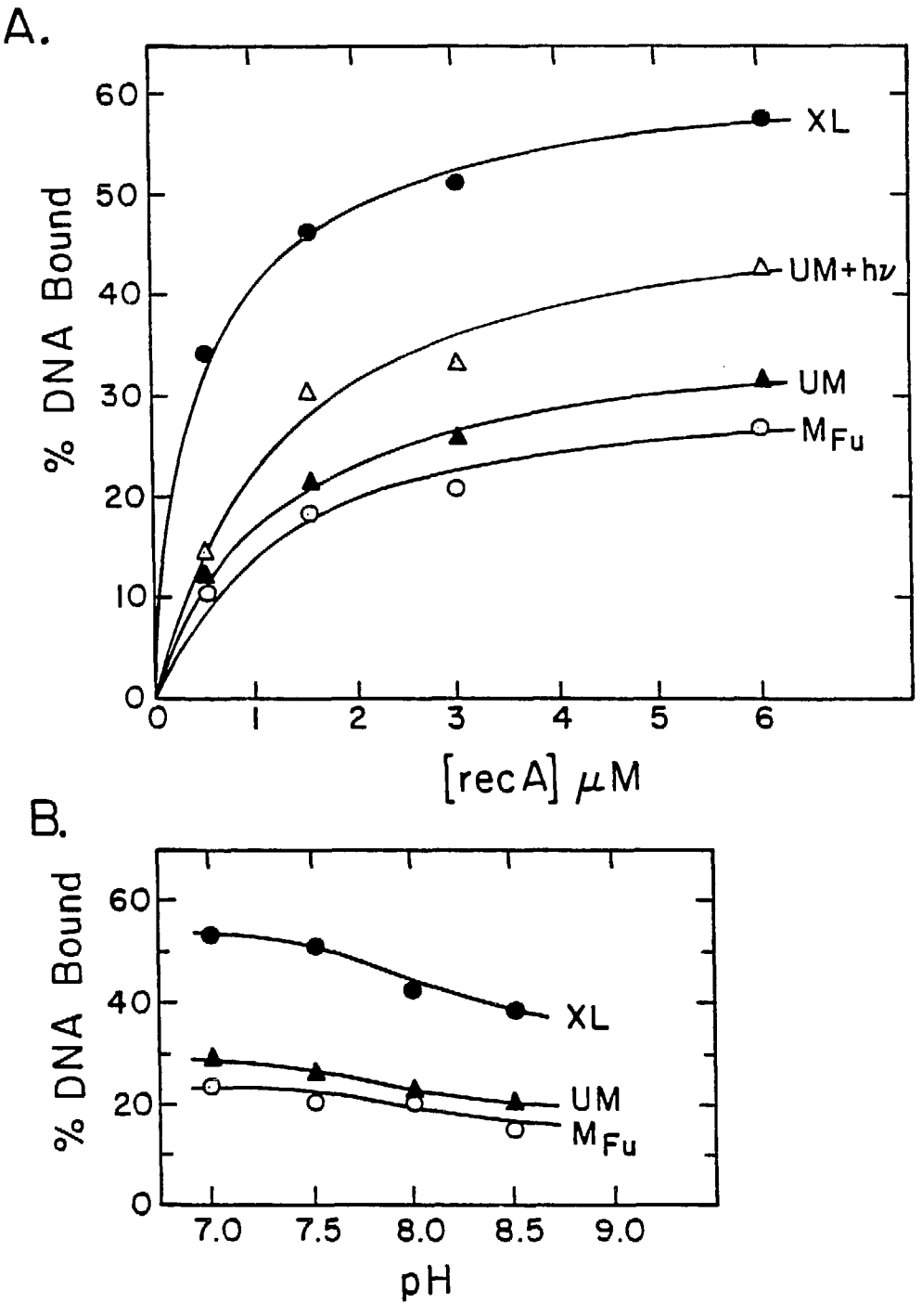
A.
% DNA Bound
60
50
40
30
20
10
0
0
1
2
3
4
5
6
[recA] μM
XL
UM+hν
UM
M Fu
B.
% DNA Bound
60
40
20
0
7.0
7.5
8.0
8.5
9.0
pH
XL
UM
M Fu

tigating DNA structures such as DNA bending and circle formation (Griffith et al., 1986). In collaboration with Dr. Jack Griffith (Lineberger Cancer Research Center, Univeristy of North Carolina at Chapel Hill), we have investigated the possible structure deformation by psoralen additions on double-stranded DNA with electron microscopy. When the unmodified and psoralen modified 138mers were examined under an electron microscope, they all looked similar and curved due to DNA flexibility (data not shown). No significant difference was observed. It is known that the binding of the drug distamycin to kinetoplast DNA fragment reduces or even abolishes DNA curvature due to the stiffening of the DNA helix (Wu and Crothers, 1984; Griffth et al., 1986). To eliminate DNA curvature due to DNA flexibility, distamycin was added during the mounting of DNA. The electron micrograms of the DNA mounted this way are shown in Figure 2. The UM-138mer appeared as straight molecules (figure 2A) and the XL-138mer appeared as molecules bent or curved at the middle where the psoralen was attached (figure 2B). M_{Fu}-138mer was similar to UM-138mer. Statistical results of the electron microscopic data shown in Tables I and II indicate that the XL-138mer was preferentially bent with a factor of 2-6 over that of the control, i.e., the UM-138mer. In contrast, the monoadducted DNA resembled the unmodified 138mer. Thus an HMT monoadduct does not bend the DNA appreciably whereas an HMT inter-strand diadduct induces a sharp kink or bent at the site of the psoralen addition under these conditions. The structure change accompanied with psoralen additions observed under an electron microscope is, therefore, consistent with

Figure 2. Electron micrograms of 138mers in the presence of distamycin. A) UM-138mer. B) XL-138mer.

B
A

Table I. Fraction of the Molecules Scored Having a Stiff Bend (Kink) 40-60% from One End of the DNA and in Which the Bend Measures between 30-52°. (Expressed as percent relative to the fraction scoring as straight.)

DNA	UM-138mer	M_{Fu}-138mer	XL-138mer
%	31	67	180

Table II. Electron Microscopic Analysis of 138mers with a Single Psoralen Molecule Bound at the Center. (861 molecules scored.)

DNA	% Molecules Straight	% Molecules with a Bend at 0-30% from one End	% Molecules with a Bend at 40-60% from one End
UM-138mer	35	36	29
M_{Fu}-138mer	26	39	35
XL-138mer	11	36	53

that revealed by recA binding experiments.

4. Discussion

The effects of psoralen additions on the structure of double-stranded DNA were first suggested by a theoretical model of a double-stranded DNA containing a psoralen diadduct based on the X-ray crytallographic data of the 8-methoxypsoralen-thymidine furan-side monoadduct Kim et al. (1983). A sharp kink due to the psoralen diadduct was predicted from the model. Since then, several independent experiments have been performed to test the model. Two dimensional proton NMR data of a double-stranded DNA containing a 4'-aminomethyl-4, 5', 8-trimethylpsoralen-tymidine diadduct show that the diadduct causes a kink in its vicinity without much effect on the DNA structure a few base pairs away from the diadduct and the diadduct unwinds the DNA helix by about 56° (Tomic et al., 1987). Our data here, especially the electron micrographic results also suggest a bend produced by a psoralen diadduct. However, Siden and Hagerman (1984) did not detect any appreciable bending due to psoralen addition by the decay of linear birefrigence. Similarly, we have failed to detect any bending by the diadduct in XL-138mer by non-denaturing gel electrophoresis, which can reveal any abnormal mobility of a bent molecule compared to a straight one (Wu and Crothers, 1984). A possible explanation for these controversial results could be that the DNA helix around a psoralen diadduct is flexible on the time scale of non-denaturing gel electrophoresis or linear birefrigence measurement. In fact, NMR data suggests significant flexibility on one side of a crosslinked DNA (Tomic et al.,

1987). Clearly, the final resolution of the controversy waits for further study.

We have found that monoaddition of HMT does not destabilize double-stranded DNA. Instead, it slightly stabilizes the helix, suggesting that the psoralen group is stacked with DNA bases (Chapter IV). Similarly, using a flow linear dichroism technique Vigny et al. (1987) have found that the psoralen moieties of the furan-side monoadducts of different psoralen derivatives are stacked with DNA base pairs with the plane of the psoralen moieties deviated slightly from normal to the helix axis. Thus the psoralen moiety in a monoadduct is intercalated in between DNA base pairs. One end of the psoralen of the monoadduct is attached with one strand and other is fairly flexible in the helix. Such a structure might not cause any bending or other dramatic structural change to the DNA helix. Consistent with this, our recA binding and electron microscopic experiments did not reveal any appreciable difference between the furan-side monoadducted and unmodified DNA fragments.

The preferential binding of recA to XL-138mer might have some significance in the repair of psoralen diadduct. Though a psoralen monoadducted DNA can be repaired by removing the short fragment containing a psoralen monoadduct by uvrABC followed by filling the gap by DNA polymerase and sealing the break by DNA ligase, the action of uvrABC can only cut around the psoralen diadduct on the DNA strand attached to the furan-end of the psoralen, leaving the psoralen adducted fragment still attached to the DNA (Van Houten et al., 1986a, b). To

completely repair a psoralen diadduct, a more complicated mechanism has be be utilized. RecA has been shown to be involved in the SOS repair (Little and Mount, 1982; Ennis et al., 1983). The preferential binding of recA to psoralen crosslinked DNA thus implicates a possible diadduct repair mechanism, in which recA is involved, for example, a mechanism involving general recombination.

PART III

APPLICATIONS OF PSORALEN-DNA PHOTOCHEMISTRY

CHAPTER VII. INTERACTION OF *E. COLI* RNA POLYMERASE WITH DNA IN AN ELONGATION COMPLEX ARRESTED AT A SPECIFIC PSORALEN ADDUCT SITE

1. Introduction

Transcription consists of three major steps: initiation, elongation, and termination (McClure, 1985). Initiation is the most well understood process in transcription. First, RNA polymerase binds to a promoter in a DNA template to form a closed complex. Second, a segment of DNA in the closed complex is melted out thereby giving the so-called open complex. Third, the binding of the first ribonucleoside triphosphate converts the open complex into an initiation complex. Elongation can then start in the presence of all four ribonucleoside triphosphates. The nature of the binding of RNA polymerases to promoters has been successfully elucidated using both chemical and enzymatic footprinting techniques (Siebenlist et al., 1980; Siebenlist and Gilbert, 1980; Spassky et al., 1985; Hofer et al., 1985; Carpousis and Gralla, 1985; Duval-Valentin and Ehrilich, 1986; Spassky, 1986; Ikeda and Richardson, 1986). These methods include DNase I footprinting, methidiumpropyl-EDTA-Fe(II) footprinting, methylation protection and interference, and ethylation interference. These aforementioned studies have shown that the binding of *E. coli* RNA polymerase, a multi-subunit enzyme with a molecular weight of 450 kD, to its promoters protects the template DNA in the region from -50 to +20 from enzymatic and chemical cleavage. In this region specific sites also exhibit enhanced cleavage due to RNA polymerase binding. These same types of experiments have revealed that the pattern of DNA protection by RNA polymerase differs

from complex to complex (Spassky et al., 1985; Hofer et al., 1985; Spassky, 1986).

Relatively little is known about transcription elongation complexes, though limited information has been obtained from footprinting experiments using incomplete ribonucleotide mixtures to stop the RNA polymerase at a specific position after synthesizing a short oligoribonucleotide (Carpousis and Gralla, 1985; Straney and Crothers, 1985). These and similar studies have shown that *E coli* RNA polymerase protects 26 to 40 bp of the template DNA (Rohrer and Zillig, 1977; Carpousis and Gralla, 1985; Straney and Crothers, 1985). Here we report the interactions of *E. coli* RNA polymerase with DNA in an elongation complex arrested at a site specific psoralen crosslink as probed by DNase I protection experiments.

As shown in Chapter V, the well understood photochemistry between psoralens and double-stranded nucleic acids has enabled us to construct a double-stranded 138mer DNA fragment containing an *E. coli* RNA polymerase promoter at one end and a psoralen diadduct at a specific site in the middle of the fragment. Transcription of the crosslinked DNA was blocked by the psoralen diadduct. DNase I footprinting experiments showed that the arrested RNA polymerase protected the DNA fragment from about 22 nucleotides upstream to 15 nucleotides downstream of the diadduct on both the coding and the noncoding strands. A model of the transcription elongation complex is presented. The results here have been published (Shi et al., 1988a).

2. Materials and Methods

A) Materials

T4 polynucleotide kinase was obtained from New England Biolabs. RNase-free DNase I (Cat. No. 8047SA, 10 μg/μl, ≥10,000 units/mg), Exonuclease III (Cat. No. 8013SA, 65 units/μl), and restriction enzymes were acquired from Bethesda Research Laboratories. See previous chapters for the rest.

B) DNase I Footprinting of Initiation and Elongation Complexes

Initiation Complexes. The initiation complex (or open complex) between *E coli* RNA polymerase and its promoter was formed by incubating the end labelled template (0.5 nM) with the polymerase (0.4-20 nM) in 50 μl 1X open-c buffer (40 mM TrisHCl, 10 mM $MgCl_2$, 20 mM KCl, 0.1 mM EDTA, and 0.1 mM DTT, pH 8.0) at room temperature (22-24°C) for 11 min with or without ATP, the first nucleotide of the transcript (Gamper and Hearst, 1982). 2 μl calf thymus DNA (1 μg/μl) and 5 μl 100 mM $CaCl_2$ were added to the complex. DNase I digestion was initiated with the addition of 2 μl of 20,000 fold diluted DNase I (prepared immediately before use by diluting the stock enzyme in 30 mM NaOAc, pH 6.4, 25% glycerol). The reaction was terminated after 4 min by adding 2.5 μl 0.25 M EDTA to the mixture and was then phenol extracted. Finally, the solution was dried in a Speedvac concentrator and analyzed by electrophoresis on an 8% polyacrylamide-8 M urea gel for the top strand labelled DNA and on a 5% polyacrylamide-8 M urea gel for the bottom strand labelled DNA. The gel was transferred to Whatman 3MM chromatography paper, dried in a Bio-Rad Model 483 Slab Dryer, and

autoradiographed. The same procedures were used for footprinting at 37°C except that the complex was formed at the higher temperature for 5 min and then digested with 2 µl of 200,000 fold diluted DNase I for 4 min at that same temperature, i.e. 10 fold less DNase I than that at room temperature since DNase I is more active at the elevated temperature.

Elongation Complexes. The end-labelled template (0.5 nM) was incubated with the polymerase (4-24 nM) in the presence of ATP or ApA in open-c buffer at 37°C for 5 min. Elongation was then started with the addition of a premixed aliquot of NTPs at 37°C. When heparin was used, it was added before the addition of NTPs. The final NTP concentrations were 0.2 mM GTP, 0.2 mM UTP, 0.2 mM CTP, and unless otherwise indicated 0.05 mM ATP. The final reaction volume was 50 µl in 1X open-c buffer. After 5 min incubation at 37°C, the samples were transferred to a room temperature water bath (22-24°C) followed by additions of 2 µl of 5 M NaCl, 2 µl of 1 µg/µl calf thymus DNA, and 5 µl of 100 mM $CaCl_2$. We have observed that the DNase I digestion was partially inhibited in the presence of high concentrations of NaCl. Consequently, in the presence of NaCl these digestions were carried out using 2.5 µl of 2,000 fold diluted DNase I, i.e., 12.5 fold more than that used in the absence of NaCl. The nuclease reaction was stopped after 4 min with 2.5 µl 0.25 M EDTA and was followed by phenol extraction. The samples were split into two equal portions. One was kept in the dark. The other was irradiated for 16 min in a 1.5 ml Eppendorf tube (coverd with Reynolds Film 910 to cut off light below 240 nm) with 1 mW/cm^2 254 nm light from

a low pressure germicidal lamp (estimated with a black-ray ultraviolet meter, Model J-225, short UV meter, Ultra-violet Products, Inc. San Gabriel, CA.) to photoreverse the HMT diadduct. Both aliquots were taken to dryness in a Speedvac concentrator and analyzed by electrophoresis on an 8% polyacrylamide-8 M urea gel. The gel was then dried and autoradiographed. DNase I footprinting of the elongation complex was also performed under the following conditions: initiation and elongation were both performed at room temperature followed by DNase I digestion at the same temperature, or initiation and elongation were performed at 37°C followed by digestion at the same temperature with 2.5 µl of 20,000 fold diluted DNase I, i.e., 10 fold less than at room temperature. All protocols yielded the same results.

C) Analysis of Transcription Complexes by Non-denaturing Polyacrylamide Gel Electrophoresis

Transcription complexes were analyzed by non-denaturing 4% polyacrylamide gel electrophoresis according to the procedure of Straney and Crothers (1985). The transcription initiation and elongation complexes were formed at 37°C as described above in a final volume of 20 µl. The samples were then adjusted to room temperature and supplemented with 0.8 µl of 1 µg/µl calf thymus DNA and, if indicated, 0.8 µl of 5 M NaCl. The samples were immediately adjusted to 6% sucrose, 0.02% bromophenol blue and 0.02% xylene cyanol FF with 10X loading buffer and loaded on a non-denaturing 4% polyacrylamide gel (40 cm x 20 cm x 0.08 cm). The gel was run at room temperature (5 W with an aluminum plate clamped on the glass plate) until xylene cyanol FF had migrated 10-15

cm. When the DNA template was labelled, the gel was dried and autoradiographed. For quantitation, the labelled bands in the dried gel were excised and counted. When the RNA transcripts were labelled, the gel was autoradiographed without drying and the labelled complexes were directly excised from the wet gel. The RNA transcripts in the complexes were eluted into 50 mM LiCl, 0.1 % SDS, and 1 mM EDTA and EtOH-precipitated in the presence of 5 μg carrier tRNA. The purified RNA transcripts were then analyzed by 8% polyacrylamide-8 M urea gel electrophoresis.

3. Results

A) Rationale and Template Construction

A homogeneous population of elongation complexes at a specific site is required in order to study the interaction of the polymerase with DNA during elongation. It is known that during transcription the RNA polymerase transiently unwinds the DNA and that a newly incorporated RNA chain forms a short RNA-DNA hybrid with the coding strand (Von Hippel et al., 1984). A covalent inter-strand crosslink blocks forward movement of RNA polymerase by preventing DNA unwinding and strand separation. When the crosslink is engineered to a site-specific location, the stalled transcription complexes are homogeneous and amenable to study by DNA footprinting techniques. Using such a complex it is also possible to determine the locations relative to the DNA substrate of the unwinding and the polymerizing sites of the enzyme.

As described in Chapter V, a double-stranded 138mer was constructed with an *E. coli* RNA polymerase tac promoter (de Boer et al., 1983)

at one end of the helix (see figure 1, note that the top strand vs. bottom strand is shown opposite to that shown in figure 1 of Chapter V). This double-stranded DNA was prepared with a 5'-end label on either the top or bottom strand. Both the UM-138mer and the psoralen modified 138mers were prepared. The psoralen was attached to T-29 of the non-coding strand as a furan-side monoadduct in M_{Fu}-138mer and to both T-29 of the non-coding strand and T-30 of the coding strand as a diadduct in XL-138mer. As shown in Chapter V, the monoadduct on the non-coding strand does not affect transcription by *E. coli* RNA polymerase whereas the diadduct, as expected, blocks transcription. Consequently, only UM-138mer and XL-138mer were used in the DNase I footprinting experiments described below.

B) DNase I Footprints of the Initiation Complexes

Correct binding of RNA polymerase to a promoter is essential for the initiation process and therefore transcription by the polymerase. The interaction of the *E coli* RNA polymerase with the synthetic tac promoter was probed by DNase I footprinting. The results obtained with the UM-138mer are shown in figure 2 and demonstrate that the polymerase protects up to +17 (all numbers related to DNase I footprints are relative to the transcription start site) on the coding strand and +22 on the noncoding strand, with characteristic enhancements around -22 on both strands and -37 on the coding strand. Analysis of the footprint on the noncoding strand using a 20% polyacrylamide-7 M urea gel revealed that the protection extended to -39 with enhanced cleavage at -40 and -41 (data not shown). These results are similar to those reported for

Figure 1. Sequence of the double-stranded 138mer and the oligonucleotides from which the 138mer was synthesized. The numbers above the sequence are relative to the *E. coli* RNA polymerase transcription start site. The arrows indicate the thymidine residues that are covalently linked to the HMT molecule in the XL-138mer. Several restriction sites are also shown.

Top Strand: 5′-51mer-18mer-12mer-14mer-43mer-3′

12mer: 5′-GAAGCTACGAGC-3′
14mer: 5′-TGAGGCCATCGATA-3′
18mer: 5′-CAGACTCAGTACGAATTC-3′
43mer: 5′-AAGGTCTAGATCTCCCTATAGTGAGTCGTATTAATTTCGACGT-3′
51mer: 5′-CCCATCCCCCTGTTGACAATTAATCATCGGCTCGTATAATGTGTGGAATTG-3′

Bottom Strand: 5′-40mer-52mer-46mer-3′

40mer: 5′-TACGTCGAAATTAATACGACTCACTATAGGGAGATCTAGA-3′
46mer: 5′-TCCACACATTATACGAGCCGATGATTAATTGTCAACAGGGGGATGG-3′
52mer: 5′-CCTTTATCGATGGCCTCAGCTCGTAGCTTCGAATTCGTACTGAGTCTGCAAT-3′

DS 138mer:

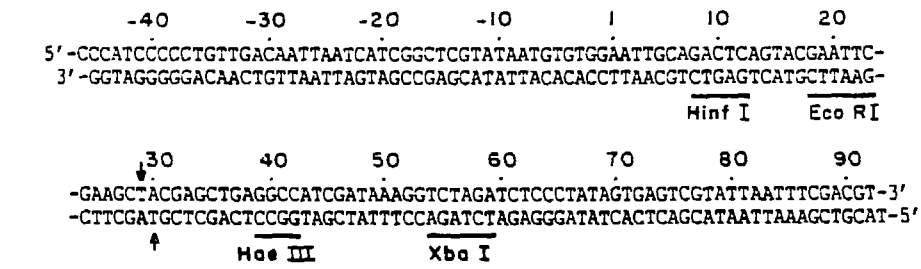

Figure 2. DNase I footprints of the initiation complex on the UM-138mer. A) Bottom strand labelled. DNA sequencing (lanes, G/A, G, C/T, C), in this figure as well as in other figures, were performed as described (Maxam and Gilbert, 1980). Lanes 1-9: footprinting at room temperature (22-24°C); Lanes 10-12: footprint at 37°C; Lanes 1 and 10: control samples without RNAP, 50 μM ATP; Lane 6: control sample without DNase I treatment; Lanes 2-6: 50 μM ATP with 1, 3, 8, 20, 8 nM RNAP, respectively; Lanes 7-9: 8 nM RNAP with 0, 20, 200 μM ATP, respectively; Lanes 11 and 12: 50 μM ATP with 8 and 20 nM RNAP, respectively. The numbers refer to the position relative to the transcription start site. B) Top strand labelled. Lanes 1 and 7: control samples without RNAP and DNase I, respectively; Lanes 1-7: RNAP was 0, 0.4, 1, 2.6, 8, 20, 20 nM, respectively.

A
G/A G C/T C 1 2 3 4 5 6 7 8 9 10 11 12
-30
-20
-10
+1
+10
+20
+30
+40
+50
B
G/A G C/T C 1 2 3 4 5 6 7
+40
+30
+20
+10
+1
-10
-20

other polymerase-promoter complexes. The exact upstream boundary of the footprint could not be determined due to the inability of DNase I to bind and incise near the termini of a helix. We assumed that the polymerase protected up to the upstream end of the DNA fragment since it is known that *E coli* RNA polymerase protects approximately 70 base pairs (-50 to +20) around a promoter in an initiation complex (see references cited in the **INTRODUCTION**). The results also show that the protection is identical at 37°C and at room temperature (22-24°C) and is independent of the concentration of the initiation nucleotide ATP. Identical footprints were obtained for the binding of the polymerase to XL-138mer (data not shown). This was expected since the HMT diadduct lies outside the binding domain of the initiation complex. The above results are summarized in figure 8.

C) DNase I Footprints of the Elongation Complexes

Transcription requires transient unwinding and separation of the DNA template as the polymerizing site of the enzyme moves through the helix. The site specific placement of an inter-strand HMT diadduct in the XL-138mer consequently stopped transcription at the diadduct, thus generating a homogeneous elongation complex. This complex, with 5'-^{32}P label on either the top strand or the bottom strand, was then probed by DNase I footprinting. To maximize the yield of the elongation complex, initiation was conducted at low ionic strength (20 mM KCl) and in the presence of the initiation nucleotide ATP or ApA. Elongation was started by adding the full complement of ribonucleotides. DNase I footprinting was performed on the elongation complex after addition of

NaCl to 0.2 M, which minimize the polymerase-promoter complex without affecting the elongation complex. Due to the inter-strand nature of the HMT diadduct, fragments generated by DNase I cleavages 3′ to the diadduct site could not be identified because they were covalently attached to the other strand, which was also partially digested. Therefore, after the removal of protein by phenol extraction, half of each footprinting sample was irratiated with 254 nm light to reverse the crosslink thereby allowing determination of the footprint 3′ to the HMT diadduct. The samples (with and without irradiation at 254 nm) were analyzed on an 8% polyacrylamide-8 M urea gel.

Figure 3 shows the DNase I footprint of the bottom strand (coding strand) under the above elongation conditions. It is apparent that the polymerase strongly protected the DNA from +7 to +37 with enhanced cleavage at +12 and +13. There is also a weakly protected region from +37 to +49, which is seen more clearly in the densitometric scans of figure 3B. The protection and enhancement upstream from +7, characteristic of the promoter-polymerase complex, has disappeared. The protection was identical whether ATP or ApA was used as the initiation nucleotide and was also independent of the temperature (room temperature vs. 37°C) at which complex formation or DNase I digestion was conducted (data not shown). Under these same conditions, the UM-138mer did not give a footprint. Analysis of the RNA product using either a DNA sequencing ladder or 3′-OCH_3 RNA sequencing as a standard showed that the UM-138mer template yielded a full length runoff transcript whereas the XL-138mer template produced a transcript of 29 nucleotides

Figure 3. DNase I footprint of bottom strand labelled elongation complex on the XL-130mer. A) Partially digested crosslinked molecules, running slower than the 138mer, are not shown here. Lanes 1′-6′ are identical to lanes 1-6 except that they were irradiated at 254 nm to photoreverse the HMT diadduct. Lanes 1, 2, 3, and 6: samples initiated in the presence of 0.05 mM ATP; Lanes 4 and 5: samples initiated in the presence of 0.2 mM ApA; Lane 6: control sample without DNase I treatment; Lanes 1 and 3-6: 50 μM ATP, 0.2 mM GTP, UTP, and CTP with 0, 12, 12, 0, 12 nM RNAP, respectively; Lane 2: no GTP, UTP, or CTP added during elongation stage, otherwise identical to lane 3. B) Densitometric scans of lanes 1′ (dashed line) and 3′ (solid line) in A). The arrows indicate the boundaries of the protected region.

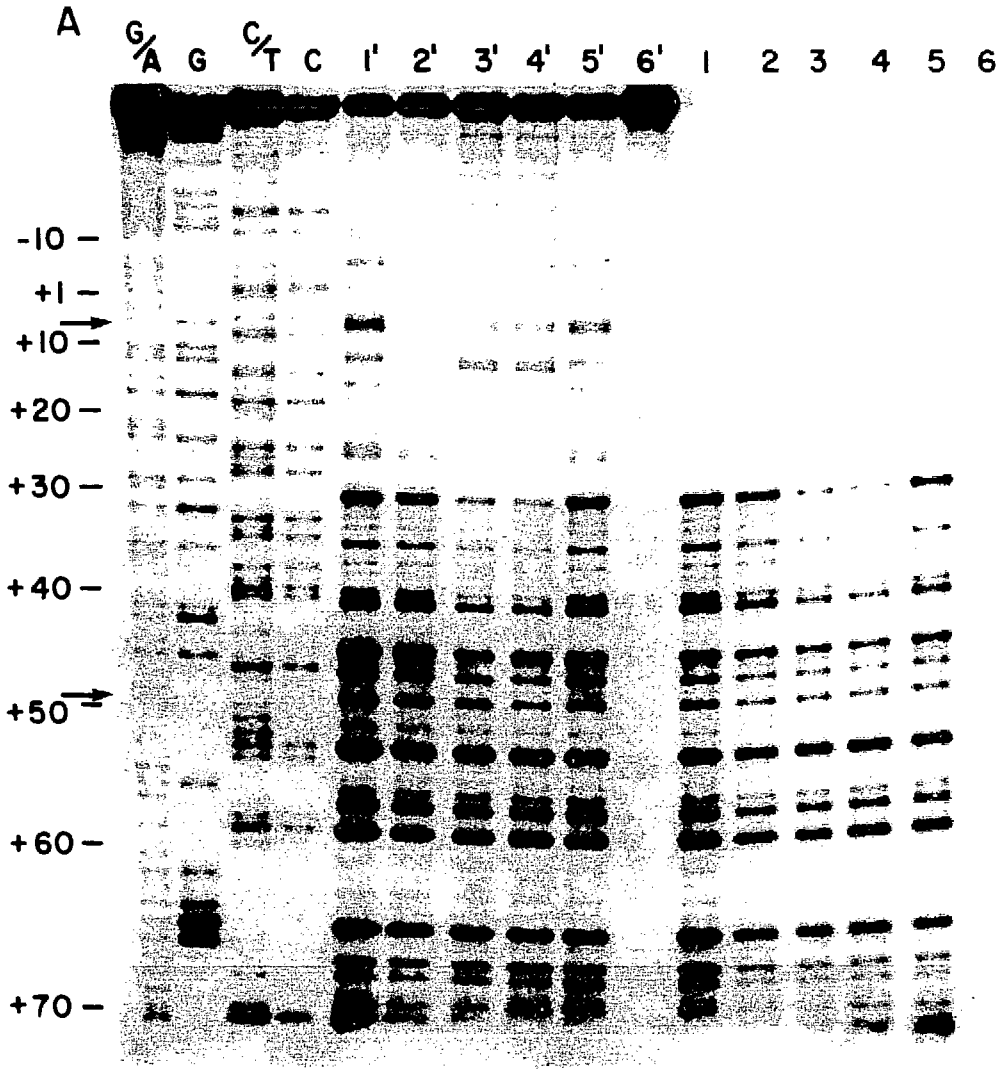
A
G/A
G
C/T
C
1'
2'
3'
4'
5'
6'
1
2
3
4
5
6
-10
+1
+10
+20
+30
+40
+50
+60
+70

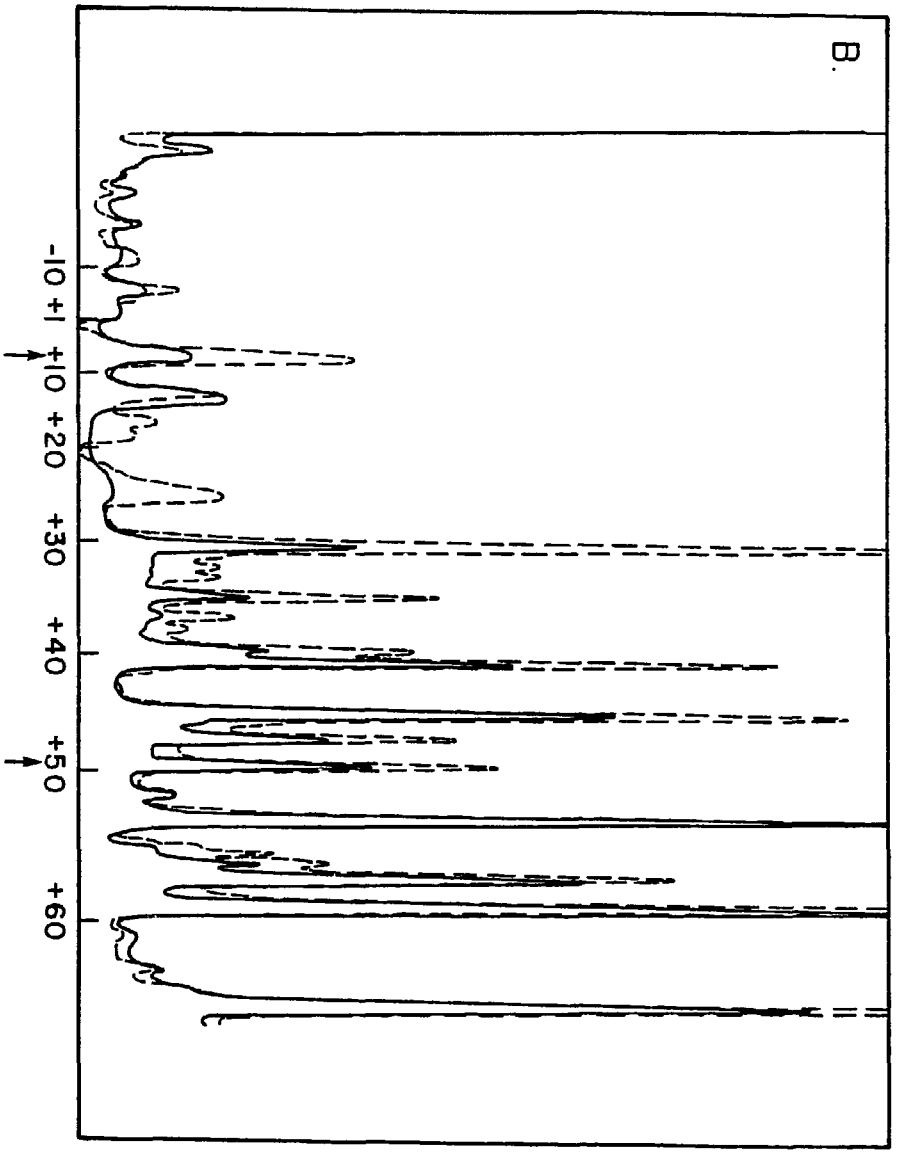
B.
-10 +1
+10
+20
+30
+40
+50
+60

long (see Chapter V and below). The short transcript reflects blockage of RNA synthesis by the HMT diadduct.

It is known that RNA polymerase can bind to the ends of a double-stranded helix and that this binding is very sensitive to heparin challenge (Melancon et al., 1982 and 1983). To eliminate the possibility that part of the footprint might result from an elongation complex formed by initiation at the nonpromoter end of the helix and transcription up to the HMT diadduct site, heparin was added to the initiation mixture prior to the addition of NTPs. DNase I footprinting was then performed in the presence of heparin. The results from such experiments (data not shown) are identical to those obtained in the absence of heparin, demonstrating that transcription from the nonpromoter end did not contribute to the observed footprint. These experiments also eliminate the possibility of two initiations occurring off the same promoter which would result in a complex with two polymerases sitting head-to-tail, thus contributing to the observed protection.

When similar footprinting experiments were performed on top strand labelled crosslinked DNA template, a 40 bp region around the HMT diadduct in the elongation complex was protected from DNase I digestion. As shown in figure 4, the protection from +8 to +36 was strong whereas the protection from +36 to + 46 was relatively weak. Identical protection was obtained in the presence of different polymerase and ATP concentrations (compare lanes 3′, 4′, 5′). The downstream boundary of the protected region on the top strand was further confirmed by an Exo III

Figure 4. DNase I footprint of top strand labelled elongation complex on the XL-138mer. Lanes 1′-6′ are identical to 1-6 except that they were irradiated at 254 nm. Lane 6: control without DNase I treatment; Lanes 1, 3, 4, and 6: 50 μM ATP, 0.2 mM GTP, UTP, and CTP with 0, 12, 24, and 12 nM RNAP, respectively; Lane 2: no GTP, UTP, and CTP added during elongation, otherwise identical to lane 3; Lane 5: 100 μM ATP, otherwise identical to lane 3. B) Densitometric scans of lanes 2′ (dashed line) and 3′ (solid line) in A). Lane 3′ was weaker than lane 2′ in the region upstream from +6. This was probably due to a salt-induced converging of lane 2′ going down to the bottom of the gel. The arrows indicate the boundaries of the protected region.

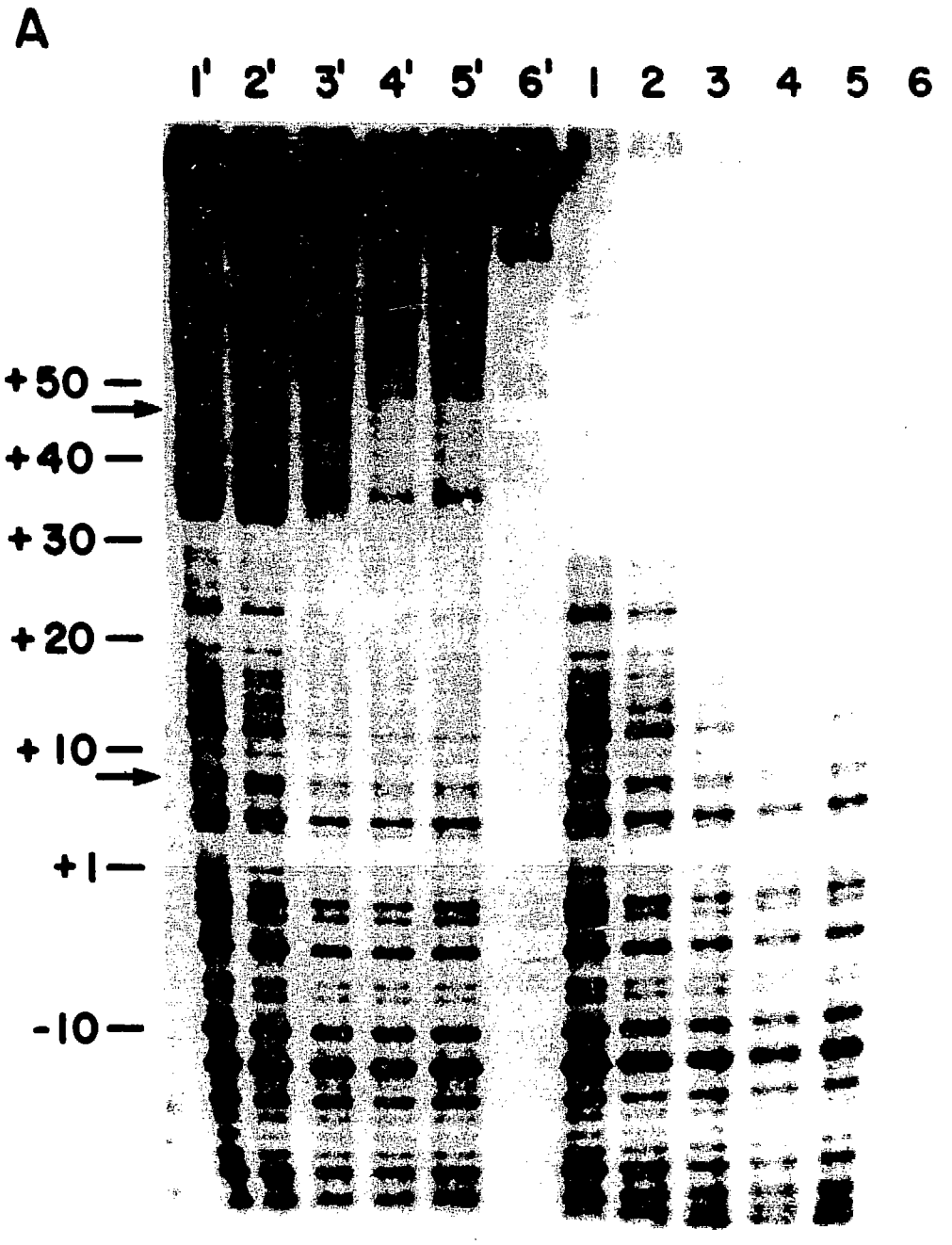
A
1'
2'
3'
4'
5'
6'
1
2
3
4
5
6
+50
+40
+30
+20
+10
+1
-10

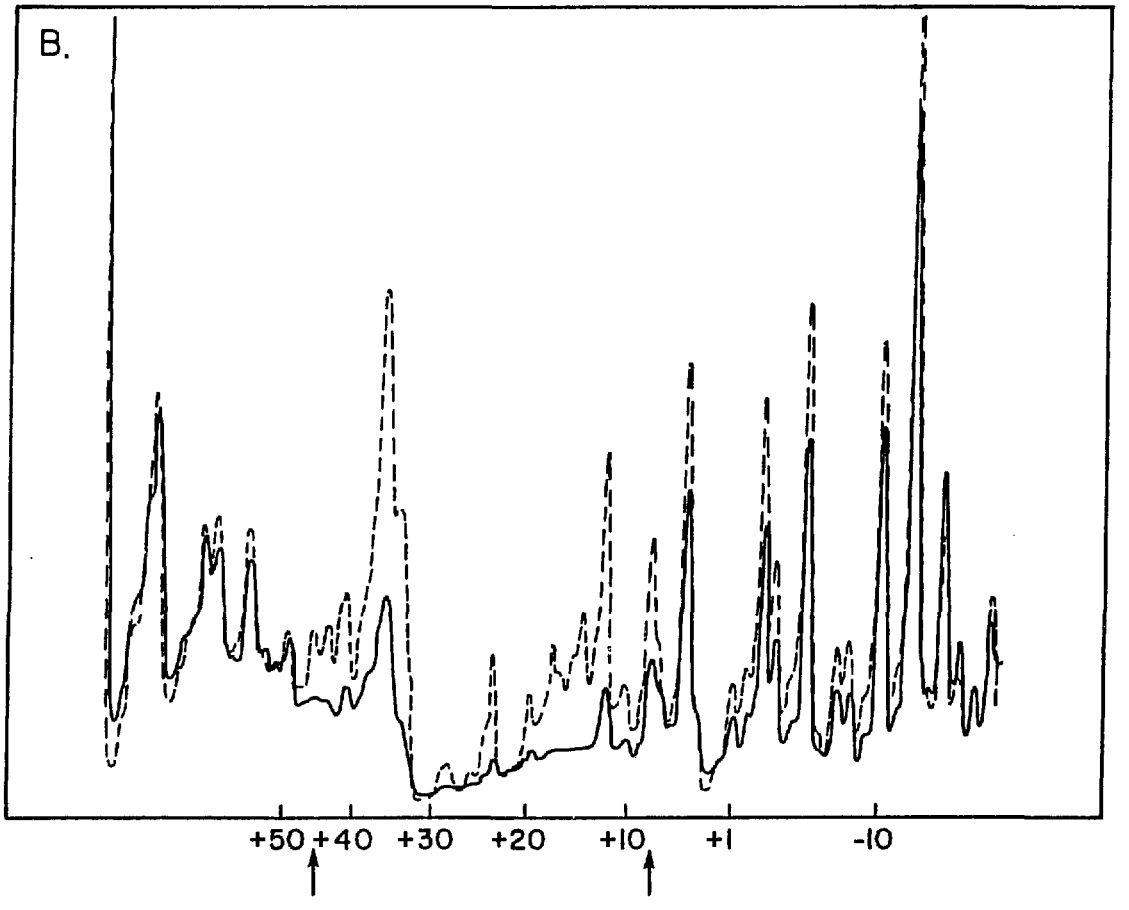
B.
+50
+40
+30
+20
+10
+1
-10

nuclease (a double-strand specific 3′ to 5′ exonuclease) digestion experiment. As shown in figure 5, treatment of the top strand labelled XL-138mer with Exo III in the absence of the RNA polymerase resulted in a band migrating slightly slower than single-stranded 138mer (lane 1). Upon photoreversal at 254 nm, this sample yielded a band corresponding to 3′-end digestion of the top strand to position +33, i.e., 4 bases from the diadduct (lane 1′). Thus the band running slower than 138mer in lanes 1 and 1′ was a product of Exo III digestion in which the residual top and bottom strands were still crosslinked by the HMT molecule. The band labelled 138mer in lanes 1′ and 2′ was single-stranded 138mer generated from the photoreversal of undigested XL-138mer. By contrast, treatment of the XL-138mer under elongation conditions with Exo III yielded no product running slightly slower than single-stranded 138mer (lane 2, DNA running much more slowly than 138mer is not shown in the figure). Photoreversal of the sample yielded three major products (lane 2′). The band labelled +33 was probably generated from DNA without polymerase while the band labelled + 42 was probably generated from over-digestion of elongation complexes by Exo III. We believe that the band labelled +48 corresponds to 3′-end digestion of the top strand to the terminus of the elongation complex. Thus Exo III digestion yielded a 3′ protection boundary 2 bases further downstream from that delineated by the DNase I protection experiments.

D) Characterization of the Elongation Complexes by Non-denaturing Polyacrylamide Gel Electrophoresis

The elongation complexes were further characterized by

Figure 5. Exo III digestion of top strand labelled elongation complex on the XL-138mer. The elongation complex was formed at 37°C in the presence of 50 μM ATP, 0.2 mM GTP, UTP, and CTP. After addition of 2 μl of 5 M NaCl, 10 μl of Exo III was added and the mixture was incubated at 37°C for 10 min. The samples were then treated the same as the DNase I digested samples. Lanes 1′ and 2′ are identical to 1 and 2 except that they were irradiated at 254 nm. Lanes 1 and 2: 0.5 nM XL-138mer with 0 and 12 nM RNAP, respectively. The numbers refer to positions relative to the transcription start site. The band labelled 138mer is single-stranded 138mer generated by photoreversal of undigested XL-138mer.


1'
2'
1
2
138 mer —
+48 —
+42 —
+33 —

non-denaturing 4% polyacrylamide gel electrophoresis. Similar to the results of Straney and Crothers (1985) and as shown in figure 6 and Table I (quantitation of the complexes in figure 6), the binding of RNA polymerase to the promoter in the double-stranded 138mer resulted in the formation of open complexes (lanes 2 and 8 for ^{32}P-labelled XL-138mer and UM-138mer, respectively) as well as other minor species including closed complexes and aggregates (using Straney and Crothers' nomenclature). Addition of 0.2 M NaCl to the samples before electrophoresis removed most of the initiation complexes (see figure 7, lane 4 and Table I). Upon addition of the four ribonucleotides, two elongation complexes formed with concomitant reduction of the initiation complexes (lane 3). The predominant complex, constituting 40% of the total DNA, was resistant to high salt, while the minor one, constituting only 10% of the DNA, was fairly sensitive to high salt and could be removed by the addition of heparin to the reaction mixture prior to the addition of ribonucleotides (compare lanes 3, 5, and 6 and see Table I). The major elongation complex migrated slightly faster than the open complex, similar to what was observed by Straney and Crothers (1985). The mobility of the major elongation complex indicates that there was only one polymerase molecule per complex.

Unexpectedly, the UM-138mer served as an excellent template for the formation of elongation complexes (Figure 6, lane 7). To further characterize the identity of the elongation complexes formed on the two DNA templates, we performed additional experiments. When complexes which contained label only in the nascent RNA were analyzed by

Figure 6. Transcription complexes with labelled DNA template assayed by non-denaturing gel electrophoresis. The nomenclature for the complexes is similar to that of Straney and Crothers (1985). Calf thymus DNA was added to all samples prior to gel electrophoresis. Lanes 1-6: XL-138mer template; Lanes 7 and 8: UM-138mer template; Lane 1: control without RNAP; Lane 2: initiation complex, 15 nM RNAP, 50 μM ATP; Lanes 3, 5, and 6: 15 nM RNAP, 50 μM ATP, 0.2 mM GTP, UTP, and CTP; Lane 3: elongation complex; Lane 4: identical to lane 2 except 0.8 μl of 5 M NaCl added before the addition of calf thymus DNA; Lane 5: identical to lane 3 except 0.8 μl of 5 M NaCl added before the addition of calf thymus DNA; Lane 6: identical to lane 5 except heparin added before the addition of NTPs; Lane 7: identical to lane 6; Lane 8, identical to lane 2.

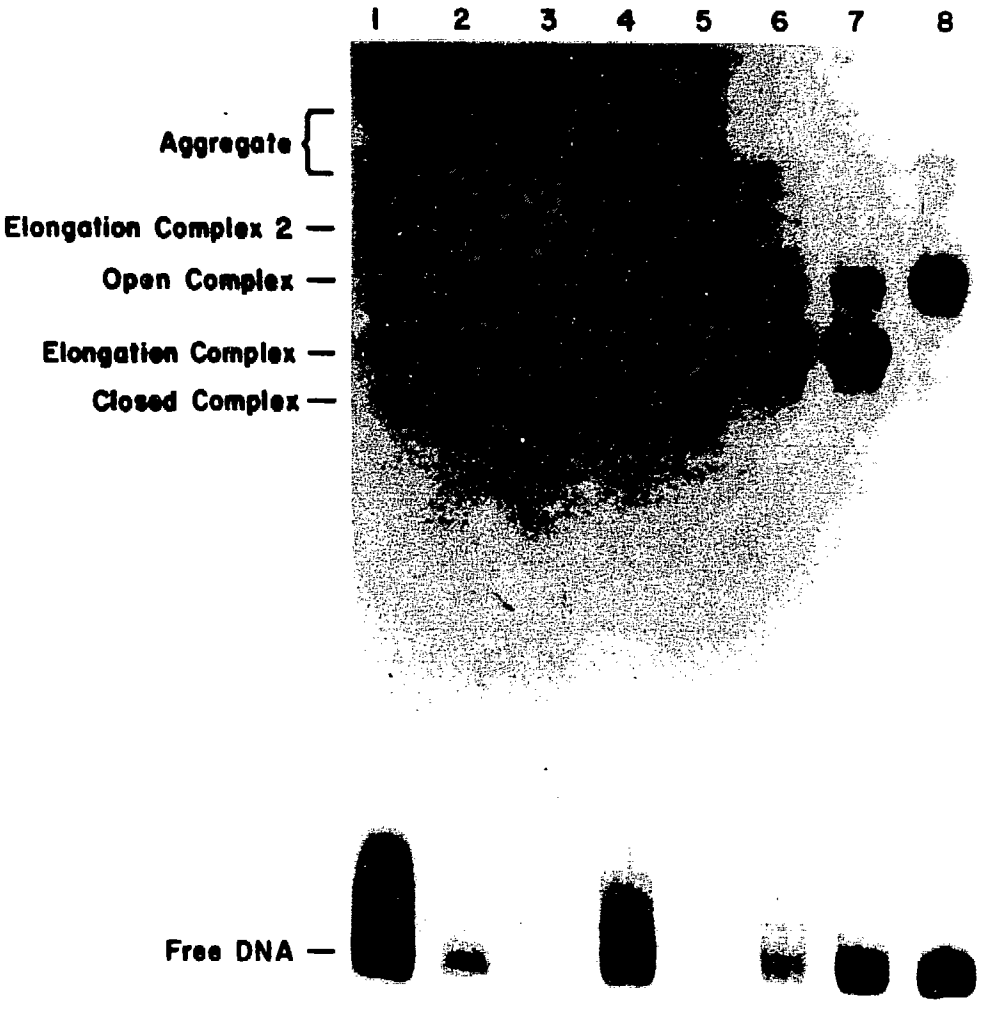
1
2
3
4
5
6
7
8
Aggregate
Elongation Complex 2
Open Complex
Elongation Complex
Closed Complex
Free DNA

Table I. Transcription Complexes as Analyzed by Native 4% Polyacrylamide Gel Electrophoresis*

Sample	1	2	3	4	5	6	7	8
Substrate	XL-138mer						UM-138mer	
Free DNA	100	44.6	13.2	72.8	30.6	46.6	48.9	51.5
Closed Complex	0	10.0	0	7.0	0	0	0	2.4
Elongation Complex	0	0	41.0	0	43.2	40.4	37.4	0
Open Complex	0	36.4	18.3	17.3	12.6	9.0	7.2	40.3
Elongation Complex 2	0	0	11.2	0	6.5	1.6	1.3	0
Aggregate	0	9.0	16.3	3.0	7.2	2.4	1.9	5.7

*The data were expressed as percent of total DNA recovered from the gels.

non-denaturing gel electrophoresis, results similar to those reported by Straney and Crothers (1985) were obtained (data not shown). While both templates supported the formation of an elongation complex, the UM-138mer gave an additional product which was not detectable when only the DNA template was labelled. This product is believed to be a DNA-free complex between nascent RNA and RNA polymerase. A similar complex was characterized by Straney and Crothers (1985). The second elongation complex seen earlier was not detectable when label was present only in the RNA. This could be due to low yield of the complex under the modified conditions, a fairly high background associated with the RNA labelling approach, or to the possibility that the RNA in this complex was short and consequently had less label. This complex was not further characterized since it is a minor component of the reaction and therefore does not affect the footprinting results. It is noteworthy that the transcription complexes detected when the RNA was labelled were insensitive to the concentration of ATP in the range from 0.7-50 μM, although more RNA-RNA polymerase complex was formed in the case of UM-138mer at a higher ATP concentration.

The labelled RNAs from the above complexes were extracted and analyzed by denaturing 8% polyacrylamide gel electrophoresis using the bottom strand DNA sequencing ladder as a length standard (figure 7). The XL-138mer elongation complex gave predominantly a 29 base long RNA transcript (later confirmed using 3'-OCH_3 RNA sequencing standard) while the UM-138mer elongation complex gave a family of transcripts up to 80 bases in length. (Similar patterns of transcript distribution

Figure 7. Analysis of RNA transcripts from the elongation complexes of the UM-138mer and XL-138mer. The RNAs were extracted from gel slices containing the elongation complexes and electrophoresed on an 8% polyacrylamide-8 M urea gel. The chemical sequencing of the bottom strand labelled UM-138mer was used as a length standard. The numbers refer to the lengths of the end-labelled fragments, which were shifted by one base relative to the fragments generated from sequencing. (Sequencing reactions remove the corresponding base from the fragment and consequently generate fragments running one base faster than normal DNA fragments of the same length.) Lane 1: RNA isolated from the elongation complex of the XL-138mer in figure 8. Lane 2: RNA isolated from the elongation complex of the UM-138mer in figure 8.

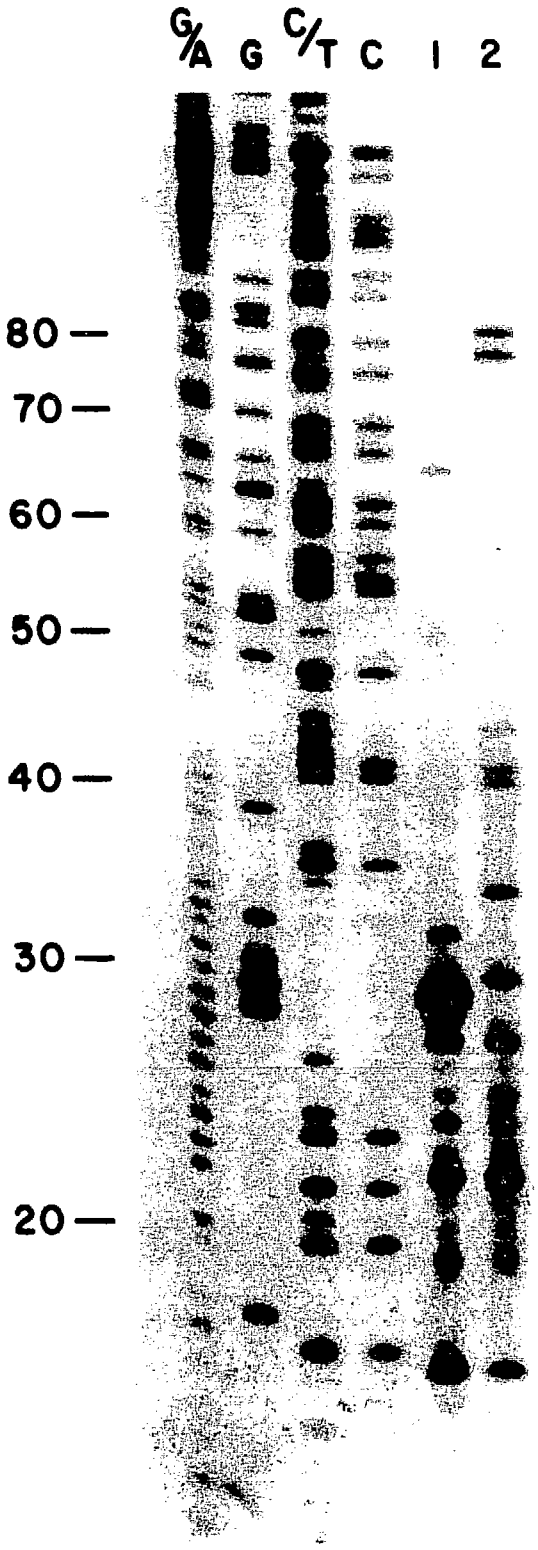
G/A
G
C/T
C
1
2
80
70
60
50
40
30
20

were observed for the complex formed at different ATP concentrations.) This suggests that the UM-138mer elongation complex represents a collection of RNA polymerases paused at different sites along the DNA template and is consistent with the fact that no specific DNase I footprint was observed on the UM-138mer under the elongation conditions. The position of the enzyme on the DNA and the length of the nascent RNA transcript did not affect the mobility of the elongation complex in a non-denaturing gel, in agreement with the findings of Straney and Crothers (1985). Analysis of the RNA from the putative RNA-RNAP complex demonstrated it to be primarily full length runoff transcript (data not shown), which is consistent with our interpretation. When this same RNA was electrophoresed through a non-denaturing polyacrylamide gel under the same conditions as described in figure 6, the runoff transcript ran faster than the double-stranded UM-138mer thus indicating that the mobility of the corresponding enzyme complex was due to the presence of the polymerase and not to partial folding of the RNA itself. No runoff transcript-polymerase complex was produced when the XL-138mer was used as the template, because the RNA polymerase was blocked at the HMT diadduct.

Although the predominant RNA transcript of the XL-138mer terminated at the HMT diadduct, there were other minor products (see figure 7). The shorter RNAs can be attributed to RNase contamination during workup or to elongation complexes paused at specific sites prior to reaching the HMT diadduct. There were also RNAs of longer length, notably a transcript 64 nucleotides long. This transcript was also detectable

when transcription aliquots containing the XL-138mer template were directly analyzed by denaturing gel electrophoresis. It is known that *E. coli* RNA polymerase can bind to nonpromoter DNA, preferentially ends of double-stranded DNA, and can possibly initiate transcription (Melancon et al., 1982 and 1983). To test the possibility that the long transcript was generated by RNA synthesis initiated at the nonpromoter end followed by termination at the HMT diadduct, we isolated this transcript and probed it with component oligonucleotides of the 138mer (see figure 1). Electrophoresis on a non-denaturing 12% polyacrylamide gel (data not shown) indicated that the top strand 43mer hybridized to the long transcript, confirming that RNA polymerase had initiated transcription from the nonpromoter end of the XL-138mer to generate a transcript 63 nucleotides long upon reaching the HMT diadduct. Initiation of transcription from the promoter end would be unlikely since the polymerase bound to this end would move to the promoter and start normal transcription there. The above results clearly demonstrate the existence of minor elongation complexes on the XL-138mer in addition to the expected complex. The RNA contents in the elongation complexes shown in figure 9, however, indicate that the total fraction of such complexes is so low that they would not be detectable in the DNase I footprinting experiments.

4. DISCUSSION

The main purpose of this study was to investigate the interaction of RNA polymerase with DNA during elongation and to determine the relative locations of the unwinding and catalytic sites of the polymerase.

To this end we have placed a psoralen (HMT) diadduct at a specific site downstream from an *E. coli* RNA polymerase promoter in a double-stranded DNA fragment. The interstrand diadduct blocks forward movement of the polymerase leading to the accumulation of a stable homogeneous elongation complex which was probed by DNase I footprinting. The length of the transcript in the arrested elongation complex was also determined.

A) Initiation Complex

The binding of *E. coli* RNA polymerase to the synthetic tac promoter was characterized by non-denaturing polyacrylamide gel electrophoresis and DNase I footprinting. The electrophoresis assay indicates that the open complex was the predominant product although there were minor amounts of closed complex and aggregate. The above assay probably underestimates the actual amount of open complex since almost complete protection of the DNA was effected by the polymerase in the DNase I footprinting experiments. These footprints, representing the open complex since the population of other complexes was too low to be detected, indicate that in the open promoter complex approximately 65 bp of DNA are protected with characteristic enhancements around -20 and -40 (figure 8). Our results are similar to those reported by others for polymerase-promoter complexes (Siebenlist and Gilbert, 1980; Siebenlist et al., 1980; Hofer et al., 1985; Carpousis and Gralla, 1985; Spassky et al., 1985; Duval-Valentin and Ehrilich, 1986; Spassky, 1986). These results indicate that the polymerase binds normally to the tac promoter in the 138mer bp DNA fragment. With the crosslinked DNA template the HMT diadduct was placed outside the polymerase protected

Figure 8. DNase I protection of double-stranded 138mer by RNA polymerase during initiation and elongation. The solid lines indicate strong protection and the dashed lines indicate weak protection. The open circles indicate the sites of enhanced cleavage. The arrows denote the thymidine residues attached to the HMT in the XL-138mer.


Elongation
Initiation
oo
ooo
-40
-30
-20
-10
1
10
20
30
40
50
5'-CCCATCCCCCTGTTGACAATTAATCATCGGCTCGTATAATGTGTGGAATTGCAGACTCAGTACGAATTCGAAGCTACGAGCTGAGGCCATCGATAAAGGTCTAGAT...3'
3'-GGTAGGGGGACAACTGTTAATTAGTAGCCGAGCATATTACACACCTTAACGTCTGAGTCATGCTTAAGCTTCGATGCTCGACTCCGGTAGCTATTTCCAGATCTA...5'
o
o o
Initiation
Elongation
oo

region and consequently should not interfere with polymerase binding and initiation. As expected, the non-denaturing gel assay and the DNase I footprinting experiments yielded identical results for the initiation complexes of the UM-138mer and XL-138mer.

B) Elongation Complex

Transcription off the XL-138mer template generated an arrested elongation complex containing a nascent RNA 29 nucleotides long. This complex electrophoresed through a non-denaturing 4% polyacrylamide gel with the expected mobility based upon the previous results of Straney and Crothers (1985). In fact, the elongation complexes formed on UM-138mer and XL-138mer comigrated with one another, indicating that the conformations of the two complexes were similar even though the polymerase was located at naturally occurring pause sites in one case while it was blocked at a specific HMT diadduct site in the other case. It is known that the σ subunit of the polymerase is released after an RNA 8 to 13 nucleotides long is synthesized (Hansen and McClure, 1980; Bernhard and Meares, 1986). The RNA polymerase in the elongation complex of the XL-138mer was blocked at the HMT diadduct site, yielding a transcript of 29 nucleotides long. We have also observed the same relative mobility of the promoter-polymerase open complex compared to the elongation complex of the XL-138mer in a non-denaturing gel that Straney and Crothers (1985) observed between open initiation complex and elongation complex, where the σ subunit was independently shown to be absent. These results strongly suggest that the XL-138mer elongation complex does not contain the σ subunit.

The DNase I footprinting experiments indicate that the RNA polymerase in the elongation complex of the XL-138mer protects 40 bp of the DNA template, with approximately 30 bp strongly protected and another 10 bp further downstream weakly protected (figure 8). This protection pattern is similar to that observed by Straney and Crothers (1985) but differs from the protection pattern reported by Carpousis and Gralla (1985), who did not observed the weakly protected downstream extension of the footprint. Both of these studies generated an elongation complex by supplying the polymerase with an incomplete mixture of ribonucleotides. As would be expected, the footprints of both the initiation and elongation complexes contract upon exposure to a limit nuclease digest. Using this method Rohrer and Zillig (1977) have reported footprints of 37 and 26 base pairs for the two respective complexes.

The general agreement of these footprints argues that the HMT diadduct does not significantly perturb the structure of the arrested elongation complex. This is further supported by the following observations. First, comparison of the DNase I cleavage patterns of the two strands of the UM-138mer with those of the XL-138mer in the absence of polymerase (compare lane 1 of figure 2A to lane 1′ of figure 3A for the bottom strand and lane 1 of figure 2B to lane 1′ of figure 4A for the top strand) indicates that the presence of the HMT diadduct does not perturb the conformation of the DNA except in the immediate vicinity of the diadduct. Second, the mobility of the elongation complex of the XL-138mer is identical to that of the UM-138mer in a non-denaturing polyacylamide gel, indicating that the conformations of the two com-

plexes are similar even though one was formed at a specific HMT diadduct site whereas the other was formed at different natural occurring pause sites. Finally, using a similar strategy we have probed the interaction of T7 RNA polymerase with its DNA template in an elongation complex arrested at a specific HMT diadduct site or HMT furan-side monoadduct site (on the coding strand) site by DNase I footprinting technique. Identical footprints were obtained for the elongation complexes sequestered on the furan-side monoadducted or crosslinked templates even though the nature of the two HMT adducts is quite different (See Chapter VIII).

DNase I footprinting experiments on the elongation complex of the XL-138mer also revealed two hypersensitive sites 17 and 18 nucleotides upstream from the HMT diadduct on the bottom strand (see figure 8). No such enhancement was oberved by Carpousis and Gralla (1985) and Straney and Crothers (1985) in their elongation complexes. Although this difference could be due to the presence of the HMT diadduct in our elongation complex, we believe that this is unlikely for the reasons mentioned above and because the hypersensitive sites are far away from the HMT diadduct site. Instead, we postulate that the hypersensitive sites may reflect a fundamental change in the structure of the elongation complex upon synthesis of a minimum length transcript. The elongation complexes characterized by Carpousis and Gralla (1985) and by Straney and Crothers (1985) contain RNA transcripts of 16 and 11 nucleotides long, respectively, i.e., about half or less the length of the RNA in the complex described here. Consequently the region 17

nucleotides upstream from the transcription stop site in their elongation complexes is located upstream from the transcription start site. The properties of the interaction of the promoter DNA with the polymerase could be expected to be different from those of other DNA sequences with polymerase in the elongation complex. In addition, if one assumes that the unwound region in the complex is 17 bp (Gamper and Hearst, 1982), the transcript in their cases would be expected to be completely hybridized with the coding strand without a 5'-end tail stretching out of the complex as in our case and the hypersensitive sites would be in the helix junction (RNA-DNA helix and DNA-DNA helix junction, see below). The properties of the DNA in the helix junction in these cases could be different. It is worth mentioning that we have observed similar hypersensitive sites 17-19 nucleotides upstream from the transcription stop site on the coding strand in a T7 elongation complexes arrested at a specific HMT diadduct or HMT monoadduct site (see Chapter VIII).

C) Model of the Elongation Complex

During the elongation process, RNA polymerase opens approximately 12 to 17 base pairs of DNA template (Gamper and Hearst, 1982; Von Hippel et al., 1984). Based on an unwinding angle analysis of *E. coli* RNA polymerase-DNA complexes at different stages of transcription, Gamper and Hearst (1982) have proposed a topological model for transcription elongation, in which they suggest the existence of unwindase and rewindase activities on the polymerase. During elongation, the unwindase open the DNA while the rewindase, lagging by 17 bp, displaces the RNA

transcript and reseals the DNA helix. Based on our DNase I footprint data and the measured length of the transcript on the psoralen crosslinked template, we present a revised model shown in figure 9. Again, the unwindase and rewindase sites are separated by about 12 to 17 bp depending on the length of the unwound region of the DNA in the complex (Gamper and Hearst, 1982; Von Hippel et al., 1984). The unwindase site is located close to the HMT diadduct site, since the polymerase cannot unwind and strand-separate the covalently linked helix, and the rewindase site is positioned near the end of the RNA-DNA hybrid helix. Our experiments show that the catalytic site of the polymerase is next to the HMT diadduct site since the length of the RNA transcript in the elongation complex demonstrates that RNA synthesis proceeds up to the diadduct. Thus the unwindase site and catalytic site are very close to each other in our arrested elongation complex. This interpretation should be tempered by the qualification that although RNA polymerase can insert its last nucleotide next to the crosslink, the result does not mean that it does so during the normal elongation process.

Another feature we add to the elongation complex is the DNA protection pattern observed on both sides of the HMT diadduct. The polymerase protects about 20 bp upstream and 10 bp downstream from the HMT diadduct not including the weakly protected region. It is interesting that the hypersensitive sites observed in the coding strand of the elongation complex occur at the postulated junction between the RNA-DNA helix and the reformed DNA-DNA helix (see figures 8 and 9), assuming

Figure 9. A model for the transcription elongation complex. The horizontal arrow indicates the direction of RNA synthesis. The curved arrows indicate the unwinding and rewinding of DNA or DNA-RNA helix by the polymerase. The filled triangles denote the hypothetical unwindase and rewindase centers of the enzyme. The open triangle denote the catalytic site of the polymerase, which is very close to the leading unwindase site. The vertical bar indicates the site of psoralen crosslinkage.

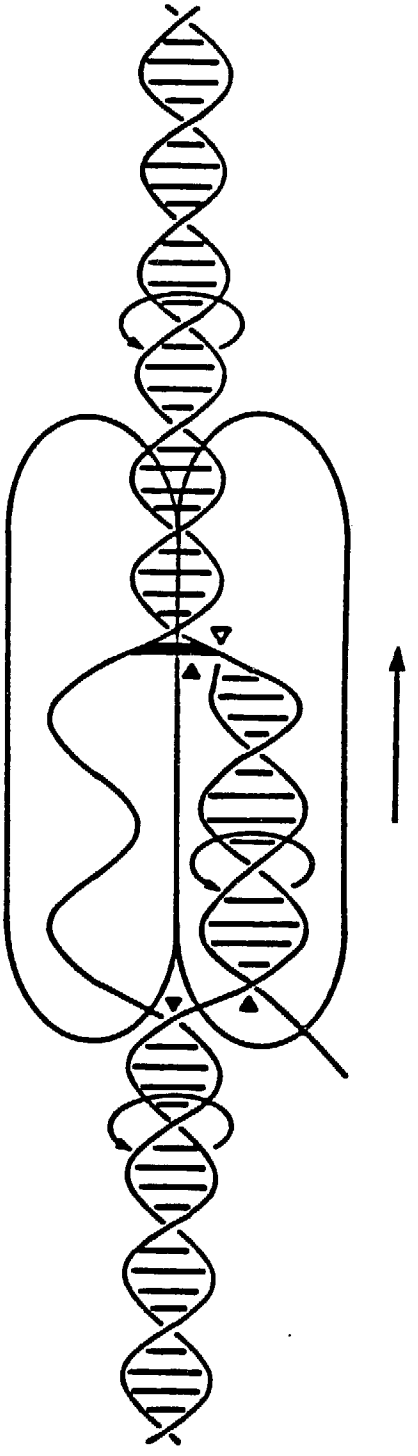

that the unwound region in the elongation complex is 17 base pairs as estimated by Gamper and Hearst (1982). Although a rigorous test of the model is difficult at present, other experimental evidence support it. First, DNase I footprinting on elongation complexes arrested using incomplete ribonucleotide mixtures yielded strong protection of the DNA template on both sides of the stop sites, though the lengths of the protected regions varied in different systems (Carpousis and Gralla, 1985; Straney and Crothers, 1985). Second, using an *in vitro* transcription assay, Phillips and Crothers (1986) have found that RNA synthesis proceeds up to 1 bp prior to preferred intercalation sites of the drug actinomycin D. Since drug intercalation requires a double-stranded helix, it follows that the unwinding does not extend more than 1 or 2 bp ahead of the catalytic site and is consistent with the model that the unwindase and catalytic sites of the polymerase are very close if not the same.

CHAPTER VIII. INTERACTION OF T7 RNA POLYMERASE WITH DNA IN AN ELONGATION COMPLEX ARRESTED AT A SPECIFIC PSORALEN ADDUCT SITE

1. Introduction

Bacteriophage T7 encoded RNA polymerase transcribes the class II and class III genes of the phage genome (Chamberlin et al., 1970; Chamberlin and Ryan, 1982). In contrast to *E. coli* RNA polymerase, a multisubunit enzyme of molecular weight 450,000 which binds to its promoter with an association constant of about 10^{11} M^{-1} (Roe and Record, 1985; Prosen and Cech, 1986), T7 RNA polymerase is a single polypeptide of molecular weight 100,000 which binds weakly to its promoter with an association constant of $\leq 10^{7}$ M^{-1} (Chamberlin and Ring, 1973; Oakley et al., 1979; Ikeda and Richardson, 1986). The reduced stability of the T7 complex renders it sensitive to high ionic strength (Smeekens and Romano, 1986; Gunderson et al., 1987). DNase I and methidiumpropyl-EDTA-Fe footprinting experiments have shown that in the presence of the initiation nucleotide GTP T7 RNA polymerase protects 28 nucleotides from -20 to +8 on the coding strand in the promoter-polymerase complex (Basu and Maitra, 1986; Ikeda and Richardson, 1986; Gunderson et al., 1987). Different results were obtained for the non-coding strand, as it was protected from methidiumpropyl-EDTA-Fe cleavage but not from DNase I cleavage. In the absence of GTP no specific DNase I footprint was observed (Basu and Maitra, 1986), although a weakly protected region from -21 to -3 on both strands was observed in the methidiumpropyl-EDTA-Fe footprinting experiments (Ikeda and Richardson, 1986; Gunderson et al., 1987).

A homogeneous population of elongation complexes is required in order to investigate the polymerase-DNA interaction during transcription. Using incomplete mixtures of ribonucleoside triphosphates, Ikeda and Richardson (1986, 1987) were able to stop transcription by T7 RNA polymerase after synthesis of short transcripts (≤15 bases in length) and obtained methidiumpropyl-EDTA-Fe footprints of the different transcription complexes as the polymerase (either the intact or a proteolytically nicked T7 RNA polymerase) moved downstream from the promoter. Here I report the DNase I footprints of homogeneous T7 elongation complexes which contain a 36 base long transcript. Blockage of transcription was accomplished by placing a site specific psoralen monoadduct or inter-strand psoralen crosslink downstream from a T7 RNA polymerase promoter. The monoadduct proved to be a noncoding lesion whereas the crosslink functioned as an absolute barrier to strand separation of the template DNA during elongation.

The unmodified and psoralen modified templates were 138mers as prepared in Chapter V. As shown in Chapter V, transcription by T7 RNA polymerase was blocked by both the psoralen diadduct and the furan-side monoadduct positioned on the coding strand. Consequently, both psoralen modified substrates have been used to investigate the interaction of T7 RNA polymerase with DNA in arrested elongation complexes by DNase I footprinting techniques. The results show that the elongation complexes protect about 15 nucleotides upstream from the adduct on the coding strand and 20 nucleotides around the adduct on the non-coding strand from DNase I digestion. The results in this chapter have been published

(Shi et al., 1988b).

2. Materials and Methods

A) Materials

See previous chapters.

B) DNase I Footprinting of Initiation and Elongation Complexes

Initiation Complex. The initiation complex between T7 RNA polymerase and its promoter was formed by incubating the end labelled template (0.5 nM) with the polymerase (0.22-0.75 μM) in 50 μl T7-trans buffer at 37°C for 5 min in the presence of GTP, the first nucleotide of the transcript. The samples were then transferred to a room temperature water bath followed by the addition of 2 μl calf thymus DNA (1 μg/μl) and 5 μl 100 mM $CaCl_2$. DNase I digestion was initiated with the addition of 2.5 μl of 20,000 fold diluted DNase I (prepared immediately before use by diluting the stock enzyme in 30 mM NaOAc, pH 6.4, 25% glycerol). The reaction was terminated after 4 min by adding 2.5 μl 0.25 M EDTA to the mixture and phenol extracting. (All phenol extractions in this paper consists of two equal volume phenol extractions, pH 7.8, one back extraction of the phenol phase with H_2O to recover any DNA in that phase, and two equal volume ether extractions of the combined aqueous phases.) Finally, the solution was dried in a Speedvac concentrator and analyzed by electrophoresis on a 20% polyacrylamide-7 M urea gel for the top strand labelled DNA and on a 5% polyacrylamide-8 M urea gel for the bottom strand labelled DNA. 20% polyacrylamide gels were autoradiographed directly on the wet gels. 5% gels were transferred to Whatman 3MM chromatography paper, dried in a Bio-Rad

Model 483 Slab Dryer, and autoradiographed.

Elongation Complex. The end-labelled template (0.5 nM) was incubated with the polymerase (0.11-0.44 μM) in 50 μl T7-trans buffer containing unless otherwise indicated 0.2 mM ATP, 0.2 mM GTP, 0.2 mM UTP, and 0.2 mM CTP at 37°C for 5 min. The samples were transferred to a room temperature water bath (22-24°C) followed by the addition of 2 μl of 5 M NaCl, 2 μl of 1 μg/μl calf thymus DNA, and 5 μl of 100 mM $CaCl_2$. We have observed that the DNase I digestion is partially inhibited in the presence of high concentrations of NaCl. Consequently, in the presence of NaCl these digestions were carried out using 2.5-4 μl of 2,000 fold diluted DNase I, i.e., ≥12.5 fold more than that used in the absence of NaCl. The nuclease reaction was stopped after 4 min with 2.5 μl 0.25 M EDTA and was followed by phenol extraction. When $^{N}_{Fu}$-138mer was the template, the samples were dried in a Speedvac concentrator and analyzed on an 8% polyacrylamide-8 M urea gel. When XL-138mer was the template, the samples were split into two equal portions. One was kept in the dark. The other was irradiated for 16 min in a 1.5 ml Eppendorf tube (covered with Reynolds Film 910 to cut off light below 240 nm) with 1 mW/cm^2 254 nm light from a low pressure germicidal lamp (estimated with a black-ray ultraviolet meter, Model J-225, short UV meter, Ultra-violet Products, Inc. San Gabriel, CA.) to photoreverse the HMT diadduct. Both aliquots were taken to dryness in a Speedvac concentrator and analyzed by electrophoresis on an 8% polyacrylamide-8 M urea gel. The gel was then dried and autoradiographed. DNase I footprinting of the elongation complex was also performed under

the following conditions: transcription was performed at 37°C followed by digestion at the same temperature for 4 min with 2 µl of 5,000 fold diluted DNase I.

C) Exonuclease III Digestion of Elongation Complexes

Elongation complexes were formed under the same conditions as in the DNase I footprinting experiments. The complexes were then digested with 1 µl (65 units/µl) Exo III at 37°C for 10 min. The digestion was terminated by adding 2.5 µl of 0.25 M EDTA. The samples were then treated exactly as described for the DNase I digested samples.

3. RESULTS

We have demonstrated in previous chapters that a psoralen diadduct or a psoralen monoadduct on the coding strand can efficiently block transcription by both *E. coli* and T7 RNA polymerases and in the case of *E. coli* RNA polymerase, the arrested elongation complex is amenable to DNase I footprint experiments. Here we used a similar strategy to study the interaction of T7 RNA polymerase with its template DNA in elongation complex arrested at psoralen adduct sites. Figure 1 shows again the double-stranded 138mer constructed with or without an HMT adduct at a specific site. Relative to T7 RNA polymerase promoter start site, the psoralen was attached to T-37 of the coding strand as a furan-side monoadduct in M_{Fu}-138mer and to both T-37 of the coding strand and T-36 of the non-coding strand as a diadduct in XL-138mer.

A) DNase I Footprints of the Initiation Complexes

The interaction of T7 RNA polymerase with the synthetic promoter was probed by DNase I footprinting. The results obtained with the

Figure 1. Sequence of the double-stranded 138mer and the oligonucleotides from which the 138mer was synthesized. The numbers above the sequence are relative to the T7 RNA polymerase transcription start site. The arrow indicates the thymidine residue on the bottom strand (coding strand) to which an HMT furan-side monoadduct is attached in the M_{Fu}-138mer. The solid triangle indicates the thymidine residue on the top strand (noncoding strand) to which the pyrone-end of the HMT is attached in the XL-138mer. The furan-end of the HMT in the XL-138mer is attached to the thymidine residue indicated by the arrow on the bottom strand. Several restriction sites are also shown.

Bottom Strand: 5′-51mer-18mer-12mer-14mer-43mer-3′

12mer: 5′-GAAGCTACGAGC-3′
14mer: 5′-TGAGGCCATCGATA-3′
18mer: 5′-CAGACTCAGTACGAATTC-3′
43mer: 5′-AAGGTCTAGATCTCCCTATAGTGAGTCGTATTAATTTCGACGT-3′
51mer: 5′-CCCATCCCCCTGTTGACAATTAATCATCGGCTCGTATAATGTGTGGAATTG-3′

Top Strand: 5′-40mer-52mer-46mer-3′

40mer: 5′-TACGTCGAAATTAATACGACTCACTATAGGGAGATCTAGA-3′
46mer: 5′-TCCACACATTATACGAGCCGATGATTAATTGTCAACAGGGGGATGG-3′
52mer: 5′-CGTTTATCGATGGCCTCAGCTCGTAGCTTCGAATTCGTACTGAGTCTGCAAT-3′

DS 138mer:

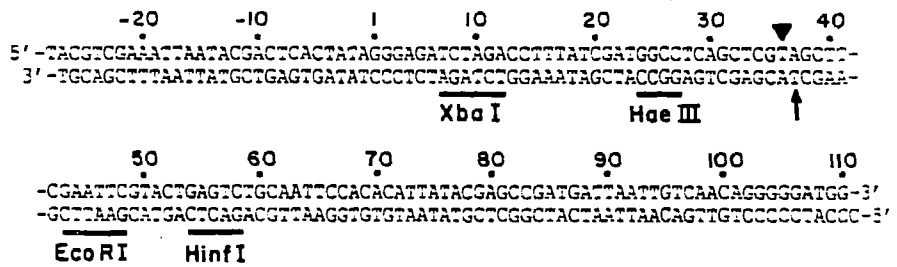

UM-138mer (data not shown and see figure 6) demonstrate that the polymerase protects up to +8 on the coding strand (bottom strand). The protection disappeared when GTP, the first nucleotide of the transcript, was omitted or when 0.2 M NaCl was added. By contrast, there was no protection on the noncoding strand (top strand) in the presence of GTP or both GTP and ATP. These results are consistent with those reported for other T7 polymerase-promoter complexes (Basu and Maitra, 1986; Smeekens and Romano, 1986; Gunderson et al., 1987). The exact upstream boundary of the footprint on the bottom strand could not be determined due to the inability of DNase I to bind and incise near the termini of a helix. We assumed that the polymerase protected up to -20 at the upstream end based on previously reported results (Basu and Maitra, 1986; Ikeda and Richardson, 1986; Gunderson et al., 1987). Identical footprints were obtained for the binding of the polymerase to M_{Fu}-138mer (data not shown). This was expected since the HMT adducts in the M_{Fu}-138mer and XL-138mer lie outside the binding domain of the initiation complex. The above results are summarized in figure 6.

B) DNase I Footprints of the Elongation Complexes

Both the HMT furan-side monoadduct on the coding strand and the HMT diadduct efficiently blocked transcription by T7 RNA polymerase on the synthetic 138mer (see Chapter V). Consequently, an arrested elongation complex could be formed using either HMT adduct. This complex, with a 5'-^{32}P label on either the top strand or the bottom strand, was probed by DNase I footprinting. To maximize the yield of the elongation complex, transcription was conducted at low ionic strength (50 mM

TrisHCl and 10 mM $MgCl_2$). DNase I footprinting was performed on the elongation complex after addition of NaCl to 0.2 M; this minimized the polymerase-promoter complex but had little effect on the elongation complex. If th M_{Fu}-138mer or UM-138mer was used as the template, the digested samples were extracted with phenol, dried in a Speedvac concentrator, and analyzed on an 8% polyacrylamide-8 M urea gel. Due to the inter-strand nature of the HMT diadduct, fragments generated by DNase I cleavages 3′ to the diadduct site in the XL-138mer elongation complex could not be identified because they were covalently attached to the other strand, which was also partially digested. Therefore, after the removal of protein by phenol extraction, half of each footprinting sample was irradiated with 254 nm light to reverse the crosslink thereby allowing determination of the footprint 3′ to the HMT diadduct. The samples (with and without irradiation at 254 nm) were analyzed on an 8% polyacrylamide-8 M urea gel.

Figure 2 shows the DNase I footprint of the bottom strand (coding strand) for the M_{Fu}-138mer elongation complex. Under the conditions described above, transcription was blocked at the HMT furan-side monoadduct, thus yielding an elongation complex with an RNA transcript ca. 36 bases long. The polymerase in the complex protected a region from +21 to +33 with enhanced cleavage at +19 and +20. The protection past +33, if any, could not be detected due to the inability of DNase I to cut in the vicinity of the adduct site. No protection or enhancement was observed when ATP, UTP, and CTP were omitted to prevent elongation. The protection was also sensitive to NTP concentrations as it can be

Figure 2. DNase I footprints of the elongation complex on the bottom strand labelled M_{Fu}-138mer. A) RNAP was 0.22 μM. Lanes 1 and 6: control samples without RNAP and DNase I digestion, respectively. GTP concentrations were 0.1, 0.1, 0.1, 0.05, 0.025, and 0.1 mM, respectively, for lanes 1-6; ATP, UTP, and CTP concentrations were equamolar at 0.1, 0, 0.1, 0.02, 0.01, and 0.1 mM, respectively, for lanes 1-6. B) Densitometric scans of lanes 1 (upper line) and 3 (lower line). The arrows indicate the boundaries of the protected region.

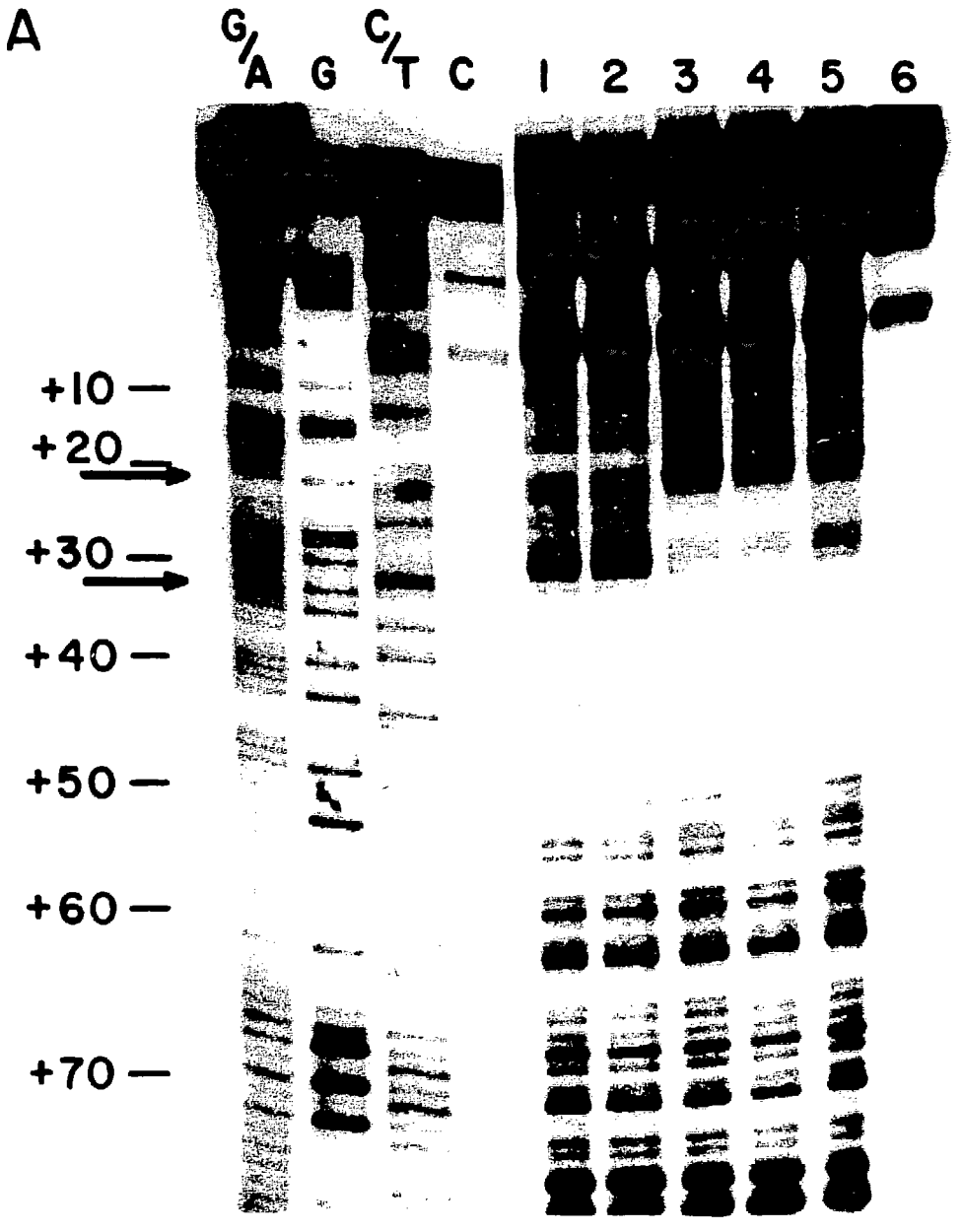
A
G/A
G
C/T
C
1
2
3
4
5
6
+10
+20
+30
+40
+50
+60
+70

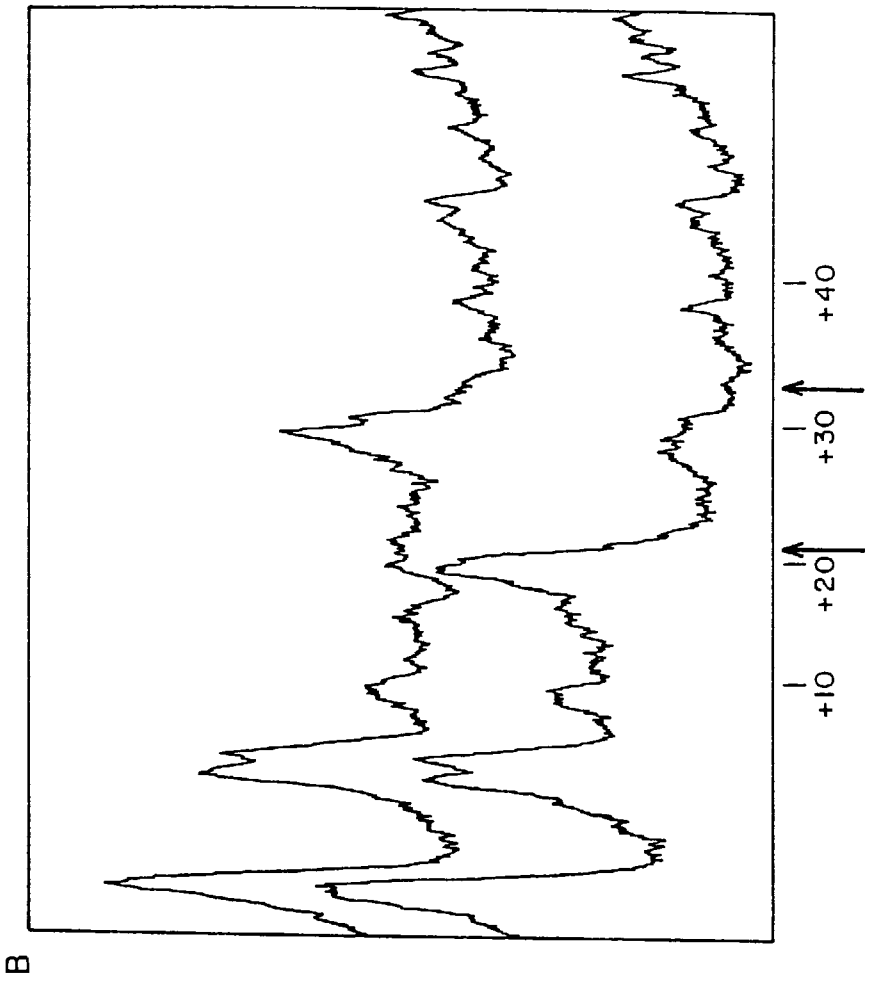
B
+10
+20
+30
+40

seen that at 0.025 mM GTP and 0.01 mM ATP, UTP, and CTP the protection was very weak (lane 5). Identical results were obtained when the bottom strand labelled XL-138mer was used as the template (figure 3).

When similar footprinting experiments were performed on top strand labelled M_{Fu}-138mer template, the results shown in figure 4 were obtained. In contrast to the initiation complex, where no protection was observed on the noncoding strand, the polymerase in the elongation complex on the M_{Fu}-138mer template protected the noncoding strand for 20 bp (from +24 to +43) around the termination site. However, no enhancement was observed on the noncoding strand. As in the case of the coding strand, the protection was independent of the polymerase concentration from 0.11tp 0.44 μM but sensitive to the NTP concentration, as it can be seen that the protection was weaker at a NTP concentration of 0.05 mM (figure 4, lane 6). Identical results were obtained when both the complex formation and the DNase I digestion were performed at 37°C or when the XL-138mer was used as the template (data not shown). When the same experiments were performed using the UM-138mer as the template, no protection was observed, consistent with the fact that transcription on this template yielded runoff transcript.

C) Exo III Digestion of the Elongation Complexes

The 3′ boundary of the protected region in an elongation complex can be delineated by digesting the complex with Exo III nuclease (a double-strand specific 3′ to 5′ exonuclease). Figure 5 shows the results of such an experiment when the bottom strand labelled UM-138mer or M_{Fu}-138mer was used as the template. In the case of the UM-138mer,

Figure 3. DNase I footprints of the elongation complex on the bottom strand labelled XL-138mer. A) Lanes 1′-6′ are identical to lanes 1-6 except that they were irradiated at 254 nm to photoreverse the HMT diadduct. Lanes 1 and 4: control samples without RNAP and DNase I digestion, respectively. Lanes 1, 3, and 4: 0.1 mM ATP, GTP, UTP, and CTP with 0, 0.22, and 0.22 μM RNAP, respectively. Lane 2: identical to lane 3 except no ATP, UTP, and CTP added. Lanes 5 and 6: repeat of lanes 1 and 3, respectively. B) Densitometric scans of lanes 5′ (upper line) and 6′ (lower line). The arrows indicate the boundaries of the protected region.

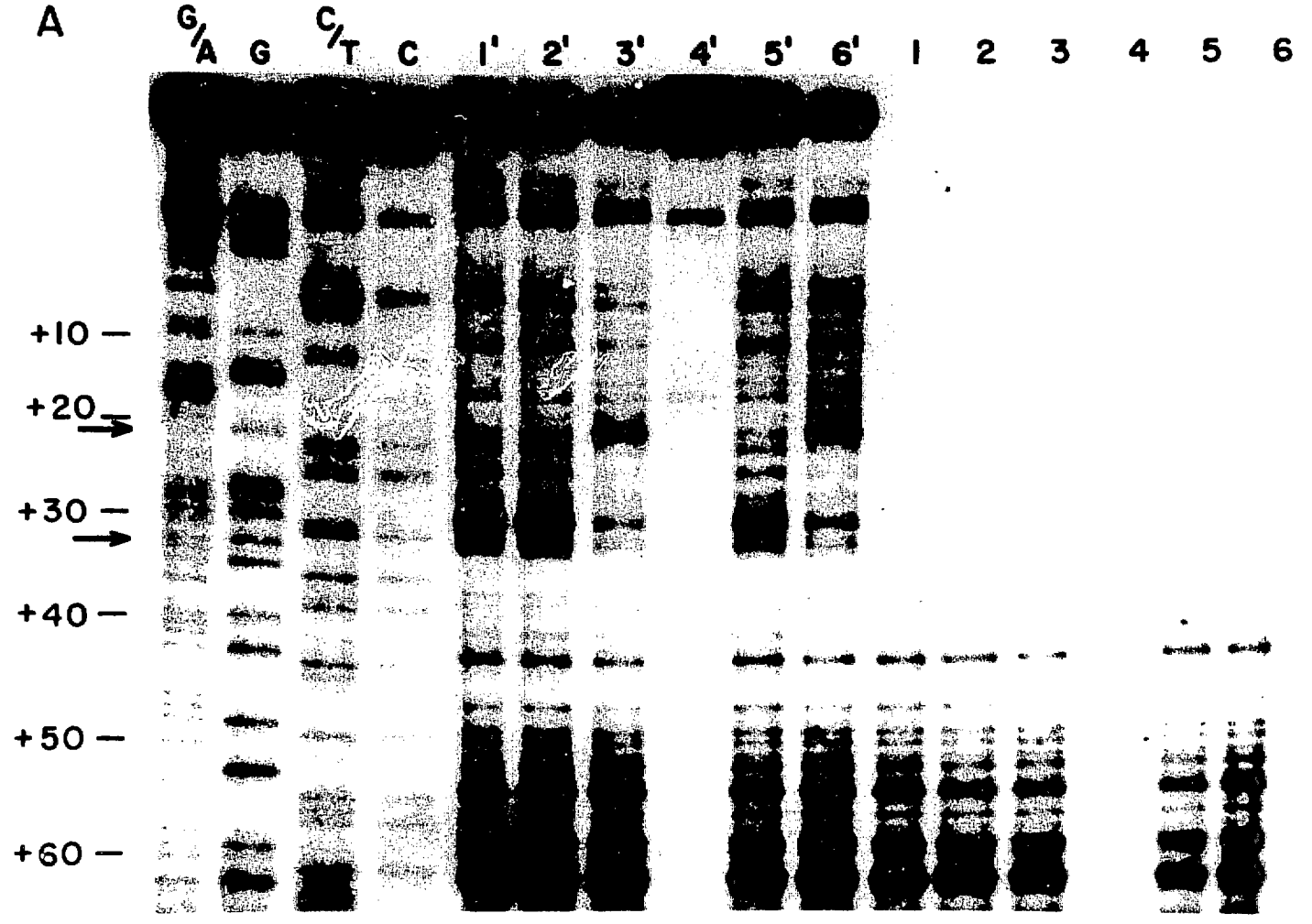
A
G/A
G
C/T
C
1'
2'
3'
4'
5'
6'
1
2
3
4
5
6
+10
+20
+30
+40
+50
+60

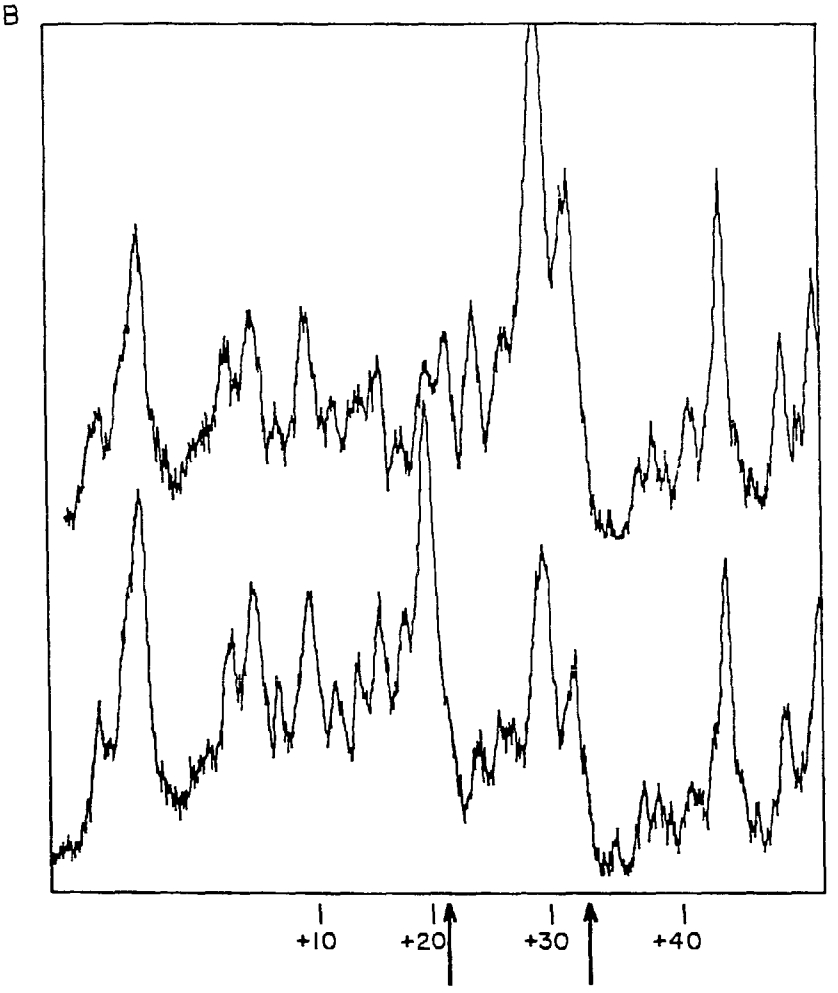
B
+10
+20
+30
+40

Figure 4. DNase I footprints of the elongation complex on the top strand labelled M_{Fu}-138mer. A) Lanes 1, 3-5: 0.2 mM ATP, GTP, UTP, and CTP with 0, 0.11, 0.22, and 0.44, μM RNAP, respectively. Lane 2: identical to lane 4 except no ATP, UTP, and CTP added. Lanes 6 and 7: identical to lane 4 except that nucleotide concentrations were 0.05 mM and 0.4 mM for lanes 6 and 7, respectively. B) Densitometric scans of lanes 1 (upper line) and 3 (lower line). The arrows indicate the boundaries of the protected region.

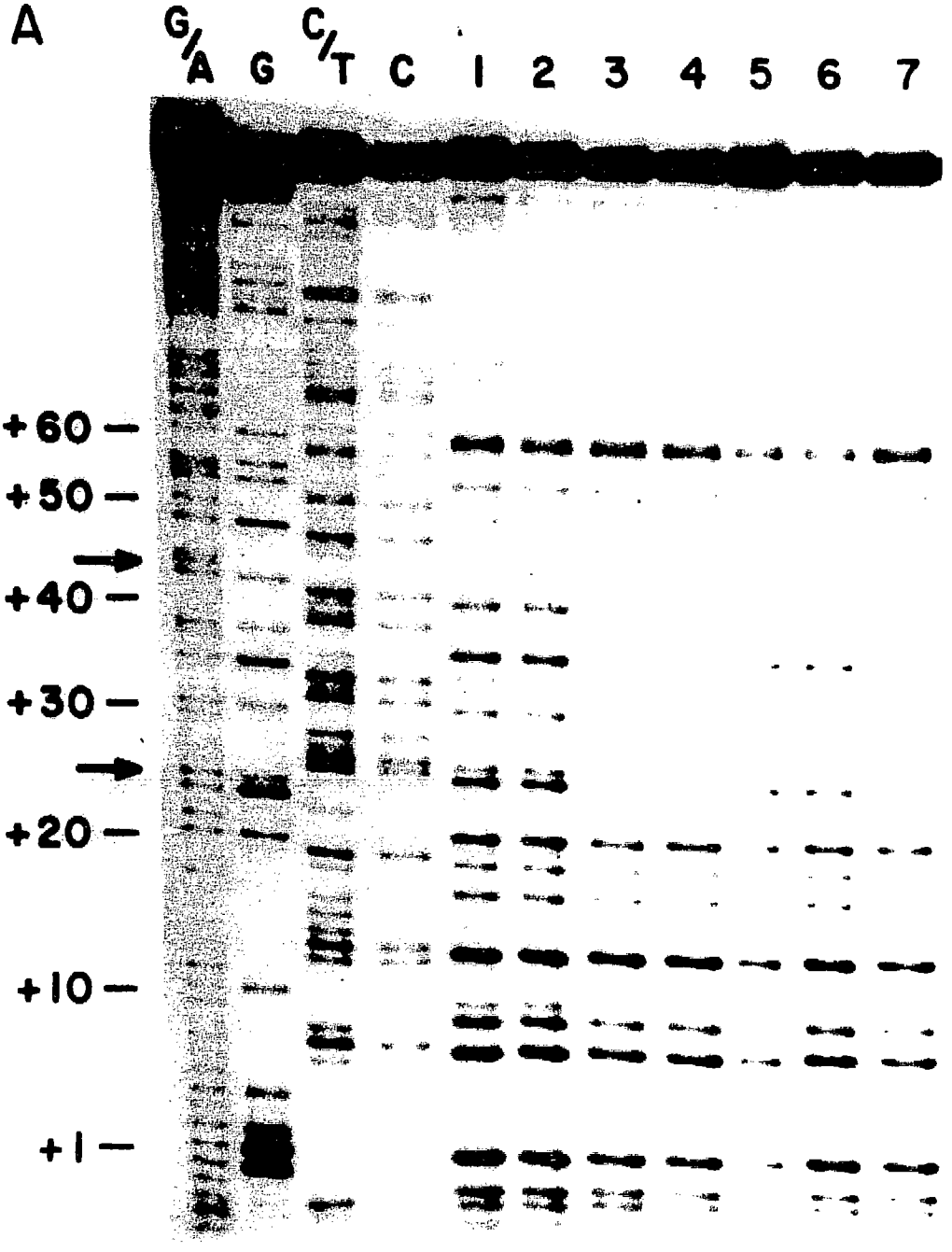
A
G/A
G
C/T
C
1
2
3
4
5
6
7
+60
+50
+40
+30
+20
+10
+1

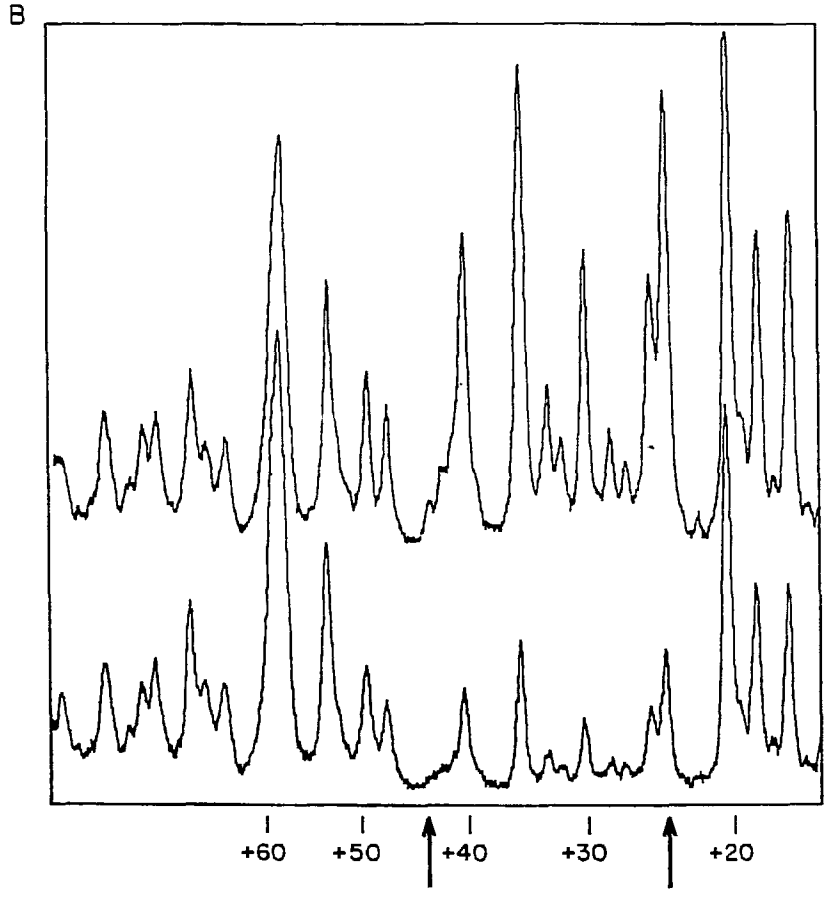
B
+60
+50
+40
+30
+20

no elongation complex was detected (compare lanes 1 and 2). In contrast, when the M_{Fu}-138mer was used as the template, Exo III digestion of the DNA under the elongation conditions yielded a unique band corresponding to 3'-end digestion of the bottom strand to position +23 (figure 5, lane 4). This band did not appear when the T7 RNA polymerase was omitted (figure 5, lane 3). Instead, in this case, Exo III digestion yielded a product corresponding to the 3'-end digestion of the bottom strand to position +34, i.e., 3 bases from the HMT furan-side monoadduct. The +34 band produced in the presence of the polymerase was probably generated from uncomplexed M_{Fu}-138mer. These results indicate that the +23 band corresponds to 3'-end digestion of the bottom strand to the terminus of the elongation complex. Thus Exo III digestion yielded a 3' protection boundary 2 bases downstream from that delineated by the DNase I protection experiments. An identical 3' protection boundary was determined when the XL-138mer was used as the template in the Exo III digestion experiment (data not shown).

When similar experiments were performed on the top strand labelled DNA templates, it was observed that Exo III nuclease frequently terminated in the right half of the DNA, which contained an *E coli* RNA polymerase promoter (Chapter V). The digestion patterns were very difficult to identify. Consequently, the 3' protection boundary on the top strand could not be accurately determined. However, the agreement between the 3' protection boundaries on the bottom strand determined by Exo III and DNase I digestions would suggest that the 3' protection boundaries on the top strand determined by the two methods would agree

Figure 5. Exonuclease III digestion of the elongation complex on bottom strand labelled templates. The elongation complex was formed at 37°C in the presence of 0.1 mM ATP, GTP, UTP, and CTP with 0 (lanes 1 and 3) and 0.22 μM (lanes 2 and 4) RNAP. 1 μl of Exo III was added and the samples were digested at 37°C for 10 min. Lanes 1 and 2: UM-138mer as the template. Lanes 3 and 4: M_{Fu}-138mer as the template.

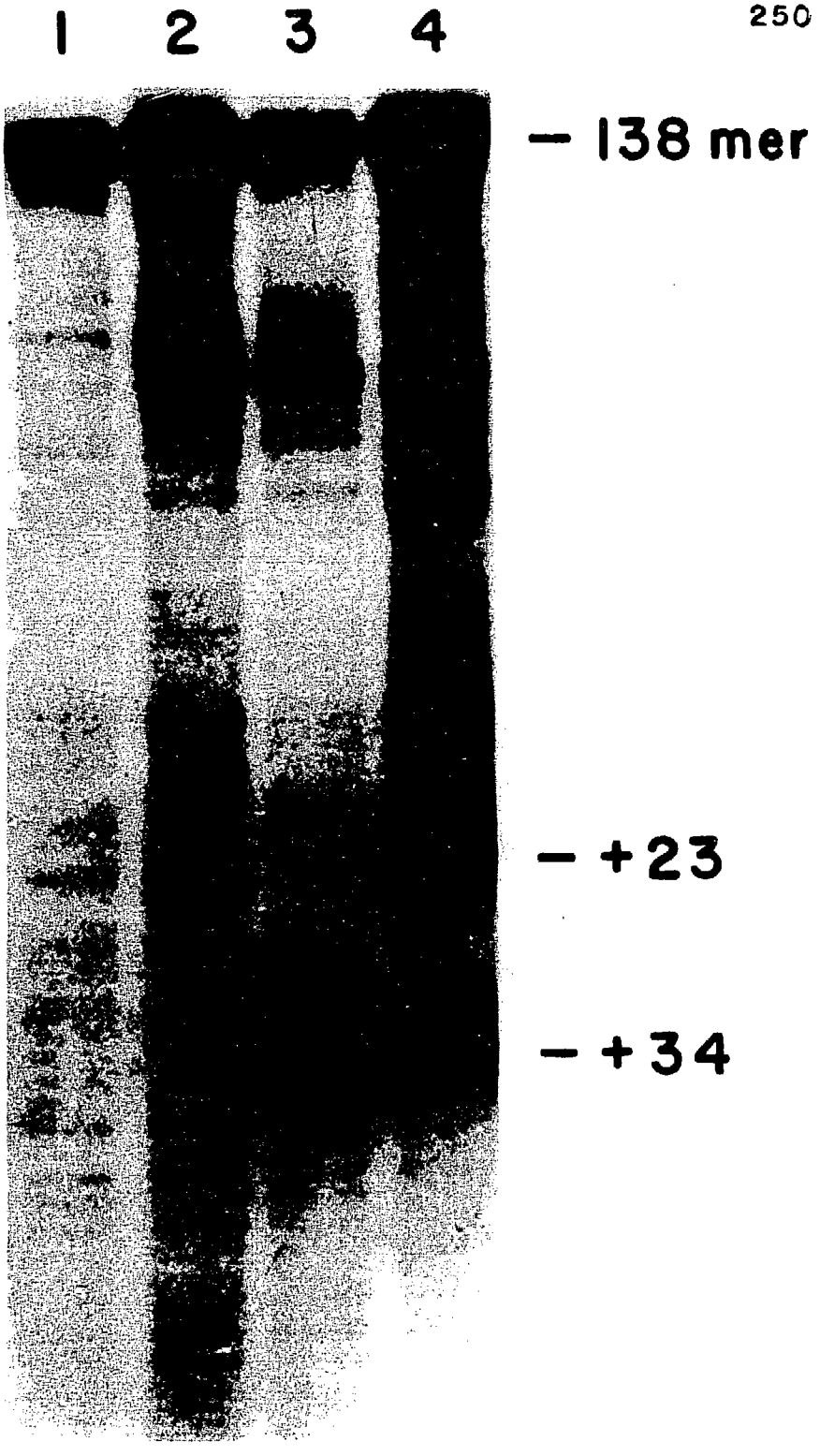
1
2
3
4
— 138 mer
— +23
— +34

with each other if the Exo III digestion were successful.

4. DISCUSSION

We have described a method to generate a homogeneous T7 RNA polymerase elongation complex. This was done by placing an HMT furan-side monoadduct at a specific site on the coding strand of a synthetic double-stranded 138mer containing the consensus T7 RNA polymerase promoter. Transcription by the polymerase was blocked by both the HMT furan-side monoadduct and the photochemically derived interstrand diadduct, thus generating the desired complex. Employing DNase I footprinting, we have investigated the initiation and elongation complexes on the 138mer substrate.

A) Initiation Complex

DNase I footprinting on the initiation complex formed on the UM-138mer template indicates that the polymerase protects up to +8 on the coding strand but affords no protection on the non-coding strand (figure 6), consistent with the results of Basu and Maitra (1986). The upstream boundary of the protected region on the coding strand was assumed to be -20 based on other reported results (Basu and Maitra, 1986; Ikeda and Richardson, 1986; Gunderson et al., 1987). The initiation complex formation requires the presence of GTP, the initiation nucleotide, and is inhibited by high NaCl concentration. These results and the transcription experiments on the synthetic template strongly indicate that the polymerase binds normally to the promoter in the double-stranded 138mer. The data reported by Basu and Maitra (1986) and those in this paper show that the noncoding strand is not protected

Figure 6. DNase I protection of the double-stranded 138mer by RNA polymerase during initiation and elongation. The solid lines indicate protection and the open circles indicate the sites of enhanced cleavage. The arrow denotes the thymidine residue on the bottom strand (coding strand) to which an HMT furan-side monoadduct is attached in the M_{Fu}-138mer. The solid triangle denotes the thymidine residue on the top strand (noncoding strand) which is additionally modified in the XL-138mer.


Elongation
-20
-10
1
10
20
30
40
50
60
70
5'-TACGTCGAAATTAATACGACTCACTATAGGGAGATCTAGACCTTTATCGATGGCCTCAGCTCGTAGCTTCGAATTCGTACTGAGTCTGCAATTCCACACATTATAC...3'
3'-TGCAGCTTTAATTATGCTGAGTGATATCCCTCTAGATCTGGAAATAGCTACCGGAGTCGAGCATCGAAGCTTAAGCATGACTCAGACGTTAAGGTGTGTAATATG...5'
Initiation
Elongation
oo

from DNase I cleavage in the initiation complex, in contrast to the methidiumpropyl-EDTA-Fe protection experiments reported by Ikeda and Richardson (1986) and Gunderson et al. (1987). The difference in the protection pattern is most likely due to the different probes used. Although the binding of the polymerase to its promoter does not protect the noncoding strand from DNase I cleavage, it can interfere with the intercalation of the methidiumpropyl group in the promoter region by either direct physical blockage or unwinding and strand separation of the helix. Since intercalation is a prerequisite for DNA cleavage, its inhibition prevents nicking of both the coding and noncoding strands. DNase I footprinting experiments also show that the HMT addition in the M_{Fu}-138mer and XL-138mer does not interfere with the polymerase-promoter interaction; this is as expected since the HMT adducts in these templates are outside the polymerase binding domain.

B) Elongation Complex

The site specific HMT addition in the M_{Fu}-138mer and XL-138mer efficiently blocked transcription by T7 RNA polymerase, thus generating an elongation complex containing a nascent RNA 36 or 37 bases long. The major RNA transcript was 36 bases long, which corresponds to transcription termination at the coding strand A(36) adjacent to the HMT-thymidine adduct. The minor transcript was one base longer. This RNA could have been generated either by transcription passing through the HMT moiety in the templates or by the nonspecific addition of a base to the 3'-terminus of the RNA in the arrested elongation complexes. We believe that the former is unlikely since the HMT moiety is

between the two A:T base pairs (bp 36 and 37) in both the M_{Fu}-138mer and XL-138mer and the crosslinked template cannot be strand separated so as to allow the polymerase to pass through the diadduct. Furthermore, it has been shown that T7 RNA polymerase can incorporate a randomly selected base at the 3'-terminus of a runoff RNA transcript before the release of template and transcript (Lowary et al., 1986). Thus the elongation complexes formed on the M_{Fu}-138mer and XL-138mer templates were heterogeneous in that the transcript in the complexes was either 36 or 37 bases long. The position of the polymerase on the template DNA in these two groups of complexes could either be shifted by one base from each other or occupy the same site relative to the HMT adduct. The latter is more likely if the 37 base-long RNA is formed by the nonspecific addition of one base to the 3'-terminus of the transcript in the arrested elongation complex (see Chapter V).

The DNase I footprinting experiments indicate that the RNA polymerase in the elongation complexes on both the M_{Fu}-138mer and XL-138mer templates protects 20 nucleotides (+24 to +43) in the vicinity of the HMT adduct on the noncoding strand and 13 nucleotides (+21 to +33) upstream from the HMT adduct on the coding strand (figure 6). In fact, the polymerase may protect the coding strand from +21 up to or even past the HMT adduct site (+37) since the RNA is synthesized up to that site in the complexes. Any protection around the adduct site, however, could not be detected due to the inability of DNase I to cut in the vicinity of the HMT furan-side monoadduct or diadduct (see figures 2-4).

The protection of the DNA template by the polymerase in the T7 elongation complexes was not as strong as that observed for the corresponding *E. coli* RNA polymerase complex (Carpousis and Gralla, 1985; Chapter VII) and this protection weakened considerably when the NTP concentrations were ≤50 μM. The weak protection stems from the fact that T7 RNA polymerase elongation complexes are less stable than the analogous *E. coli* RNA polymerase complexes. It has been shown, for example, that *E. coli* elongation complexes can survive non-denaturing polyacrylamide gel electrophoresis and gel filtration (Rohrer and Zillig, 1977; Straney and Crothers, 1985; Chapter VII). However, analysis of the T7 elongation complexes by non-denaturing polyacrylamide gel electrophoresis failed to detect any descrete nucleoprotein complex, although the DNA template was slightly retarded on the gel in the presence of the polymerase under both the initiation and elongation conditions (data not shown). Based on the amount of RNA transcript synthesized from the M_{Fu}-138mer and XL-138mer templates, we estimate that more than one copy of the transcript per template was synthesized during the 5 min incubation at 37°C under our standard transcription conditions, suggesting a lifetime for the arrested elongation complex of approximately 5 min. or so. This short lifetime explains the weak protection of the template from DNase I digestion and the inability to detect any elongation complexes by non-denaturing gel electrophoresis.

Our results demonstrate that a dramatic conformational change occurs upon conversion of the initiation complex to the elongation complex. During initiation T7 RNA polymerase protects only the coding

strand, whereas both strands are protected in the elongation complex. The size of the protected region also decreases upon the conversion and is reminescent of a similar contraction observed for the footprints of *E. coli* RNA polymerase complexes (Rohrer and Zillig, 1977; Carpousis and Gralla, 1985; Straney and Crothers, 1985; Chapter VII). The structural significance of these changes remains to be elucidated.

Although the elongation complexes described here were generated using a site specific HMT adduct to arrest the transcription process, the DNase I footprints of the complexes agree with those obtained by Ikeda and Richardson (1986), who used methidiumpropyl-EDTA-Fe to footprint a T7 RNA polymerase elongation complex stalled by omitting one ribonucleoside triphosphate. This agreement, which argues that the HMT adducts do not significantly perturb the structure of the arrested complex, is further supported by the following observations. First, a comparison of the DNase I cleavage patterns of both the top and bottom strands in the absence of T7 RNA polymerase indicates that the presence of the HMT adduct in the M_{Fu}-138mer or the XL-138mer does not perturb the conformation of the DNA helix except in the immediate vicinity of the adduct (Chapter VII and data not shown). Second, both the M_{Fu}-138mer and XL-138mer elongation complexes yielded identical footprints even though the nature of the HMT adduct in each template is quite different.

The agreement between the protection of the DNA from DNase I digestion in our elongation complexes, which contain an RNA transcript 36 bases in length, and the protection of the DNA from

methidiumpropyl-EDTA-Fe cleavage in an elongation complex which contains an RNA transcript 15 bases in length (Ikeda and Richardson, 1986) suggests that transcription enters the elongation stage after synthesizing a transcript 15 bases long. This in not apparent from Ikeda and Richardson's data alone since they obtained a different protection pattern for each complex (containing nascent RNAs up to 15 bases in length) examined.

The DNase I footprints of the elongation complexes formed on the M_{Fu}-138mer and XL-138mer templates have revealed two hypersensitive sites on the coding strand 17 and 18 nucleotides upstream from the HMT adduct site (figure 6). The HMT adduct and the DNase I hypersensitive sites may bracket a hypothetical unwound region encompassing approximately 17 bp, a conclusion in good agreement with similar experiments on the *E. coli* complex. Hypersensitive sites have been observed in the DNase I footprints of an *E. coli* RNA polymerase elongation complex arrested at a site specific HMT diadduct site (Chapter VII). It is known that during the elongation process, *E. coli* RNA polymerase unwinds approximately 12 to 17 base pairs of DNA template and maintains a short RNA-DNA hybrid helix between the nascent RNA chain and the DNA coding strand in the unwound region (Gamper and Hearst, 1982; Von Hippel et al., 1984). Based on this, we have proposed that the hypersensitive sites in the *E. coli* elongation complex correspond to the junction between the RNA-DNA helix and the reformed DNA-DNA helix (Chapter VII). If similar DNA unwinding and RNA-DNA helix formation occurs during transcription by T7 RNA polymerase, the hypersensitive

sites we have observed here would be at the postulated junction between the RNA-DNA helix and the reformed DNA-DNA helix.

APPENDIX

ABBREVIATIONS

ATP	Adenosine 5′-triphosphate
ATP-γ-S	Adenosine 5′-[γ-thio]-triphosphate
bp	Base pair
BSA	Bovine serum albumin
C-HMT-C	Cytidine-HMT-Cytidine diadduct
DTT	Dithiothreitol
EDTA	Ethylenediaminetetraacetic acid
EtOH	Ethanol
HMT	4′-Hydroxymethyl-4, 5′, 8-trimethylpsoralen
HPLC	High-performance liquid chromatography
M_{Fu}	Furan-side monoadduct
M_{Py}	Pyrone-side monoadduct
RNAP	RNA polymerase
SDS	Sodium dodecyl sulfate
T-HMT-C	Thymidine-HMT-Cytydine diadduct
5′-[T(HMT)$_{Fu}$]-3′	Thymidine-HMT furan-side monoadduct with HMT on the 3′-side of the thymidine
5′-[T(HMT)$_{Py}$]-3′	thymidine-HMT pyrone-side monoadduct with HMT on the 3′-side of the thymidine
T-HMT-T	Thymidine-HMT-Thymidine diadduct
Tris	Tris (hydroxymethyl) aminomethane
XL	HMT-DNA crosslink

BIBLIOGRAPHY

Aboul-ela, F., Koh, D., Tinoco, I. Jr., Martin, F. H. (1985) Nucleic Acids Res. 13, 4811-4824.

Axelrod, V. D., Vartikyan, R. M., Airazashvili, V., A., and Beabealashvili, R. Sh. (1978) Nucleic Acids Res. 5, 3549-3563.

Baba, Y., Beatty, C. L., Kagemoto, A. (1981) Org. Coat. Plast. Chem. 44, 223-227.

Basu, S., and Maitra, U. (1986) J. Mol. Biol. 190, 425-437.

Bensasson, R. V., Salet, C., Land, E. J., and Rushton, F. A. P. (1980) Photochem. Photobiol. 31, 129-133.

Ben-Hur, E., and Song, P. S. (1984) Adv. Radiat. Biol. 11, 131-171.

Bernhard, S. L., and Meares, C. F. (1986) Biochem. 25, 5914-5919.

Black, D. L., Chabot, B., and Steitz, J. A. (1985) Cell (Cambridge, Mass.) 42, 737-750.

Blais, J., Ronfard-Haret, J. C., Vigny, P., Cadet, J., and Voituriez, L. (1985) Photochem. Photobiol. 42, 599-602.

Bohr, V., and Nielsen, P. E. (1984) Biochimica et Biophysica Acta. 783, 183-186.

Borer, P. N., Dengler, B., Tinoco, I. Jr., Uhlenbeck, O. C. (1974) J. Mol. Biol. 86, 843-853.

Bose, S. N., and Davies, R. J. H. (1984) Nucleic Acids Research 12, 7903-7914.

Calvet, J. P., Meyer, L. M., and Pederson, T. (1982) Science 217, 456-458.

Carpousis, A. J., and Gralla, J. D. (1985) J. Mol. Biol. 183, 165-177.

Cassier, C., Chanet, R., and Moustacchi, E. (1984) Photochem. Photobiol. 39, 799-803.

Cassier, C., Chanet, R., and Moustacchi, E. (1985) Photochem. Photobiol. 41, 289-294.

Chamberlin, M., and Ring, J. (1973) J. Biol. Chem. 248, 2235-2244.

Chamberlin, M., and Ryan, T. (1982) in The Enzymes, ed. boyer, P. D. (Academic, New York), Vol. 15, pp. 87-108.

Chamberlin, M., McGrath, J., and Waskell, L. (1970) Nature 228, 227-231.

Chan, G. L., Doetsch, P. W., and Haseltine, W. A. (1985) Biochem. 24, 5723-5728.

Cimino, G. D., Gamper, H. B., Isaacs, S. T., and Hearst, J. E. (1985) Ann. Rev. Biochem. 54, 1151-1193.

Cimino, G. D., Shi, Y.-B., Hearst, J. E. (1986) Biochem. 25, 3013-3020.

Clark, J. M. and Beardsley, G. P. (1986) Nucleic Acids Res. 14, 737-749.

Deering, R. A., and Setlow, R. B. (1963) Biochim. Biophys. Acta 68, 526-534.

de Boer, H. A., Comstock, L. J., and Vasser, M. (1983) Proc. Natl. Acad. Sci. USA 80, 21-25.

de Mayo, P., and Shizuk, H. (1976) in Creation and Detection of the Excited State (Ware, W. R., Ed.) Vol. 4, pp 164-182), Marcel Dekk-

er, New York, Basel.

Duval-Valentin, G., and Ehrlich, R. (1986) Nucleic Acids Res. 14, 1967-1983.

Ennis, D. G., Fisher, B., Edmiston, S., and Mount, D. W. (1985) Proc. Natl. Acad. Sci. USA 82, 3325-3329.

Fasman, G. D. (1975) Biochem., Mol. Biol., 3rd Ed., Vol. 1, 589.

Fitzpatrick, J. B., Stern, R. S., and Parrish, J. A. (1982) In Psoriasis -Proc. 3rd Int. Symp. (Farber, E.M., Ed) pp149-156, Grune and stratton, New York.

Fujita, H. (1984) Photochem. Photobiol. 39, 835-839.

Gamper, H. B., and Hearst, J. E. (1982) Cell 29, 81-90.

Gamper, H. B., Piette, J., and Hearst, J. E. (1984) Photochem. Photobiol. 40, 29-34.

Gamper, H. B., Cimino, G. D., Isaacs, S. T., Ferguson, M., and Hearst, J. E. (1986) Nucleic Acids Res. 14, 9943-9954.

Gamper, H. B., Cimino, G. D., and Hearst, J. E. (1987) J. Mol. Biol. In press.

Garrett-Wheeler, E., Lockard, R. E., and Kumar, A. (1984) Nucleic Acids Res. 12, 3405-3423.

Gasparro, F. P., Saffron, W. A., Cantor, C. R., and Edelson, R. L. (1984) Photochem. and photobiol. 40, 215-219.

Griffith, J., Bleyman, M., Rauch, C. A., Kitchin, P. A., and Englun T. (1986) Cell 46, 7171-724.

Grossman, L. (1968) Photobiochem. and Photobiol. 7, 727-735.

Gunderson, S. I., Chapman, K. A., and Burgess, R. R. (1987)

Biochem. 26, 1539-1546.

Hanawalt, P. C. (1986) In Basic Life Sciences: Mechanism of DNA Damage and Repair (Eds. Simic, M. G., Grossman, K., and Upton, A. C.) 38, 489-498, Plenum Press, New York.

Hansen, U. M., and McClure, W. (1980) J. Biol. Chem. 255, 9564-9570.

Hariharan, P. V., and Cerutti, P. A. (1977) Biochem. 16, 2791-2795.

Hearst, J. E., Isaacs, S. T., Kanne, D., Rapoport, H., and Straub, K. (1984) Q. Rev. Biophys. 17, 1-44.

Hofer, B., Muller, D, and Koster, H. (1985) Nucleic Acids Res. 13, 5995-6013.

Ide, H., Kow, Y. W., and Wallace, S. S. (1985) Nucleic Acids Res. 13, 8035-8052.

Ikeda, R. A., and Richardson, C. C. (1986) Proc. Natl. Acad. Sci. USA 83, 3614-3618.

Ikeda, R., and Richardson, C. C. (1987) J. Biol. Chem. 262, 3800-3808.

Isaacs, S. T., Shen, C. -K. J., Hearst, J. E., and Rapoport, H. (1977) Biochem. 16, 1058-1064.

Isaacs, S. T., Rapoport, H., and Hearst, J. E. (1982a) J. Labelled Compounds and Radiopharmaceuticals 19, 345-356.

Issacs, S. T., Chun, C., Hyde, J. E., Rapoport, H., and Hearst,J. E. (1982b) In Trends In Photobiology(Helene, C., Charlier, M., Montenay-Carestier, Th., and Laustriat, G., Eds) pp279-294, Plenum

Publishing Corp.

Johnston, B. H., Johnson, M. A., Moore, C. B., Hearst, J. E. (1977) Science 197, 906-908.

Johnston, B. H., Kung, A. H., Moore, C. B., Hearst, J. E. (1981) Biochem. 20, 735-738.

Kanne, D., Straub, K., Hearst, J. E., and Rapoport, H. (1982a) J. Am. Chem. Soc. 104, 6754-6764.

Kanne, D., Straub, K., Rapoport, H., and Hearst, J. E. (1982b) Biochem. 21, 861-871.

Kao, J. P.-Y. (1984) Ph. D. Thesis pp. 126-190. Lawrence Berkeley Laboratory, University of California, Chemical Biodynamics Division.

Kim, S.-H., Peckler, S., Graves, B., Kanne, D., Rapoport, H., and Hearst, J. E. (1983) Cold Spring Harbor Symposia on Quantitative Biology XLVII, 361-365.

Kodadek, T. and Gamper, H. (1987) Submitted.

Krainer, A., and Maniatis, T. (1985) Cell (Cambridge, Mass.) 42, 725-736.

Land, E. J., and Truscott, T. G. (1979) Photochem. Photobiol. 29, 861-866.

Little, J. W., and Mount, D. M. (1982) Cell 29, 11-22.

Lowary, R., Sampson, J., Milligan, J., Groebe, D., and Uhlenbeck, O. C. (1986) In Structure and Dynamics of RNA (Eds. P. Van Knippenberg and C. W. Hilbers) NATO ASI Series vol. 110, pp 69-76. Plenum Press, New York.

Lu, C., Scheuermann, R. H., and Echols, H. (1986) Proc. Natl.

Acad. Sci. USA 83, 619-623.

Maniatis, T., Fritsch, E. F., and Sambrook, J. (1982) In Molecular Cloning pp125-127, Cold Spring Harbor Laboratory.

Martin, F. H., Uhlenbeck, O. C., Doty, P. (1971) J. Mol. Biol. 57, 201-215.

Maxam, A. M., and Gilbert, W. (1980) Methods in Enzymology 65, 499-560.

McClure, W. R. (1985) Ann. Rev. Biochem. 54, 171-204.

Melancon, P., Burgess, R. R., and Record, M. T. Jr. (1982) Biochem. 21, 4318-4331.

Melancon, P., Burgess, R. R., and Record, M. T. Jr. (1983) Biochem. 22, 5169-5176.

Moore, P. D., Bose, K. K., Rabkin, S. D., and Strauss, B. S. (1981) Proc. Natl. Acad. Sci. USA 78, 110-114.

Moore, P. D., Rabkin, S. D., Osborn, A. L., King, C. M., and Strauss, B. S. (1982) Proc. Natl. Acad. Sci. USA 79, 7166-7170.

Morden, K. M., Chu, Y. C., Martin, F. H., Tinoco, I. Jr. (1983) Biochem. 22, 5557-5563.

Nelson, J. W., Tinoco, I. Jr. (1984) Biopolymers 23, 213-233.

Nocentini, S. (1978) Biochim. Biophys. Acta 521, 160-168.

Oakley, J. L., Strothkamp, R. E., Sarris, A. H., and Coleman, J. E. (1979) Biochem. 18, 528-537.

Ou, C.-N., Tsai, C.-H., Tapley, K. J., Jr., and Song, P.-S. (1978) Biochem. 17, 1047-1053.

Parrish, J. A., Stern, F. S., Pathak, M. A., and Fitzpatrick, J.

B. (1982) In Science of Photomedicine (Regan, J. D. and Parrish, J. A., Eds.) pp. 595-623, Plenum Press, New York.

Parsons, B. J. (1980) Photochem. Photobiol. 32, 813-821.

Patel, D. J., Kozlowski, S. A., Marky, L. A., Rice, J. A., Broka, C., Itakura, K., Breslauer, K. J. (1982) Biochem. 21, 445-451.

Peak, M. J., and Peak, J. G. (1982) Photobiochem. and Photobiol. 35, 675-680.

Peak, M. J., Peak, J. G., Moehring, M. P., and Webb, R. B. (1984) Photobiochem. and Photobiol. 40, 613-620

Pearlman, D. A., Holbrook, S. R., Pirkle, D. H., and Kim, S. H. (1985) Science 227, 1304-1308.

Pearson, M., Whillans, D. W., LeBlanc, J. C., and Jones, H. E. (1966) J. Mol. Biol. 20, 245-261.

Peckler, S., Graves, B., Kanne, D., Rapoport, H., Hearst, J. E., and Kim, S. H. (1982) J. Mol. Biol. 162, 157-172.

Phillips, D. R., and Crothers, D. M. (1986) Biochem. 25, 7355-7362.

Piette, J. and Moore, P. D. (1982) Photochem. Photobiol. 35, 705-708.

Piette, J. and Hearst, J. E. (1983) Proc. Natl. Acad. Sci. USA. 80, 5540-5544.

Piette, J., Decuyper-Debergh, D., and Gamper, H. (1985) Proc. Natl. Acad. Sci. USA 82, 7355-7359.

Piette, J. and Hearst, J. E. (1985) Int. J. Radiat. Biol. 48, 381-388.

Prager, A., Green, M., and Ben-Hur, E. (1983) Photochem. Photobiol. 37, 525-528.

Prosen, D. E., and Cech, C. L. (1986) Biochem. 25, 5378-5387.

Reisbig, R. R. and Hearst, J. E. (1981) Biochem. 20, 1907-1918.

Rinke, J., Appel, B., Digweed, M., and Luhrmann, R. (1985) J. Mol. Biol. 185, 721-731.

Roe, J.-H., and Record, M. T., Jr. (1985) Biochem. 24, 4721-4726.

Rohrer, H., and Zillig, W. (1977) Eur. J. Biochem. 79, 401-409.

Rosenstein, B. S., and Ducore, J. M. (1983) Photobiochem. and Photobiol. 38, 51-55.

Rothman, R. H., and Setlow, R. B. (1979) Photobiochem. and Photobiol. 29, 57-61.

Saffran, W. A., and Cantor, C. R. (1984) J. Mol. Biol. 178, 595-609.

Sagher D. and Strauss, B. (1985) Nucleic Acids Res. 13, 4285-4298.

Setyono, B., and Pederson, T. (1984) J. Mol. Biol. 174, 285-295.

Shames, B., Kalma, S., Heimer, Y. M., and Tal, J. (1983) Nucleic Acids Res. 11, 6453-6464.

Shi, Y.-B., and Hearst, J. E. (1986) Biochem. 25, 5895-5902.

Shi, Y.-B., and Hearst, J. E. (1987a) Biochem. 26, 3786-3792.

Shi, Y.-B., and Hearst, J. E. (1987b) Biochem. 26, 3792-3898.

Shi, Y.-B., Gamper, H., and Hearst, J. E. (1987) Nucleic Acids Res. 15, 6843-6854.

Shi, Y.-B., Gamper, H., Van Houten, B., and Hearst, J. E. (1988a) J. Mol. Biol. 199, 277-293.

Shi, Y.-B., Gamper, H., and Hearst, J. E. (1988b) J. Biol. Chem. 263, 527-534

Siden, R., and Hagerman, P. J. (1984) Biochem. 23, 6299-6303.

Siebenlist, U., and Gilbert, W. (1980) Proc. Natl. Acad. Sci. USA 77, 122-126.

Siebenlist, U., Simpson, R. B., and Gilbert, W. (1980) Cell 20, 269-281.

Smeekens, S. P., and Romano, L. J. (1986) Nucleic Acids Res. 14, 2811-2827.

Song, P. S., and Tapley, K. J. Jr. (1979) Photochem. Photobiol. 29, 1177-1197.

Spassky, A., Kirkegaard, K., and Buc, H. (1985) Biochem. 24, 2723-2731.

Spassky, A. (1986) J. Mol. Biol. 188, 99-103.

Straney, D. C., and Crothers, D. M. (1985) Cell 43, 449-459.

Straub, K., Kanne, D., Hearst, J. E., and Rapoport, H. (1981) J. Am. Chem. Soc. 103, 2347-2355.

Tessman, J. W., Isaacs, S., T., and Hearst, J. E. (1985) Biochem. 24, 1669-1676.

Thompson, J. F., and Hearst, J. E. (1983) Cell 32, 1355-1365.

Tomic, M. T., Wemmer, D. E., and Kim, S.-H. (1987) Science 238, 1722-1725.

Turner, S., and Noller, H. F. (1983) Biochem. 22, 4159-4164.

Van Dyke, M. W., and Dervan, P. B. (1983) Biochem. 22, 2373-2377.

Van Houten, B., Gamper, H., Hearst, J. E., and Sancar, A. (1986a)

J. Biol. Chem. 261, 14135-14141.

Van Houten, B., Gamper, H., Holbrook, S. R., Hearst, J. E., and Sancar, A. (1986b) Proc. Natl. Acad. Sci. USA 83, 8077-8081.

Vigny, P., Blais, J., Ibanez, V., and Geacintov, N. E. (1987) Photochem. Photobiol. 45, 601-607.

Von Hippel, P. H., Bear, D. G., Morgan, W. D., and McSwiggen, J. A. (1984) Ann. Rev. Biochem. 53, 389-446.

Vos, J.-M. H., and Hanawalt, P. C. (1987) Cell 50, 789-799.

Witkin, E. M., and Kogoma, T. (1984) Proc. Natl. Acad. Sci. USA 81, 7539-7543.

Wu, H.-M., and Crothers, D. (1984) Nature 308, 509-513.

Zhen, W.-P., Jeppesen, C., and Nielsen, P. E. (1986) Photochem. Photobiol. 44, 47-51.